2021

Cerebral Amyloid Angiopathy-Causing Beta-Amyloid Variants Have Altered Effects on the Clotting System

Steven Cajamarca

CEREBRAL AMYLOID ANGIOPATHY-CAUSING BETA-AMYLOID VARIANTS HAVE ALTERED EFFECTS ON THE CLOTTING SYSTEM

A Thesis Presented to the Faculty of
The Rockefeller University
in Partial Fulfillment of the Requirements for
the degree of Doctor of Philosophy

by
Steven Cajamarca
June 2021

CEREBRAL AMYLOID ANGIOPATHY-CAUSING BETA-AMYLOID VARIANTS HAVE ALTERED EFFECTS ON THE CLOTTING SYSTEM

Steven Cajamarca, Ph.D.
The Rockefeller University 2021

Cerebral amyloid angiopathy (CAA), where beta-amyloid (Aβ) deposits around cerebral blood vessels, is a major contributor of vascular dysfunction in Alzheimer's disease (AD) patients. However, the molecular mechanism underlying CAA formation and CAA-induced cerebrovascular pathologies, including intracerebral hemorrhage (ICH) is unclear. Hereditary cerebral amyloid angiopathy (HCAA) is a rare familial form of CAA in which mutations within the Aβ peptide cause an increase in vascular deposits. Since the interaction between normal wild-type (WT) Aβ and fibrinogen increases CAA and plays an important role in cerebrovascular damage in AD, I investigated the role of the Aβ-fibrinogen interaction in HCAA pathology. My work revealed the most common forms of HCAA-linked mutations resulted in up to a 50-fold stronger binding affinity of Aβ for fibrinogen, increased perturbation of clot structure and fibrinolysis, and increased cortical fibrin(ogen)/Aβ co-deposition. Consistent with these *in vitro* results, HCAA patients have increased fibrin deposits compared to early-onset AD patients and non-demented individuals. In addition, because of the known WT Aβ enhancements to proteolytic/fibrinolytic system activation, I examined the effects of HCAA Aβ on the fibrinolytic system. I found that the majority of HCAA Aβ variants led to increased tPA-mediated plasminogen activation. The HCAA Arctic variant (E22G) did not, which may partially explain the unique clinical features of this mutation. To expand our understanding of the continuum of Aβs that can interact with fibrin(ogen) and the fibrinolytic system, I also explore the possible role of longer length Aβs in facets of AD-related vascular pathologies.

My results suggest the HCAA-type mutations, with special emphasis on the Dutch and Iowa mutations, increase the interaction between Aβ, fibrinogen, and the fibrinolytic enzyme system. These findings provide a novel molecular mechanism for how CAA-linked mutations may lead to severe cerebrovascular pathology in HCAA patients by enhancing the Aβ-fibrin interaction and fibrinolytic activity.

To my parents, Jorge and Nanci, who sacrificed everything and dreamt of a brighter future for their children.

ACKNOWLEDGMENTS

I wish to thank Sid Strickland and Erin Norris for their exceptional guidance, support, and mentorship. They created a friendly, stimulating, and engaging lab environment that made me feel like I had a second home. They also provided extremely helpful feedback helped shape the questions that I sought to answer in my thesis. I am very grateful to Dr. Hyung Jin Ahn, who's expertise in biochemistry and previous biochemical work elucidating the interaction between Aβ and fibrinogen, were the basis of my studies in this thesis. He provided excellent mentorship and experimental assistance that allowed me to accomplish the body of work presented here. I am eternally thankful to Drs. Louise van der Weerd and Dr. Michael Farrell, who very generously shared precious and very limited HCAA-Dutch and -Iowa, respectively, brain samples for the tissue analysis conducted here.

I am grateful to my faculty advisory committee members, Drs. Barry Coller, Mary B. Hatten, and Costantino Iadecola who pushed me to think more critically about the significance of my work and provided excellent guidance as to how to narrow the scope of the questions I was asking in my thesis. I also thank Dr. Katerina Akassaglou for her amazing contributions to the scientific field advancing the role of fibrinogen in neurodegeneration and for taking the time to act as my external committee member during these odd times amidst a frightening pandemic.

I am very appreciative of the amazing friendships I was able to form during my time in the Strickland Laboratory, especially with Sarah, Anna, Pradeep, and Shigeru. They kept me sane and helped create a fun lab environment. Sarah and Pradeep provided excellent scientific advice when things were not working.

I am very indebted to current and former Rockefeller Resource Center scientists including Hiro, Dee, Amalia, Carolina, Christina, Tao, and Carlos. Their expertise and generous allotment of time to help me enabled the completion of this work. Without them, the work would have been infinitely times more difficult.

Finally, I cannot fathom how thankful I am for the immense patience, understanding, and love directed at me by my family, close friends, and Jenna, who have supported me through the lows and highs that I have experienced as an MD-PhD student; first, during the hardships of the preclinical portion of medical school, the transition to graduate school, and most recently through the innumerable uncertainties experienced during my thesis work.

TABLE OF CONTENTS **Page**

ACKNOWLEDGMENTS ..... **iv**
TABLE OF CONTENTS ..... **v**
LIST OF FIGURES ..... **vii**
LIST OF TABLES ..... **ix**
LIST OF ABBREVIATIONS ..... **x**

CHAPTER 1: INTRODUCTION **1**
1.1. Cerebral Amyloid Angiopathy in Alzheimer's Disease (AD) and in AD-associated cerebrovascular pathology 1
1.2. Hereditary Cerebral Amyloid Angiopathy: clinical features and pathology 3
1.3. Role of Aβ-fibrinogen interaction in HCAA pathology 6
1.4. A possible role for HCAA-linked Aβ's interaction with Fbg in HCAA pathology 7
1.5. A possible role for Aβ's (WT & HCAA-linked Aβ) interaction with the tPA-Plg fibrinolytic system in AD and HCAA pathology 8
1.6. A possible role for longer length Aβ (>Aβ42) in facets of AD-related vascular pathology 9
1.7. Conclusion 10

CHAPTER 2: MATERIALS AND METHODS **11**
2.1. Preparation of WT Aβ, HCAA mutant-type Aβ peptides, Aβ (1-n) peptides, and fibrinogen 11
2.2. Probe of Aβ-fibrin(ogen) interaction in fibrinogen-binding central region of Aβ using AlphaLISA assay 11
2.3. Examination of Aβ binding to fibrinogen using SPR analysis 11
2.4. Transmission Electron Microscopy 12
2.5. *In vitro* fibrin clot fibrinolysis 12
2.6. Examination of effects of HCAA Aβ *in vitro* clot structure 12
2.7. Patient brain tissue samples 13
2.8. Brain tissue processing 13
2.9. Antibodies and immunofluorescence 14
2.10. Image acquisition and processing 14
2.11. Higher magnification image acquisition and processing of Aβ-Fbg co-localization in HCAA brains 14
2.12. Digital image analysis for cortical fibrin(ogen), Aβ deposits (plaques), and Aβ oligomer quantification 15
2.13. Aβ stimulates tPA-Plg activation and enhances proteolytic enzyme activity 15
2.14. Analysis of Aβ-tPA-Plg activation in human control plasma by Western blot 15
2.15. Statistical Analysis. 16

CHAPTER 3: Aβ VARIANTS DIFFERENTIALLY INTERACT WITH FIBRIN(OGEN) AND FIBRIN CLOTS **17**
3.1. HCAA-linked Aβs have increased binding to fibrinogen 17

3.2. Specificity of Aβ and Fbg interaction in SPR assays 19
3.3. HCAA Aβs used in vitro assays have increased aggregation propensity 20
3.4. Inducing a more aggregated state in Aβ does not increase binding to Fbg 22
3.5. HCAA Aβs lead to further alterations to fibrin architecture relative to WT Aβ 23
3.6. The majority of HCAA Aβ mutants further delay *in vitro* fibrinolysis 26
3.7. Increased vascular Aβ and fibrino(gen) co-deposition in HCAA Dutch and Iowa patients' cerebral cortex blood vessel walls 29
3.8. Probe of other HCAA-linked Aβs' interaction with Fbg 40
3.8.1. HCAA-linked Arctic Aβ has increased binding to Fbg 41
3.8.2. HCAA-linked Italian Aβ further delays fibrinolysis compared to WT Aβ40 42
3.9. Longer length Aβs (>Aβ42) & Fbg 43
3.9.1. Profiling longer length Aβ peptides aggregation propensity via EM 44
3.9.2. Probing the binding affinity for Fbg of longer length Aβs 44
3.10. Longer length Aβs alterations to fibrin architecture 46
3.10.1. Longer length Aβs effect on *in vitro* fibrinolysis 47

CHAPTER 4: Aβ VARIANTS FEATURE DIFFERENTIAL ACTIVATION OF tPA-MEDIATED PLASMINOGEN ACTIVATION 50
4.1. Most HCAA Aβ mutant variants greatly stimulate and enhance Plg activation 50
4.2. HCAA Dutch and Iowa Aβ lead to more Plg activation in healthy control human plasma 56
4.3. Longer length Aβs enhance tPA-Plg activation, Pn activity, and tPA activity 58
4.4. Aβs' role in "enzymatic approximation effect" in tPA-Plg activation 61

CHAPTER 5: DISCUSSION 64
5.1. Overview 64
5.2. HCAA-linked Aβs' strong interaction with fibrin(ogen) and alteration to fibrin(ogen) structure and function 64
5.3. The overlapping role of WT- and HCAA-linked Aβs and fibrino(gen) interaction in cerebral co-deposition AD and HCAA 65
5.4. HCAA-linked Aβ mutant variants greatly enhance tPA-Plg activation and components of the fibrinolytic system 69
5.5. The spectrum of effects of different HCAA Aβs on fibrinolysis and the fibrinolytic system 74
5.6. Longer length Aβs' interaction with fibrin(ogen) and the fibrinolytic system 77
5.7. Future directions 79
5.8. Conclusion 81

REFERENCES 82

LIST OF FIGURES **Page**

Figure 1.1. APP processing leads to Aβ generation. 2
Figure 1.2. Alanine scan of the central regions of Aβ highlight its importance as a key Fbg-binding region. 8
Figure 3.1. Surface plasmon resonance schematic to probe Aβ-Fbg binding. 18
Figure 3.2. HCAA-type mutations increase Aβ's binding affinity for Fbg. 19
Figure 3.3. Specificity of Aβ and Fbg interaction in surface plasmon resonance binding assays. 20
Figure 3.4. Transmission electron microscopy (TEM) of HCAA -Aβ42 and -Aβ40. 21
Figure 3.5. The average hydrodynamic radii of HCAA Aβ peptide particles varied relative to WT Aβ. 22
Figure 3. 6. Inducing a more aggregated state in WT Aβ42 does not affect binding affinity to Fbg. 23
Figure 3.7. HCAA Aβ-induced fibrin clots demonstrate greater structural alterations than WT Aβ-induced clots. 25
Figure 3.8. HCAA Aβ-induced fibrin clots made with nanomolar Aβ concentration still shows signs of increased structural perturbations compared WT Aβ-induced clots. 26
Figure 3.9. HCAA-type Aβs increase resistance to fibrinolysis. 27
Figure 3.10. Lower Dutch42 concentrations delays clot lysis compared to WT Aβ42. 28
Figure 3.11. Lower nanomolar HCAA Aβ concentrations still perturb clot lysis. 29
Figure 3.12. Increased fibrin(ogen) deposits and Aβ-fibrino(gen) co-deposition in HCAA patients' occipital cortex. 32
Figure 3.13. Increased cerebrovascular Aβ oligomer and fibrin(ogen) co-deposition in HCAA patients' cortical blood vessels. 35
Figure 3.14. Abundant Aβ deposit/oligomer-fibrino(gen) co-deposition in HCAA patients' occipital cortical CAA-laden vessels. 37
Figure 3.15. Increased Aβ deposits/oligomer-fibrin(ogen) co-deposition across small and large HCAA patients' cortical blood vessels. 39
Figure 3.16. Distribution of cerebral vessels in HCAA patients' occipital cortex is not significantly different compared to EOAD and ND brains. 40
Figure 3.17. HCAA-type mutant Arctic Aβ has increased binding affinity for Fbg. 41
Figure 3.18. HCAA-type Italian Aβ40 increases resistance to fibrinolysis, while Arctic Aβ40 lowers maximum clot turbidity. 43
Figure 3.19. TEM analysis of different length Aβ (1-n) peptides. 44
Figure 3.20. Assessing the increased binding affinity for Fbg of Aβs (1-n). 46
Figure 3.21. ScEM analysis of Aβ (1-n)-induced fibrin clots. 47
Figure 3.22. Longer length Aβs also prolong in vitro fibrinolysis. 49
Figure 4.1. HCAA Aβ42 and Aβ40 mutant peptides further enhance tPA-Plg activation. 51
Figure 4.2. Components of the fibrinolytic system are enhanced by HCAA Aβ. 53
Figure 4.3. A few HCAA Aβ40 variants exhibit differential effects on fibrinolytic enzymatic activity. 56
Figure 4.4. Most HCAA Aβ40 mutant peptides demonstrate higher tPA-Plg activation in normal human plasma relative to WT Aβ40. 58
Figure 4.5. Differential effects of Aβ (1-n) on fibrinolytic enzymatic activity. 60

Figure 4.6. Longer length Aβ46 featured a higher trend in tPA-Plg activation in normal human plasma. 61
Figure 4.7. Increasing Plg concentration abolishes WT Aβ42-induced stimulation of in vitro tPA-Plg activation. 62
Figure 4.8. Increasing Plg concentration also abolishes the more aggregation prone WT Aβ42-induced stimulation of in vitro tPA-Plg activation. 63
Figure 5.1. Model scheme: HCAA Aβ's effects on fibrin(ogen) structure/function and fibrinolytic enzyme activity are interconnected leading to HCAA pathology. 72
Figure 5.2. Model schematic of mechanisms of various HCAA-linked Aβ leading to HCAA pathology. 76

LIST OF TABLES

Table 3.1. Characteristics of HCAA patients used in our immunofluorescence analysis of cortical fibrin(ogen), Aβ, and Aβ-Fbg co-deposition levels. 30

Table 5.1. Effect of HCAA Aβ-linked mutations on the Aβ-Fbg interaction and fibrinolytic enzymatic system compared to WT Aβ. 70

Table 5.2. Effects of Aβ (1-n) on the Aβ-Fbg interaction and fibrinolytic enzymatic system relative to Aβ42 78

LIST OF ABBREVIATIONS

Aβ	beta(β)-amyloid or amyloid-beta(β) peptide
Aβ(1-n)	different length beta(β)-amyloid peptides
AD	Alzheimer's disease
ApoE	apolipoprotein E
APP	amyloid precursor protein
ASO	anti-sense oligonucleotide
BBB	blood brain barrier
BCA	bicinchoninic acid
BSA	bovine Serum Albumin
CAA	Cerebral Amyloid Angiopathy
CR	congo red
CSF	cerebrospinal fluid
Col IV	collagen IV
DLS	dynamic light scattering
ECM	extracellular matrix
EOAD	early onset Alzheimer's disease
Fbg	fibrinogen
HCAA	Hereditary Cerebral Amyloid Angiopathy
HFIP	hexafluoroisopropanol
HRP	horseradish peroxidase
ICH	intracerebral hemorrhage
IF	immunofluorescence
KD	Equilibrium dissociation constant
LOAD	late onset Alzheimer's disease
LRP1	lipoprotein receptor-related protein 1
MMP-2	matrix metalloproteinase-2
MRI	magnetic resonance imaging

ND	non-demented
NFT	neurofibrillary tangle
NS	not significant
OD	optical density
Plg	plasminogen
Pn	plasmin
PSEN	presenilin
RAGE	receptor for advanced-glycation end products
RU	resonance units
SMC	smooth muscle cell
ScEM	scanning electron microscopy
SD	standard deviation
SDS-PAGE	sodium dodecyl sulfate-polyacrylamide gel electrophoresis
SEM	standard error mean
TEM	transmission electron microscopy
tPA	tissue-type plasminogen activator
tPA-Plg	tPA-mediated plasminogen activation
WB	western blot
WT	wild-type
SPR	surface plasmon resonance
SVD	small vessel disease
Sw	Swedish

CHAPTER 1: INTRODUCTION

1.1. Cerebral Amyloid Angiopathy in Alzheimer's Disease (AD) and in AD-associated cerebrovascular pathology

Alzheimer's Disease (AD) is a complex disease with a heterogeneous presentation. The cardinal clinical symptoms include memory impairment and executive dysfunction which eventually leads to AD dementia. The greatest biological risk factor for AD is age. A United States (U.S.) census data analysis has estimated that by 2050, there will be 13.8 million people over the age of 65 with AD dementia (1). On a global scale, the elderly population (e.g. individuals over the age of 65) is expected to reach 1 billion by 2030 due to advances in modern medicine, which indicates that the incidence of AD is expected to grow significantly without a viable treatment or cure. Care for AD individuals is and will continue to be a significant burden on the economy, the healthcare system, caregivers, and family members. By 2050, U.S. costs associated with dementia, including AD-dementia, is projected to reach $1.1 trillion (2).

Among the main pathologies seen in AD are extracellular beta-amyloid (Aβ) plaque deposits in the brain parenchyma, intracellular neurofibrillary tangles (NFTs) consisting of hyperphosphorylated tau, and neuronal death leading to brain atrophy with widening of the sulci (3). Inclusions of alpha-synuclein, also known as Lewy bodies, are also commonly found. Another common pathogenic feature found in many but not all AD patients is cerebrovasculature abnormalities (4-7). While Aβ plaques and NFTs contribute to cognitive impairment in AD, concurrent vascular pathologies including cerebral amyloid angiopathy (CAA) and small-vessel diseases (SVDs), such as hippocampal sclerosis and ischemic changes, are correlated with cognitive dysfunction (3). Approximately a third of AD cases may exhibit significant SVDs (6). CAA, which involves the deposition of Aβ in cerebral blood vessels, affects up to 80-95% of AD patients (3, 8).

There are several types of CAA according to the amyloid protein involved. Sporadic Aβ-type of CAA is most commonly found in elderly individuals and AD patients (9). While the origin of vascular amyloid has not been clearly elucidated, the mechanism by which Aβ is produced follows the "amyloid cascade hypothesis" (10). The extracellular Aβ found in parenchymal Aβ plaques and in CAA is produced by the processing of transmembrane amyloid precursor protein (APP) by sequential proteolytic activity of β-secretase and the γ-secretase/presenilin (PSEN) complex (11) releasing a 43-51 peptide, which can be further cleaved by γ-secretase leading to the production of Aβ 1-42 and 1-40 (Aβ42 and Aβ40, respectively). The two pathways leading to these Aβ peptides are: (Aβ49→Aβ46→Aβ43→Aβ40 and Aβ48→Aβ45→Aβ42) (Figure 1.1)(12, 13). Familial forms of AD and Aβ-type CAA involve mutations in the genes *APP*, *PSEN1*, and *PSEN2*, which lead to overproduction of Aβ or an altered form of Aβ (13). Aβ can self-aggregate and assume higher order aggregated states including oligomers, protofibrils, and fibrils (14) (Figure 1.1). Aβ40 has a decreased propensity to aggregate in the brain parenchyma relative to Aβ42, which might allow its more facile removal through interstitial fluid drainage along vessels. This might be the basis for the increased Aβ40/Aβ42 ratio observed CAA pathology (15, 16). However, studies in AD

patients (17, 18) and transgenic mice overexpressing human APP (19) show that Aβ42, which adopts more beta(β)-sheet structure relative to Aβ40, is also essential for vascular amyloid deposition. Interestingly, in Aβ-type CAA deposits, many serum proteins have been found including complement system proteins, serum amyloid-P components, apolipoprotein E (ApoE), ApoJ, and many other extracellular matrix (ECM)-proteins (20, 21).

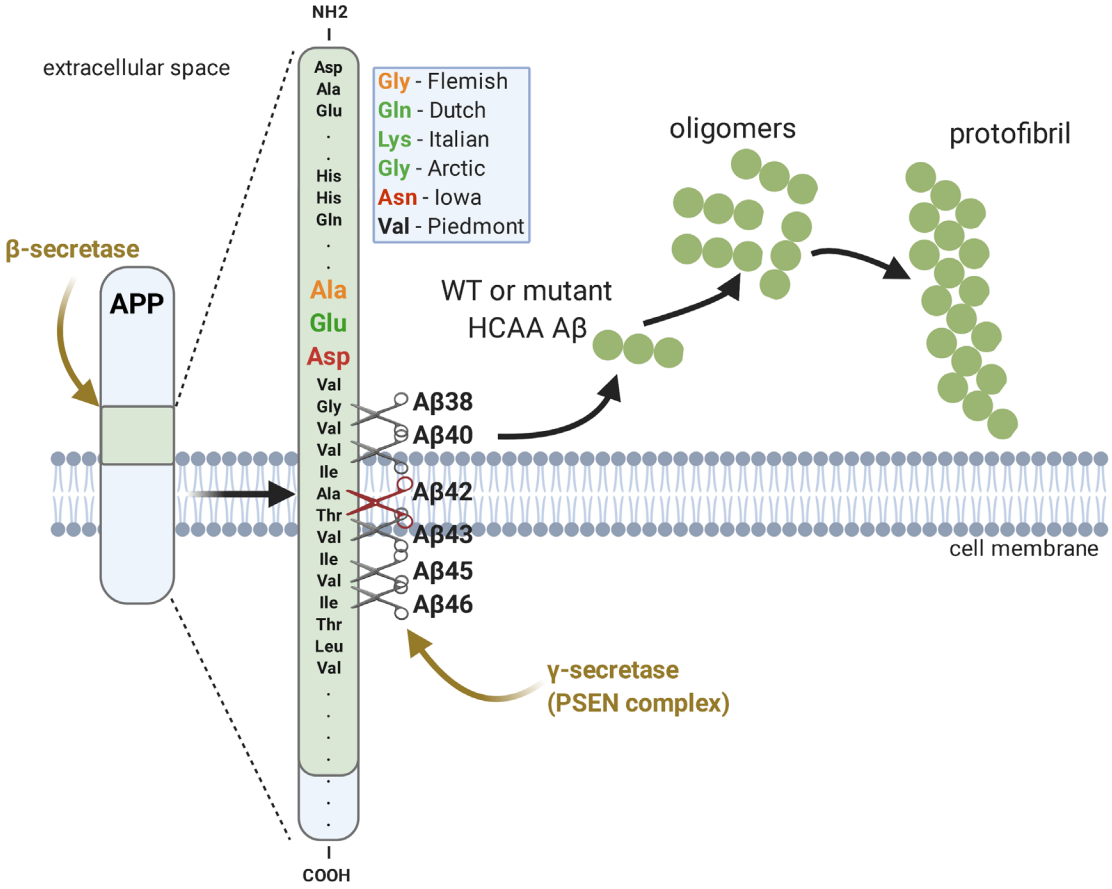

Figure 1.1. APP processing leads to Aβ generation.
Transmembrane amyloid precursor protein (APP) is processed by sequential proteolytic activity of the β- and γ-secretase/presenilin complex releasing Aβ peptides. The APP-γ-secretase complex can lead to variant sequential cleavage of Aβ leading to the generation of Aβ of various lengths (Aβ(1-n)). Aβ-type HCAA-linked Aβ mutations are concentrated around amino acids 21-23, which is also an important fibrinogen-binding region. They include HCAA-Dutch (E22Q), -Italian (E22K), -Arctic (E22G), and -Iowa (D23N). Aβ can self-aggregate and assume higher order aggregated states including oligomers, protofibrils, and fibrils.

The incidence of CAA is approximately 50% in individuals over 70 years and is even higher, 80%, in all AD cases (21).This form of CAA occurs along the walls of capillaries and the tunica media and adventia of arterioles (15), middle-sized cerebral arteries, and leptomeningeal arteries (3, 7, 22). Many studies closely associate CAA with cerebral hemorrhagic lesions, such as lobar intracerebral hemorrhage (ICH) and cortical microhemorrhages, and ischemic lesions (9). More recently it has been implicated as a

major cause of spontaneous ICH (23, 24). Depending on the severity of the CAA pathology and the caliber and location of the vessel afflicted, small microbleeds or large lobar ICHs can ensue. Given the large overlap in pathology between sporadic CAA and severe AD (21, 25) and reports indicating cognitive impairment in CAA-positive individuals presenting with our without AD, it is difficult to study the independent impact of CAA on cognition. Nevertheless, CAA can contribute to dementia and is associated with cognitive impairment in AD patients, since they are often comorbidities (26-28). The frequency and severity of CAA is increased in AD (29) and cognitively normal individuals who are CAA-positive are at high risk for developing dementia (30).

The presence and/or formation of CAA is closely connected to cerebral microvascular dysfunction and degeneration abnormalities observed in AD pathology, including blood-brain barrier (BBB) dysfunction, structural changes to the cerebrovasculature, and neurovascular decoupling (31-33). Vascular Aβ deposition can be toxic to pericytes and endothelial cells *in vitro*, which are important in BBB formation/integrity and cerebral blood flow (31, 34), and can lead to loss of smooth muscle in vessel walls, therefore weakening them (24). CAA can impair cerebral Aβ clearance via various pathways including disrupted Aβ-LRP1 binding at the BBB, Aβ-mediated increased receptor for advanced glycation end products (RAGE) expression at the BBB, and impaired perivascular drainage(23). Severe CAA can lead to significant neurovascular decoupling whereby there is reduced vasodilation in response to physiological stimuli (35). CAA's connection to these AD-associated pathologies suggest that it can contribute to and/or exacerbate cerebrovascular dysfunction in AD brains.

1.2. Hereditary Cerebral Amyloid Angiopathy: clinical features and pathology

While CAA is mostly observed in the sporadic form (sporadic Aβ-type CAA) in late onset AD (LOAD) patients, rare familial forms occur in early-to-mid-adulthood and lead to more severe cerebrovascular disease, including severe hemorrhagic and ischemic strokes, early onset dementia, and ultimately death (25, 36, 37). While there are several variant types of HCAA that have been identified with mutations in other genes (e.g. cystatin C, BRI, transthyretin(25)) with their own unique pathophysiology, most familial forms of CAA involve mutations in the *APP* gene. Although most pathogenic AD-linked APP mutations elevate total Aβ production or promote formation of the more toxic Aβ42 peptide, a subset of fully penetrant, autosomal-dominantly inherited mutations induces a dramatic increase in vascular deposits of Aβ (CAA formation). The most common form of HCAA results from the Dutch mutation (E22Q) giving rise to HCAA-Dutch disease, which is also the most known and studied HCAA variant. The exact prevalence of HCAA disease is not known, but recent studies indicate there are approximately 200 HCAA-Dutch individuals reported in the literature (38, 39). Other identified HCAA-mutation variants underlying the development of HCAA with a hemorrhagic phenotype, also known as hereditary cerebral hemorrhage with amyloidosis (HCHWA), similar to HCAA-Dutch, include the Iowa (D23N), Italian (E22K), and Flemish (A21G). These HCAA-linked mutations are clustered in the amino acid 21-23 region of Aβ (Figure 1.1), with the exception of Piedmont (L34V). The disease variants are given geographic names of the origin/founder family or individuals, in which the variant was first genetically identified (25). These HCAA-linked Aβ variants correspond to mutations at

codons 692-694 of the *APP* gene (21, 25). Patients afflicted by these HCAA mutations have severe cerebrovascular disorders including severe CAA pathology and cerebral hemorrhages in midlife (25) making HCAA an ideal disease to examine the pathogenic mechanisms of CAA (40). Mutations in this region of Aβ (amino acid 21-23) seem to dramatically increase vascular amyloid deposits, but do not lead to the same magnitude increases of parenchymal Aβ plaques (9). The mechanism behind this phenomenon is not well understood, although it suggests that this region plays an important role in vascular Aβ deposition in HCAA disease. Given the autosomal dominant nature of this disease, most HCAA patients are heterozygous carriers of the mutant APP and express both the wild-type (WT) and mutant HCAA Aβ species in CAA deposits in an approximately 50:50 ratio (25).

HCAA-Arctic (E22G) disease variant is similar to HCAA-Dutch, wherein the glutamate residue at the 22nd position in Aβ is mutated into glycine (Figure 1.1). However, HCAA-Arctic's pathophysiology stands out as an interesting outlier compared the other HCAA types. While the literature surround HCAA-Arctic disease is scarce, it appears that its clinical features are similar to other HCAA variants, with memory impairment at presentation at a mean age of onset 57 ± 2.9 years and cognitive decline (25). Arctic-carriers also demonstrate moderate to severe CAA in cerebral vessels, NFTs, and parenchymal Aβ plaques(41, 42). More akin to AD pathology, Arctic-carrier patients display brain atrophy and reduced cerebral blood flow (25, 43). However, unlike most other HCAA disease variants, Arctic-carriers do not show signs of hemorrhagic and/or ischemic strokes (43) and show more gradual cognitive decline (25).

Although symptoms and clinical markers resulting from different HCAA mutations are variable, the key common distinguishing clinical feature of most HCAA disease variants is recurring cerebral strokes of the hemorrhagic (macro- and micro-hemorrhages) and non-hemorrhagic type (25). Nevertheless, there are many similarities in the clinical profiles between HCAA and other forms of CAA, including sporadic Aβ-type CAA, which is found in over 80% all AD cases (21) (Table 1.1). However, the clinical profile for HCAA is more severe and aggressive because it is a fully penetrant early-onset, autosomal dominant disease where the age of onset can be as early as 40 years of age (4). In contrast, the incidence of sporadic CAA increases with age, with an approximate 50% incidence of CAA in elderly individuals 70 years and older (5). In HCAA-Dutch disease, the first stroke is lethal in one-third of patients and cognitive deterioration is more rampant with presentation of dementia in around 75% of the patients over the age of 40, usually proceeding the first stroke (6). Half of HCAA-Dutch patients who have suffered one or more strokes also commonly present with epilepsy (39). Similar to HCAA-Dutch, sporadic CAA can present with recurrent cortical ICH and large, symptomatic to small, asymptomatic microbleeds (9, 25). Sporadic CAA can also present with sudden onset or transient cognitive decline depending on the scale of the ICH. In HCAA, larger vessels, including leptomeningeal and cerebral cortical blood vessels, are mainly affected by severe CAA, while in sporadic Aβ-type CAA, CAA ranges from mild to severe with more capillary involvement (5). These larger vessels afflicted by severe CAA are also usually the sites of hemorrhagic and ischemic strokes. In HCAA, vascular Aβ deposits start in the occipital lobe, but in advanced cases all brain

regions are involved (39, 44). Aβ40 is the major species of Aβ of HCAA vascular Aβ (45), similar to sporadic Aβ-type CAA.

Table 1.1. Comparison of sporadic (Aβ-type) and Aβ-type HCAA.

	SPORADIC CEREBRAL AMYLOID ANGIOPATHY (Aβ-TYPE)	COMMON TRENDS	HEREDITARY CEREBRAL AMYLOID ANGIOPATHY (Aβ-TYPE)
Age of onset:	60-80s – increases with age		30-60s
APP mutation	no APP mutation		Yes: 692-694 and 705 mutation
Aβ-involvement	Vascular WT Aβ40 prevalence	Vascular Aβ40 prevalence	Vascular mutant Aβ40 prevalence
AD-prevalence	80% of AD patients		Not clear, not classified as AD
Stroke	Yes	Yes (vary in caliber and type)	Yes (not Arctic-variant)
• **Type**	Ischemic & hemorrhagic (less common)		Ischemic and hemorrhagic
• **Location**	Lobar		Lobar
• **Caliber**	Micro- and macro (less common)-bleeds		More severe: micro and macro
Seizures	Yes	Yes	Yes – more common
Dementia	+/- (varies on caliber of stroke)	Yes	+ (linked to vascular incident)
Recurrent ICH risk	Yes	Yes	Yes – high
ApoE-related risk	Yes (ApoE: ε4>ε2>ε3)		Not clear, no clear evidence
Site of CAA	More capillary involvement		Larger vessel involvement
Radiology Marks:	Yes	Yes	Yes
	Multiple lobar hemorrhages		Multiple lobar hemorrhages
	White matter lesions		Hemorrhagic/non-hemorrhagic infarcts
	• CAA-related vasculitis		Diffuse white matter changes
	• Perivascular inflammation		White matter hyperintensities

One of the main genetic risk factors for both sporadic AD, specifically LOAD, and sporadic CAA is the apolipoprotein E (apoE) gene (*APOE*), but not for HCAA-Dutch disease and other Aβ-type HCAA variants. *APOE* has three polymorphic alleles (ε2, ε3, and ε4) giving rise to apoE isoforms (apoE2, apoE3, and apoE4). The ε4 allele is the most well-known and strongest risk factor for LOAD. Inheritance of one copy of the e4-allele increases AD risk 4-fold, and 10 to 15-fold when two copies are inherited (46, 47). While produced systemically in the liver, ApoE4 is abundantly produced by astrocytes in the brain and functions as a cholesterol-carrier lipoprotein that delivers lipids to neurons. It is known to bind to Aβ and facilitates deposition of fibrillar Aβ in blood vessels and plaques (48). In CAA, it is associated with increased vascular Aβ deposition and earlier onset of ICH as well as increased recurrence of ICH (25). However, multiple studies have revealed that there is not a strong association between ApoE4 and the severity of HCAA-Dutch disease (25, 27, 49).

The exact mechanism of how ApoE4 increases cerebral Aβ burden remains to be resolved, but could involve impaired Aβ removal by either binding to Aβ, which could have “seeding effect”, thereby inducing Aβ aggregation (50). Increased aggregation would affect Aβ clearance or its binding to LRP1 that is responsible for Aβ efflux/clearance across the BBB (51, 52). LRP1 mediates transcytosis of Aβ-ApoE complexes (53). There are a few discrepancies in the literature highlighting clear associations between ApoE genotype and CAA severity. Studies have shown that the severity of CAA in patients with minimal AD pathology was more strongly correlated with the ε4 genotype compared CAA severity in AD patients (54). There are also indications that the ε2 allele, which is protective in AD (relative to ε4 genotype), is also associated with CAA disease (55), can lead to more CAA-associated vasculopathies, and is more common in individuals with non-capillary CAA (55).

Molecular mechanisms explaining how HCAA-type mutations induce severe CAA formation and stroke remain largely unknown. Furthermore, analogous to AD, HCAA disease is complex and, although the genetic causes HCAA disease variants are known, the disease lacks treatments to slow the progression of CAA and prevent ICH (40). Its more morbid clinical features, ICH and CAA-related inflammation, can be managed by surgical removal of hematomas, avoidance of anticoagulants and antiplatelets, the use of pharmacological agents such as antihypertensives and statins, and immunosuppressive therapy to relieve CAA-related angiitis (56).

1.3. Role of Aβ-fibrinogen interaction in HCAA pathology

Alterations in vascular hemostasis are evident in many AD patients and AD mouse models (57). Indeed, there is evidence suggesting a strong correlation between concurrent vascular disease and cognitive dysfunction seen in AD (3). Various vasculature defects, including clot formation and clearance, have been implicated in the progression of AD pathology (58).

Accumulating evidence implicates fibrin(ogen), the main protein component of blood clots, in AD pathogenesis (59-62). Soluble fibrinogen (Fbg) is converted into fibrin through activation of the coagulation cascade, which normally serves a beneficial hemostatic role. However, persistent fibrin deposited on cerebral vessel walls can lead to vessel occlusions and brain parenchymal ischemia (60, 62). Fibrinogen binds to Aβ42 which leads to the formation of structurally abnormal fibrin clots that are more resistant to plasmin(Pn)-mediated degradation/fibrinolysis than normal clots (63-65). Fibrinogen binding to oligomeric Aβ also promotes fibrin(ogen) oligomerization and their co-aggregation *in vitro* and contributes to the development of CAA in AD mouse models (59, 60, 63, 66). In addition, fibrin(ogen) co-localizes with Aβ along cerebral vessel walls in AD patients and AD mouse models (59, 66). Oligomeric Aβ42 binds specifically to Fbg with a K_D of 26.3 ± 6.7 nM (63) with known sites including the C-terminus of the β-chain of fibrinogen near the b-hole (63), and to a region of the αC-region of fibrinogen (Aα239-421) (67), which is known to bind plasminogen (Plg) and includes Pn cleavage sites (68). These binding interactions delay fibrinolysis by physically interfering with the binding of Plg and Pn to fibrin (64).

Although the binding strength for Fbg is highest for oligomeric Aβ compared to monomeric or fibrillar Aβ (63, 69), it remains unclear if the β-sheet structure found in the oligomeric/aggregated state of Aβ alone contributes to this delay in fibrinolysis. Clots formed in the presence of amyloidogenic human amylin peptides or truncated Aβ (Aβ1-28) do not exhibit delayed fibrinolysis (64), which suggests the interaction between Aβ and fibrin(ogen) is specific, strong, and necessary for perturbed fibrinolysis.

Fibrin(ogen) is normally contained within vascular vessels and does not extravasate into the brain, yet it has been found in the extravascular space (62, 70-72) and cerebrospinal fluid (CSF) of AD (73-75) and HCAA patients (45). One possible explanation for this finding is that the BBB is often disrupted in AD (62, 76-78) and HCAA patients (39, 79), which could allow fibrin(ogen) to penetrate into the brain parenchyma. While previous analysis of HCAA and AD patient plasma, cerebrospinal, and cerebral interstitial fluid show Aβ concentration ranges in the picomolar to

nanomolar range (80, 81), several studies suggest that insoluble Aβ deposits in the brain are in equilibrium with the interstitial Aβ and serve as a reservoir for soluble oligomers (82, 83). Furthermore, soluble, non-fibrillar Aβ species are highly concentrated, found up to in the micromolar range, around CAA-positive (CAA+) vessels (18, 84). Other factors contributing to high local vascular Aβ concentrations include impaired perivascular clearance of Aβ from CAA vessels by LRP1 receptors (23, 85) and a leaky BBB in AD and HCAA patients, which would allow fibrin(ogen) to encounter high levels of cerebrovascular Aβ. Therefore, local concentrations of Aβ around parenchymal plaques and sites of vascular Aβ deposition in cerebral blood vessels may exceed plasma concentrations, especially provided these depositions increase over the lifespan of an individual afflicted by CAA pathology. The presence of elevated Aβ in the brain could promote its binding to fibrin(ogen) and would be further incorporated into fibrin clots.

The alterations in fibrin clot structure, delayed fibrinolysis, and increased co-localization in CAA+ vessels in AD human cerebral vessels indicate that fibrin in the presence of Aβ can create a vascular environment where altered hemostasis occurs concomitantly with CAA. In addition, genetic and pharmacological depletion of Fbg in an AD mouse model reduced neuroinflammation, amyloid pathology, and vascular pathology, which lessened CAA burden and BBB dysfunction (59, 62). These findings suggest that fibrin plays a significant role in AD cerebrovascular pathology including CAA. The persistence and accumulation of Aβ-bound fibrin(ogen) cerebral vessel walls could be detrimental to neurons downstream. The exact mechanism illustrating how Aβ and fibrin(ogen) interact to contribute to persistent fibrin deposition, CAA, and cognitive dysfunction has not yet been elucidated.

1.4. A possible role for HCAA-linked Aβ's interaction with Fbg in HCAA pathology

Patients afflicted by HCAA-linked Aβ mutations have severe cerebrovascular disorders, including severe CAA pathology, in midlife (25) making HCAA an ideal disease to examine the pathogenic mechanisms of CAA and to elucidate the role of the Aβ-fibrinogen (Aβ-Fbg) interaction in AD vascular pathology. Previous analysis has revealed that the central region of Aβ42, including amino acids 17-23, is a critical Fbg-binding region (67). This Fbg-binding region in Aβ overlaps with Aβ sites that are mutated in various HCAA disease variants (amino acids 21-23), including amino acid 22 in HCAA-Dutch, -Arctic, and -Italian, and amino acid 23 in HCAA-Iowa (21, 25). Furthermore, past Fbg-binding experiments using alanine-scanning peptide analog of Aβ (L17A, E22A, D23A, and V24A) (Figure 1.2) demonstrate that E22A and D23A mutants have up to 40-times stronger binding affinity for Fbg compared to WT Aβ42 and the other mutant analogs. These results suggest that mutations within Aβ's Fbg-binding region, specifically at sites commonly mutated in HCAA (amino acids 22-23), increase its binding affinity for Fbg. Fibrin(ogen) interacts with the tertiary structure of Aβ's Fbg-binding region, which is stabilized by Aβ C-terminal residues (67), which may explain why higher order structured or oligomeric Aβ have a stronger binding affinity to Fbg compared to monomeric Aβ (69). Interestingly, HCAA Aβ (including Dutch, Iowa, Arctic, and Italian) are highly prone to self-aggregation and exist in more multimeric forms including oligomeric and protofibrillar structural states with increased β-sheet structure

(86-90). Therefore, HCAA Aβs, which have a higher propensity to oligomerize, may interact with Fbg more strongly relative to WT Aβ. A stronger interaction may further impair fibrinolysis, increase Fbg oligomerization, and lead to further co-aggregation in the cerebrovasculature, and thus have a role in the development of exacerbated CAA pathology observed in HCAA patients.

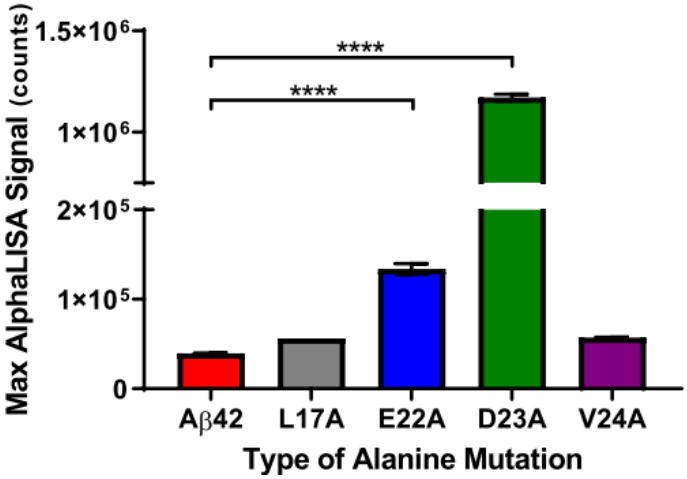

Figure 1.2. Alanine scan of the central regions of Aβ highlight its importance as a key Fbg-binding region.
AlphaLISA binding assay was performed using human purified Fbg and various concentrations of biotinylated alanine-scanning peptide analogs of Aβ42 (L17A, E22A, D23A, and V24A). Bar graph indicates the maximum binding between Fbg and the various Aβ fragments and wildtype (WT) Aβ42. Alanine mutations in amino acid positions 22 and 23 increased Aβ's binding to Fbg compared to WT Aβ42 (red bar) and other alanine-scanning analogs (****p<0.0001; n=3-6/group). Statistical analyses were performed using one-way ANOVA followed by Tukey's post-hoc test.

1.5. A possible role for Aβ's (WT & HCAA-linked Aβ) interaction with the tPA-Plg fibrinolytic system in AD and HCAA pathology

Fibrinogen, the inactive precursor of fibrin, is a 340 kDa glycoprotein that circulates in human blood plasma at a concentration of 4.5-11 μM or 1.5-4 g/L (91, 92). Due to either vessel wall injury, activated blood cells, or a foreign surface, the serine protease, thrombin, is activated and converts Fbg into an insoluble network of fibrin fibrils (clot). Clots are then degraded and cleared by the proteolytic activity of the fibrinolytic system, which mainly encompasses of plasmin(ogen) and tissue-type plasminogen activator (tPA). Through the action of tPA and other activators, Plg is converted into Pn, a serine protease, which is the main enzyme involved in fibrinolysis. Pn also cleaves other substrates, such as extracellular matrix proteins, growth factors, and has been shown to degrade Aβ (93, 94). Fibrinolysis is regulated by a complex system of biochemical reactions that have negative and positive feedback mechanisms. Interestingly, fibrin(ogen) can enhance Plg activation by exposing cryptic tPA and Plg binding sites, which initiate fibrinolysis, and additional plasmin(ogen)-binding sites composed of lysine residues that are exposed through the fibrinolytic process (68, 91).

The mechanism by which fibrin binds, stimulates tPA, and potentiates Pn generation involves fibrin acting as a template and substrate simultaneously, which enhances

catalysis by approximation (95). The network of fibrin fibers acts as a template onto which tPA and Plg can both bind and co-localize together, which enhances tPA-Plg activation leading to more Pn generation. Studies suggest that the formation of cross-β sheet structure by fibrin, fibrin analogues, and amyloid proteins, such as Aβ, is important in tPA binding, tPA activation, and tPA-mediated plasminogen (tPA-Plg) activation (94, 96). The increase in Pn levels could be vital to the removal of these amyloid aggregates such as fibrin in fibrinolysis under normal hemostasis. Furthermore, WT Aβ42 increases tPA-Plg activation (64) and although the exact mechanism of this process remains to be elucidated, it appears to be mediated by further enhancing tPA activity. *In vitro* studies have revealed that formation of β-sheet secondary structure in full length WT Aβ is important in enhancement of tPA-Plg activation (93, 94, 96-98).

Previous studies have shown peptide fragments (residues 1-28) of WT and Dutch Aβ can lead to further stimulation of Plg activation. However, very short Aβ fragments (residues 5-16, 16-28) containing simple β-sheet structures were not enough for tPA stimulation (97) suggesting that additional structural motifs and the electrostatic properties of Aβ may be additional components of fibrinolytic enzyme activity enhancement. Increases in Pn generation can lead to increased Pn-mediated collateral damage to cerebral vessels, which could underline the cerebrovascular pathology observed in AD and HCAA individuals. Aβ can exert functional fibrin(ogen) mimicry to replace fibrin(ogen), bind, and stimulate tPA (94, 96), which in the context of CAA, can lead to local high concentration of tPA and consequently Pn, which could then lead to detrimental proteolysis of extracellular matrix tissue and rupturing of vessel walls (97). Due to the extensive vascular Aβ accumulation in cerebral vessels in HCAA patients and increased fibrillization properties of HCAA Aβ, it is possible that in HCAA disease, CAA sites may lead to dramatically higher fibrinolytic (or proteolytic) activity of tPA and plasmin(ogen).

Given that Aβ can also lead to enhancement of the proteolytic system involved in fibrinolysis seems contradictory to its impairment to fibrin(ogen) structure and function and adds layers of complexity to the relationship of Aβ and Fbg in CAA deposition. The precise mechanism behind how Aβ-Fbg interaction leads to impaired fibrinolysis, alterations to clot structure, and co-deposition in cerebral vessels is not clear, but it appears to involve Aβ-mediated impairment of plasmin(ogen) access to and activity on the αC region of fibrin(ogen) (64, 67). Key regulators of fibrinolysis in the vasculature such as tPA, Plg, α2-antiplasmin bind to this αC region (68), but they do not bind to soluble Fbg. At sites of CAA, both fibrin and Aβ are often co-deposited (59), and therefore, are both having significant roles in tPA-Plg activation. It is possible that both processes are in occurring in tandem.

1.6. A possible role for longer length Aβ (>Aβ42) in facets of AD-related vascular pathology

Although Aβ42 is thought to be the primary pathogenic and neurotoxic species in AD senile plaques and Aβ40 in vascular amyloid deposits (99-101), parenchymal and vascular amyloid deposits in AD patients' brains often consist of many serum proteins (20, 102-104) and/or a heterogenous mixture of Aβ species (103). Several studies

suggest that longer Aβ species such as Aβ43, which is an often overlooked Aβ species, may play a key role in AD pathogenicity. Abundant Aβ43 levels have been found in parenchymal plaques in AD mouse models and in human AD brains (105) and in vascular amyloid in human CAA deposits (106). Biochemical/biophysical studies show that Aβ43 has an increased aggregation propensity and fibrillization capacity relative to shorter Aβs (106, 107). Aβ43 also features increased neural cell toxicity. Recent studies show that familial AD-linked PSEN or APP mutations enhance the production of long amyloidogenic Aβ species (≥ Aβ43), including Aβ45 and Aβ46 (108), by destabilizing the APP-γ-secretase/presenilin complex leading to premature Aβ release (Figure 1.1). The detection of longer length Aβs in immunohistochemical studies remains difficult. In order to detect longer Aβs (≥ Aβ43) usually requires mass spectrometry analysis approaches. Nevertheless, it is possible that there are abundant longer Aβs present in parenchymal and vascular amyloid deposits. Their increased fibrillization capacity suggest that they may interact with fibrin(ogen) more strongly and could also further stimulate the fibrinolytic enzyme system (tPA-Plg activation).

1.7. Conclusion

CAA is a major pathology in HCAA disease and contributes to vascular dysfunction in AD patients. While many neuropathological and radiological studies have detailed CAA pathology, the molecular mechanisms underlying CAA formation and CAA-induced cerebrovascular pathology is unclear. By focusing on Aβ-type HCAA disease forms, in which mutations within the Aβ peptide leads to severe cerebrovascular pathology, this research seeks to advance our understanding of the molecular mechanisms explaining how these mutations induce HCAA associated pathology. Since the interaction between WT Aβ and fibrin(ogen) increases CAA, plays an important role in cerebrovascular damage in AD patients and AD mouse models, and because of the known WT Aβ enhancements to proteolytic system activation, we investigated the role of the interaction between HCAA Aβ, fibrin(ogen), and the fibrinolytic system (tPA-Plg activation and tPA/Pn activity) in HCAA pathology. A closer inspection of these interactions could advance our understanding of the pathogenesis and pathophysiology of the cerebrovascular pathology in HCAA patients and could highlight a new role for fibrin(ogen) in HCAA disease. This work could also help us further understand the molecular mechanisms underlying CAA formation and CAA-induced cerebrovascular pathology in AD. Furthermore, insights into the mechanism underlying CAA pathology could provide new therapeutic targets for patients with HCAA or AD patients afflicted by CAA pathology.

As an extension of the main body of work in this thesis, I also investigated the possible effects of longer length Aβs in Aβ-Fbg interaction and in fibrinolytic system activation. While the aggregation and neurotoxicity properties of longer Aβs have been the focus of recent studies, the effects of their interaction with fibrin(ogen) remains to be explored.

CHAPTER 2: MATERIALS AND METHODS

2.1. Preparation of WT Aβ, HCAA mutant-type Aβ peptides, Aβ (1-n) peptides, and fibrinogen

WT and HCAA mutant, Dutch-, Iowa-, Arctic-, Italian-, and double mutant Dutch-Iowa-type, Aβ42 and Aβ40 peptides, and Aβ (1-n) (Aβ38, Aβ43, Aβ46) where obtained from Anaspec or Bachem. Aβ oligomers were prepared following established protocols (109), with the exception that for surface plasmon resonance (SPR) assays, the peptides were re-constituted in 5% DMSO in phosphate-buffered saline (PBS) (pH 7.4) instead of 5% DMSO in 50 mM Tris-HCl (pH 7.4). Purified human fibrinogen (EMD Millipore) was prepared in PBS (pH 7.4) for SPR experiments and in 50 mM Tris-HCl (pH 7.4) for clot turbidity assays and for clot formations viewed under scanning electron microscopy (ScEM). For SPR experiments, fibrinogen was prepared in the following manner: (1) biotinylated using the Sulfo-NHS-LC-Biotin kit (Thermo Scientific) with 10-fold molar excess of biotin reagent resulting in 1-3 biotin groups per molecule of fibrinogen, (2) desalted and removed of excess biotin using Zeba Spin Desalting Columns (Thermo Scientific). Aβ peptides, fibrinogen, and biotinylated-fibrinogen were diluted to desired concentrations with same reconstitution buffer. Concentrations for these peptides were established by BCA (Thermo Scientific).

2.2. Probe of Aβ-fibrin(ogen) interaction in fibrinogen-binding central region of Aβ using AlphaLISA assay

Four alanine-scanning peptide analogs of Aβ (L17A, E22A, D23A, and V24A) were synthesized by replacing L17, E22, D23, and V24 in Aβ42 with alanine and subsequently biotinylated at the N-terminus (Chinese Peptide Company). Various concentrations (0.01-20 mM) of these alanine-scanning Aβ42 peptide fragments were incubated with 1 nM fibrinogen for 30 minutes at room temperature in a final volume of 10 mL of assay buffer (25 mM Tris-HCl, pH 7.4, 150mM NaCl, 0.05%Tween-20, 0.1%BSA) in white 384-well plates (Greiner). The mixture was incubated with the anti-fibrinogen antibody, 20 mg/mL streptavidin-conjugated donor, and protein A-conjugated acceptor beads (PerkinElmer) for 90 minutes at RT. Samples were read by a PerkinElmer EnVision plate reader.

2.3. Examination of Aβ binding to fibrinogen using SPR analysis

Surface plasmon resonance (SPR) experiments were performed to determine the binding affinity (K_D) of WT- and HCAA mutant Aβ peptides to fibrinogen. The SPR Bio-Rad ProteOn XPR36 instrument was able to generate association (ka) and dissociation (kd) rate constants for the biomolecular binding interactions between individual analytes (the various Aβ peptides) and the ligand, biotinylated-purified human fibrinogen (final 0.5 mg/ml), immobilized on a ProteOn NLC sensor chip containing NeutrAvidin layer for binding biotin-labeled molecules. The various Aβ peptides were each diluted to various concentrations (Fig. 1) using PBS with 0.005% Tween-20 (PBST) as running buffer (final 0.5% DMSO-PBST). They were injected for 2 minutes at a rate of 30 μm/min for the association phase. After the dissociation phase, the SPR chip was rinsed with 1M NaCl and 50 mM NaOH. Corresponding 0.5% DMSO-PBST dilutions were used as a buffer blank. Ka's and kd's for each analyte interaction with fibrinogen were used to calculate the equilibrium dissociation constant (Kd). Additional SPR experiments were

performed to determine the specificity of the interaction between Aβ and fibrinogen in SPR binding assays (Figure 3.3). The SPR Bio-Rad ProteOn XPR36 instrument was able to generate association (ka) and dissociation (kd) rate constants for the biomolecular binding interactions between the individual analytes, WT Aβ42, and amylin, and the immobilized ligands, biotinylated-purified bovine serum albumin (BSA) and -purified human fibrinogen (final concentration 0.5 mg/ml). Purified human amylin was prepared and diluted in the same manner as all the Aβ peptides in this thesis. The SPR instrument is available at Rockefeller's High Throughput Screening Resource Center

2.4. Transmission Electron Microscopy

To assess the aggregation state of the Aβ peptides (Fig. S2) used in the *in vitro* experiments (Fig. 1,2,3), WT and HCAA mutant Aβ42 and Aβ40 peptides were diluted to 0.1 mg/ml in 50 mM Tris-HCl (pH 7.4), applied to glow-discharged CF200-Cu carbon film grids (Electron Microscopy Sciences), was washed 3 times with deionized distilled water, and negatively stained with 2% uranyl acetate. Images were acquired using transmission electron microscopes ThermoFisher (FEI) TECNAI G2 with AMT BioSprint29 camera available at the EMRC at The Rockefeller University.

2.5. *In vitro* fibrin clot fibrinolysis

Clot Turbidity assays to assess the functional impact of the various Aβ peptides on clot formation and dissolution (clot lysis) were performed at room temperature in high binding 96-well plates (Fisher Scientific) using a Spectramax Plus384 reader (Molecular Devices). Clot formation and lysis involved first incubating fibrinogen (1.5μM) without or with the individual Aβ oligomers (at various concentrations including 3, 1.5, 0.75, 0.375μM) and purified human plasminogen (final 250 nM; purified from human plasma in the Strickland Lab) for 20 minutes. To induce fibrin formation and subsequent lysis, thrombin (0.75 U/mL), $CaCl_2$ (5 mM), and purified human tissue-type plasminogen activator (tPA; final 1 nM) in 20 mM HEPES buffer (pH 7.4) with 137 mM NaCl in a volume of 200 μl was mixed in. As fibrin forms due to thrombin activity, tPA activity is enhanced leading to the activation of plasminogen into Pn, which then subsequently starts degrading the fibrin clot. Clot formation and dissolution was monitored by measuring the changes in turbidity (optical density, OD) at 350 nm (A_{350}) over time, reading at 30 second intervals. Fibrin clot lysis rates were compared using half-lysis times, which were calculated from the time when max OD was achieved to the time when the clot reached half its maximum turbidity after OD started decreasing.

2.6. Examination of effects of HCAA Aβ *in vitro* clot structure

To view fibrin clots using Scanning Electron Microscopy (ScEM), clots were formed using fibrinogen (1.5 μM or 1 μM) on round glass coverslips at room temperature. Fibrinogen was incubated in the absence or presence of the various Aβ peptides (WT and HCAA mutant-type Aβ; each at final 3 μM or 0.375 μM) oligomers for 20 minutes at room temperature. Fibrin clots were induced with the addition of thrombin (0.75 U/mL), $CaCl_2$ (5 mM), 137 mM NaCl in 20 mM HEPES (pH 7.4). 1 hour after adding thrombin, clots were gently washed twice with cold sodium cacodylate buffer (0.1 M) for 2 minutes each time and fixed with 2% glutaraldehyde on ice for 30 minutes. After ascending

serial dehydration with ice cold ethanol (20-100%), the fibrin clots on the glass coverslips were sputter-coated with gold palladium. Images were obtained using Leo 1550SEMat the Electron Microscopy Resource Center (EMRC) at The Rockefeller University and the Gemini300SEM at New York University Langone Health (NYULH), operating at 4.0 kV and using SmartSEM software. ImageJ (NIH) software was used for structural analysis of fiber diameter and number of clot aggregates and clumps present with the various Aβ peptides tested used. Three images per clot at a pixel size of 14.3 nm (fibrin alone and Aβ-induced clot) were used for quantification. The diameter of 6 fibers at 5 non-overlapping regions for each clot were measured. Clumps were qualitatively defined and chosen by selecting fiber conjunctions that contained 6 or more intersecting fibers. The clumps were usually concentrically amorphous in shape. Figures were assembled using Image J software.

2.7. Patient brain tissue samples

Postmortem tissue samples were obtained from various sources and were requested to derive from patients that are age-matched, specifically from the occipital cortical region, and for sections to be processed as described in **Brain tissue processing** section in Methods (see Table 3.1 for table of patient characteristics and more information). HCAA patient brain tissue was derived from non-hemorrhagic regions and in all cases was derived from the occipital lobe contralateral to the lethal stroke leading to or contributing to patient's death. The EOAD group consisted of patients affected by early-onset AD phenotype and confirmed by postmortem analysis. EOAD patient in our analysis do not contain any mutation within Aβ or near Aβ cleavage site as we confirmed by sequencing of exon 16 and 17 of APP gene. Brain tissue from a HCAA Iowa-type patient was limited due to very scarce availability. Out of 4 reported Iowa cases reported on PubMed, only one was available. One Iowa patient brain tissue was obtained through collaboration with Dr. Michael A. Farrell (Beumont Hospital, Dublin, Ireland). HCAA Dutch-type patients (n=5) tissue sections were obtained from Leiden University Medical Center (Leiden, Netherlands) from 5 different individuals. Collectively, the HCAA group consisted of 6 individual patients (n=6, 3 male, 3 female, age 53 ± 1 years, PMI/Autolysis Time of 9 ± 3 hours, mean ± SEM (standard error mean)). Early-onset Alzheimer's disease (EOAD) and control non-AD (non-dementia, ND) human tissue was obtained from the NIH NeuroBioBank's Brain and Tissue repository at the University of Maryland, Baltimore and from the repository at the VA Greater Los Angeles Healthcare System. Collectively, the EOAD group consisted of 5 individuals (n=5, 2 male, 3 female, age 58 ± 1 years, PMI/Autolysis Time of 12 ± 2 hours, mean ± SEM). Collectively, the ND group consisted of 7 individuals (n=7, 4 male, 3 female, age 58 ± 1 years, PMI/Autolysis Time of 16 ± 2 hours, mean ± SEM).

2.8. Brain tissue processing

Human HCAA-Dutch and -Iowa, EOAD, and control (ND) brain sections were obtained processed by the following manner: Fixed in 20% formalin, paraffin-embedded, sectioned at 5 μm thickness, except for HCAA-Iowa tissue, which was sectioned at 4 μm thickness. For immunofluorescence analysis, these brain sections were de-paraffinized using CitriSolv (Decon Labs) and rehydrated serially with descending

ethanol concentrations (100%-70%) and then treated with proteinase K (Dako) before performing the staining protocol listed above.

2.9. Antibodies and immunofluorescence

The following primary antibodies were used for HCAA, EOAD, and ND patient cortical brain immunofluorescence probe for fibrin(ogen), Aβ plaques/deposits, and Aβ oligomer staining: Goat polyclonal anti-collagen IV (EMD Millipore, 1:200) antibody, rabbit polyclonal anti-fibrin(ogen) (Dako, 1:800) antibody, mouse monoclonal anti-Aβ-oligomer antibody "NAB61" (Dr. Virginia Lee's Lab, University of Pennsylvania, 1:200)(110). Brain sections were initially blocked for 1 hour with 2% donkey:horse serum (1:1) and then incubated in each of the primary antibodies overnight at 4˚C. The following day, sections were incubated with the following fluorescent secondary antibodies and dyes: fluorescent secondary antibodies corresponded to the primary antibody using either Alexa Fluor 350 or 555 for donkey anti-goat (for anti-collagen IV antibody), Alexa Fluor 488 anti-mouse (for NAB61), and Alexa Fluor 488 or 647 donkey anti-rabbit (for anti-fibrin(ogen)). Next, Aβ deposits or plaques were visualized with 0.2% Congo Red in 70% 2-propanol and subsequently counterstained with 0.3% Sudan Black B in 70% ethanol to reduce lipofuscin green auto-fluorescence. Sections were then covered with Vectashield (Vector Labs) and mounted on glass slides and imaged.

2.10. Image acquisition and processing

Following immunostaining, our Aβ and fibrin(ogen) co-localization analysis of the patient brain sections were imaged with laser scanning microcopy using Inverted Zeiss Axio Observer Z1 confocal microscope (ZEISS) available at the Bio-Imaging Resource Center at The Rockefeller University. Two large sections per patient sample were used for quantifying the staining. We captured two non-overlapping 8 x 8 tiled images at 20X for every sample for analysis. We probed for fibrin(ogen) and Aβ using Congo Red staining and the NAB61 probe in two separate sets of tissue sections. 405 nm, 488, and 633 confocal laser lines were used to view fluorescent secondary antibodies and Congo Red dye signal. Stitched (20% overlap) 8 x 8 tiled images for every patient section were captured with Zen Black software (ZEISS) using a 20.0x water objective to view as much tissue as possible for analysis.

2.11. Higher magnification image acquisition and processing of Aβ-Fbg co-localization in HCAA brains

Following our immunostaining protocol (Materials and Methods) using Congo Red for aggregated congophillic Aβ and NAB61 for Aβ oligomer probes, patient brain sections were imaged with laser scanning microcopy using Inverted Zeiss Axio Observer Z1 confocal microscope (ZEISS) available at the Bio-Imaging Resource Center (BIRC) at The Rockefeller University. 63x oil-immersion was used for higher magnification images of representative CAA-laden vessel in HCAA-Dutch and EOAD patient samples. Z-stacks showing multiple depths of tissue were obtained with 16 z-planes captured at 0.5 µm intervals. Z-stacks were made into composite z-stack images where all three probes/channels (ex. collagen IV, Fbg, and NAB61) were merged, which were then converted into 3D movie files using ImageJ's plug-in 3D Viewer software and saved as Audio Video Interleave (AVI) files.

2.12. Digital image analysis for cortical fibrin(ogen), Aβ deposits (plaques), and Aβ oligomer quantification

For percent analysis of fibrin(ogen), collagen IV, NAB61, and Aβ signal, patient brain sections that were immunostained and imaged with confocal microscopy were analyzed using NIS-Elements Advanced Research software suite version 5.1 (Nikon). Each multichannel RGB image was analyzed by processing each of its single RGB channel (red, blue, green). Each channel was thresholded to collect the total number of pixels with numeric values inside the thresholded interval, which was then converted to a binary layer. The binary layer provided the total area of positive staining as a percentage of total image area. Data indicating % area of immunofluorescent targets (ex. % fibrin(ogen)) were organized into graphs using Prism 8 (GraphPad Software, San Diego, California USA), one-way ANOVA followed by Tukey's multiple comparisons post-hoc test was performed using GraphPad Prism version 8.0.0 for Windows. For co-localization analysis of images captured with confocal microscopy, 8 x 8 tiles images were thresholded using ImageJ (NIH). Figures were assembled using Image J software. *Due to the differences in section thickness between the HCAA-Iowa and other brain tissue sections, the HCAA-Iowa (n=1) image analysis data was not included in our immunofluorescence analysis.

For analyses indicating % area of target (ex. % fibrin(ogen)) based on vessels size, the collagen IV channel in the Congo Red probe and NAB61 probe was size thresholded in the following manner: For selection of "larger vessels", the size threshold was set to include only objects 20 to 250 μM in size, whereas "smaller vessels" were size thresholded to include objects between 5 to 20 μM in size. We excluded large blood vessels greater than 250 μm in diameter because large blood vessels were unevenly distributed between samples.

2.13. Aβ stimulates tPA-Plg activation and enhances proteolytic enzyme activity

Chromogenic enzyme assays were performed at room temperature in high binding 96-well plates (Fisher Scientific) using a Spectramax Plus384 reader (Molecular Devices) with a reaction volume of 200μl. For Pn activity, chromogenic substrate Pefa-5264 (Pentapharm; 200μM) was added to plasmin (110nM) with the various Aβ40/42 peptides (1μM). For tPA, activity, chromogenic substrate S-2288 (Diapharma; 210μM) was added to tPA (12.5nM) with the various Aβ40/42 peptides (1μM) at 37^0C. For tPA-mediated plasminogen (tPA-Plg) activation, purified human plasminogen (250nM or concentrations ranging from 125nM-4000nM for dose-response Plg experiment in Figure 4.7), and tPA (125pM) were mixed the various Aβ40/42 peptides (1μM) and Pefa-5264 was added to monitor plasmin generation or Plg activation. Enzyme activity readings were monitored and recorded at wavelength 405nm (A_{405}) every 1 minute.

2.14. Analysis of Aβ-tPA-Plg activation in human control plasma by Western blot

Experiments with human plasma were approved by the Rockefeller University Institutional Review Board. Blood from healthy control individuals was drawn into Vacutainer tubes and was anti-coagulated with sodium citrate and frozen at -80^0C. Plasmas were thawed gradually on ice and diluted 20-fold using 20mM HEPES buffer

(pH 7.4). Plasma concentration was measured by BCA to ensure equal amounts of total protein if more than one individual's plasma was used in experiment. Reaction consisted of mixtures of diluted plasma with the various the various Aβ40/42 peptides (4μM) or vehicle buffer (5% DMSO-Tris pH 7.4) and tPA (125pM). Reactions were then incubated at 37^0C with gentle rotation at 50 rotations per minute. Reaction samples were collected at various timepoints (0-hr, 12-hr, and 36-hr) and were reduced with 1M DTT and 4x sample buffer. Reduced samples were subjected to SDS-PAGE on 4-20% Tris-Glycine gradient gels (Bio-Rad), transferred to polyvinylidene fluoride (PVDF) membranes (EMD millipore), and incubated in blocking buffer (5% milk in TBS containing 0.1% Tween20 (TBS-T)) for 1 hour at room temperature. Membranes were then incubated with primary plasmin(ogen)-specific antibody (rabbit anti-Plg (Abcam-ab154560)) or transferring antibody (Abcam) overnight. After washing with TBS-T, membranes were incubated with an appropriate HRP-conjugated secondary antibody for 1 hr. Blots were developed with enhanced chemiluminescent substrate (Perkin-Elmer) and imaged with our Chemidoc chemiluminescent system (Bio-rad). Protein levels were quantified using densitometry with ImageJ (NIH). Blots were stripped with stripping buffer (Thermo Scientific) for subsequent probes with a different primary antibody. Western blot results for brain protein extracts were normalized to transferrin and control buffer groups.

2.15. Statistical Analysis.

Bar graphs and line plots were created using GraphPad Prism 8 (GraphPad Software, San Diego, California USA). Statistical analyses were conducted using Prism 8. All numerical values presented in graphs are mean ± SEM (standard error mean). Statistical analyses were assessed as described in text using either one-way ANOVA followed by Tukey's multiple comparisons test, two-tailed unpaired t-test, or linear regression analysis. P values below 0.05 were considered significant. ****$p<0.0001$; ***$p<0.001$; **$p<0.01$; *$p<0.05$, n.s.= not significant. Bar graphs of AlphaLISA, SPR, *in vitro* turbidity, and fibrinolytic enzyme experiments represent mean ± SEM of ≥3 separate experiment, unless not stated in figure legend.

CHAPTER 3: Aβ VARIANTS DIFFERENTIALLY INTERACT WITH FIBRIN(OGEN) AND FIBRIN CLOTS

3.1. HCAA-linked Aβs have increased binding to fibrinogen

As mentioned in Chapter 1.3, previous biochemical analysis revealed that specific mutations (Figure 1.2) in the central region of Aβ42 (amino acids 17-23), which are critical to its interaction with fibrinogen (Fbg) (67), greatly increased Aβ's binding affinity for Fbg. Specifically, mutations at the 22nd and 23rd amino acid sites (E22A and D23A mutants, respectively) resulted in up to a 40-fold increase in binding to Fbg compared to WT Aβ42, while L17A and V24A mutants showed similar binding affinities for Fbg comparable to WT Aβ42 (Figure 1.2). These results showed that mutations in Aβ sites commonly found in HCAA disease (amino acids 22-23) increase Aβ's binding affinity for Fbg and warranted further examination to see if HCAA-type Aβs, specifically Dutch (E22Q) and Iowa (D23N) Aβ, interact with fibrin(ogen) differently compared to WT Aβ.

To determine the binding specificity of HCAA-type Aβ mutants for Fbg, we compared the interaction between the various Aβ peptides and Fbg using surface plasmon resonance (SPR) (schematic depicted in Figure 3.1). We immobilized biotinylated Fbg on an NLC sensor chip and infused various concentrations of oligomeric WT, Iowa (D23N), or Dutch (E22Q) Aβ42 or Aβ40, in a dose-dependent manner, into the chip for 2 minutes (Figure 3.2A-F). Equilibrium dissociation constant (K_D) (Figure 3.2G,H) were calculated from association (ka) and dissociation (kd) rate constants for the complex generated from every association (from 0 – 120 seconds) and dissociation (120 – 10,000 seconds) events between the different Aβ42 (Figure 3.2A-C) or Aβ40 (Figure 3.2D-F) peptides and Fbg. Dutch and Iowa Aβ42 (Dutch42 and Iowa42) peptides had lower K_D values with Fbg compared to WT Aβ42, indicating ~4-8 times stronger binding affinity (Figure 3.2G). Dutch and Iowa Aβ40 (Dutch40 and Iowa40) peptides had ~30-50 times stronger binding affinity to Fbg compared to WT Aβ40 (Figure 3.2H). Overall, HCAA Aβ peptides revealed a stronger binding interaction with Fbg compared to their respective WT Aβ counterparts.

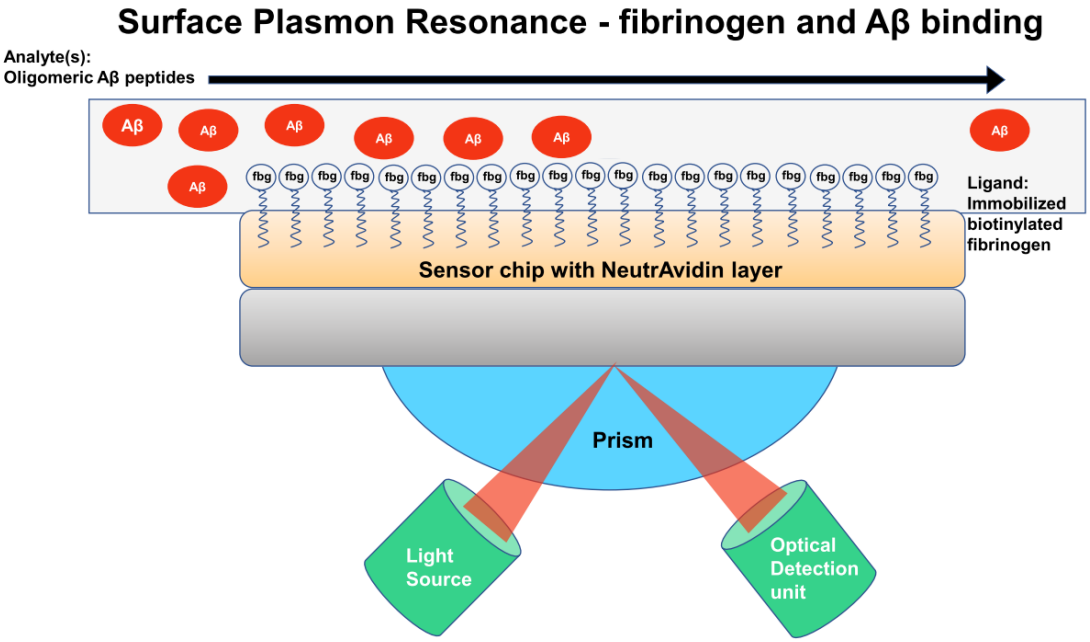

Figure 3.1. Surface plasmon resonance schematic to probe Aβ-Fbg binding. Purified human Fbg was biotinylated and immobilized on a ProteOn NLC sensor chip containing NeutrAvidin layer for binding biotin-labeled molecules. The various Aβ peptides were each diluted to various concentrations using PBS with 0.005% Tween-20 (PBST) as running buffer (final 0.5% DMSO-PBST) and injected for 2 minutes at a rate of 30 µm/min through the SPR's microfluidic channels.

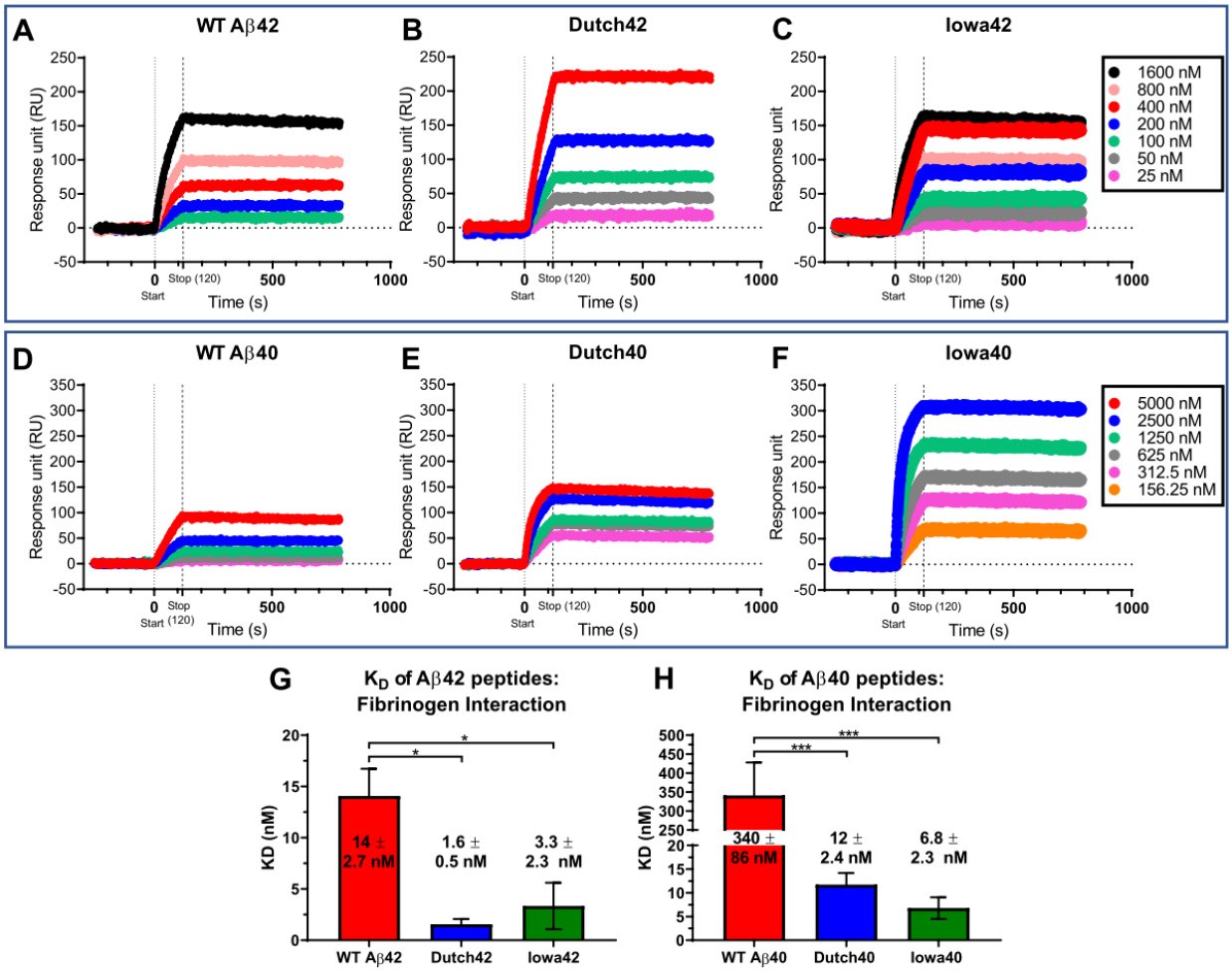

Figure 3.2. HCAA-type mutations increase Aβ's binding affinity for Fbg.
(A-F) Representative SPR response curves of WT, Dutch, and Iowa Aβ42 (A-C) and Aβ40 (D-F) peptides, respectively, that were infused over immobilized Fbg indicate that HCAA Aβ exhibited higher SPR association response signal compared to WT Aβ. (G, H) Bar graphs generated from SPR curves show that K_D of Fbg binding of HCAA-type Aβ42 (G) and Aβ40 (H) is stronger than the binding affinity of their WT Aβ counterparts. (***p<0.001; *p<0.05. n = 3-6). Bar graphs represent mean ± SEM (standard error mean) of ≥3 separate experiments. Statistical analyses were performed using one-way ANOVA followed by Tukey's post-hoc test.

3.2. Specificity of Aβ and Fbg interaction in SPR assays

To determine if the interaction to Fbg was specific to Aβ, we immobilized biotinylated BSA and infused the different Aβ peptides over the sensor chip and found no interaction (Figure 3.3A). In addition, to analyze whether another amyloidogenic protein could interact with Fbg, we infused amylin at similar concentrations as the Aβ peptides over immobilized Fbg but did not observe any interaction (Figure 3.3B). These results suggest the HCAA-type single amino acid mutations increase Aβ's binding affinity for Fbg.

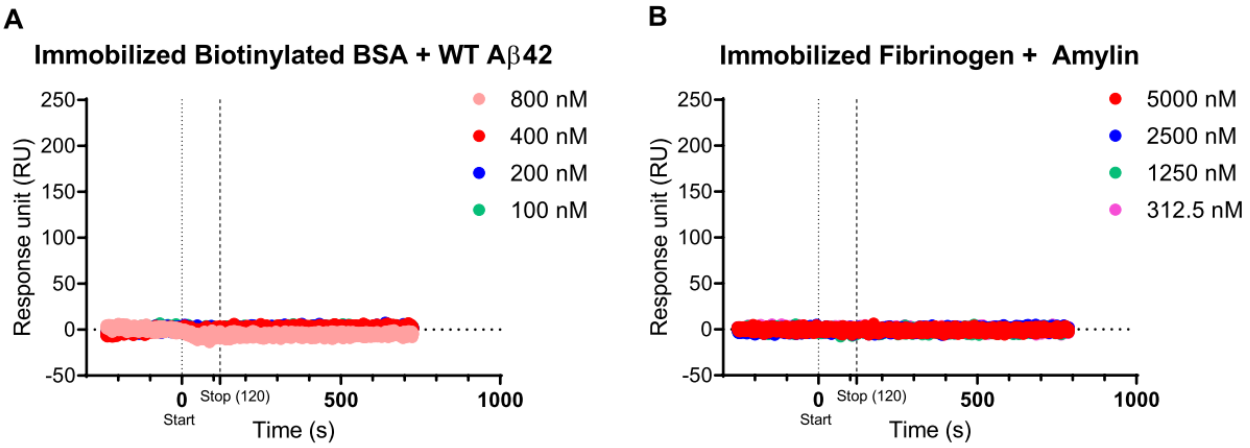

Figure 3.3. Specificity of Aβ and Fbg interaction in surface plasmon resonance binding assays.
(A) Absence of binding interaction as seen as a lack of SPR RU response between biotinylated-BSA immobilized on a SPR sensor chip and Aβ42 infused into the SPR chip in a dose-response manner. (B) Specificity of Aβ and Fbg interaction was further confirmed by the absence of an SPR response using increasing concentrations of amyloidogenic amylin infused into the SPR chip while fibrin(ogen) was immobilized.

3.3. HCAA Aβs used in vitro assays have increased aggregation propensity

The aggregated state and solubility of Aβ is important in driving Aβ deposition in AD brains (99-101), where soluble oligomeric Aβ is thought to be the primary toxic species. Oligomeric WT Aβ42 has a higher binding affinity to Fbg compared to WT Aβ40 (63), possibly due to Aβ42's higher aggregation propensity. HCAA Aβs are highly prone to self-aggregation (86-88), which could explain their observed higher binding affinity to Fbg compared to WT Aβ42. To assess the aggregation state of the WT and HCAA Aβ42 and Aβ40 peptides used for our *in vitro* experiments, we viewed each peptide via transmission electron microcopy (TEM) (Figure 3.4). Compared to WT Aβ42/40 (Figure 3.4A,D), Dutch42/40 (Figure 3.4B,E) and Iowa42/40 (Figure 3.4C,F) peptides oligomerized to a greater extent, forming larger oligomers and protofibrils. These results indicate that the mutant HCAA Aβ used in our *in vitro* experiments are more aggregated, which can have a meaningful impact on fibrin(ogen) binding.

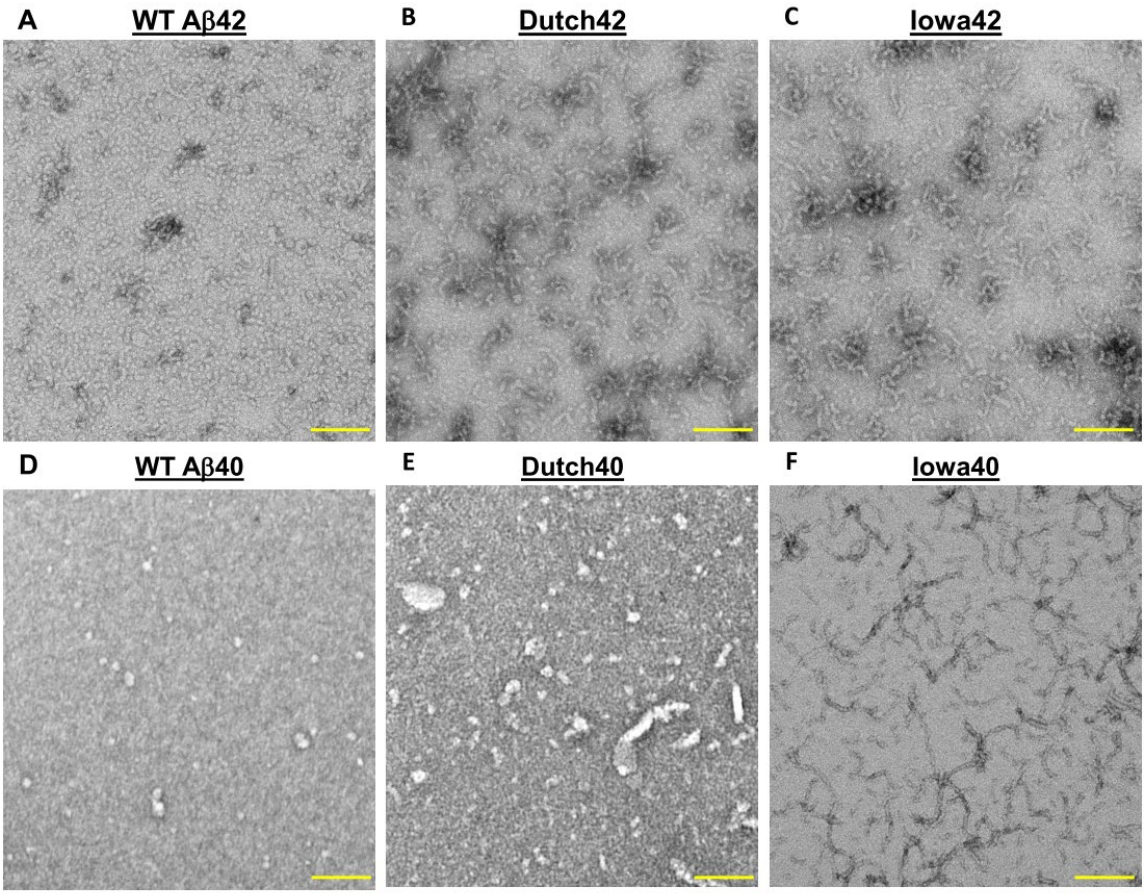

Figure 3.4. Transmission electron microscopy (TEM) of HCAA -Aβ42 and -Aβ40. The Aβ peptides used for all in vitro experiments were initially monomerized with hexafluoroisopropanol (HFIP), then allowed to oligomerize overnight at 4°C, and subsequently placed on carbon grids for transmission electron microscopy (TEM) imaging. Representative TEM images of Aβ42 peptides (A) WT Aβ42, (B) Dutch42, (C) Iowa42, and Aβ40 peptides, (D) WT Aβ40, (E) Dutch40, and (F) Iowa40. HCAA Iowa42 and Iowa40 peptides. Images of (B) Dutch42 and (C) Iowa42 peptides show more extensive aggregation and protofibril formation compared to (A) WT Aβ42. While (F) Iowa40 shows a more aggregated state, (E) Dutch40 shows marginal propensity to aggregate relative to (B) WT Aβ40. Scale bar is 50 nm.

Additionally, I performed Dynamic Light Scattering (DLS) (Figure 3.5) experiments to analyze the size distribution of the WT and HCAA Aβ peptides used in our *in vitro* experiments, including the SPR binding experiments. DLS can measure the theoretical size of particles by analyzing their Brownian motion as they scatter light in solution. The autocorrelations function of our Aβ peptides in our DLS analysis (Figure 3.5A) revealed that there was a significant amount of peptide particles detected in solution compared to buffer alone (no Aβ). Extrapolation of the autocorrelation functions using a regularization fit allowed to us to view size distribution histograms of the different particle sizes for WT Aβ, Dutch40, and Iowa40 (Figure 3.5B-D). All peptides exhibited polydisperse profiles with their own respective hydrodynamic radii and % polydispersity. There were mean (average) differences in hydrodynamic radii among all the peptides (Figure 3.5E). WT

Aβ40 had a larger hydrodynamic radius than Dutch40 and lower hydrodynamic radius than Iowa40. The mean % polydispersity of the different sized-particles populations of all the Aβ peptides showed no significant differences. My results address whether HCAA Aβ peptides have increased populations of larger and more oligomeric & aggregated particles relative to WT Aβ since this could impact our SPR Fbg binding experiments (Figure 3.1). Overall, the average hydrodynamic radii differences among the various Aβ40 peptides did not correlate with the differences in binding affinity to Fbg as seen in Figure 3.1H. This would suggest that differences in particle size populations between WT and HCAA Aβ did not affect our SPR binding affinity results.

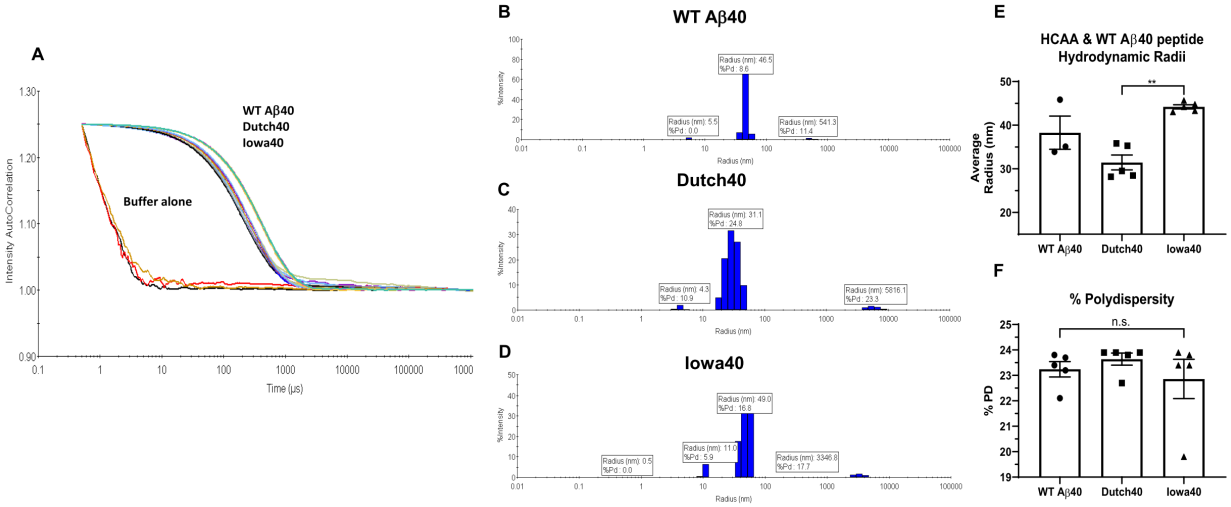

Figure 3.5. The average hydrodynamic radii of HCAA Aβ peptide particles varied relative to WT Aβ.
(A) Dynamic Light Scattering (DLS) autocorrelation function of WT and HCAA Aβ peptides and the background buffer of the Aβ peptides (Buffer alone) showing characteristic smooth and continuous extinction for particles in solution and empty solution, respectively. (B-D) Representative histograms of Regularization fit analyses of WT and HCAA Aβ40 peptides. WT, Dutch40, and Iowa40 Aβ peptides demonstrated multimodal characteristics with various population of peptide particles in solution. Each population particle size corresponds to a peak in the histogram of the radii distribution and has the average radius and % polydispersity listed in the white box insert. (E, F) Bar graphs represent mean ± SEM (standard error mean) of ≥3 separate experiments. ns (not significant) =p>0.05.

3.4. Inducing a more aggregated state in Aβ does not increase binding to Fbg

To further understand whether the aggregation state of Aβ could affect the binding affinity for Fbg, we compared the aggregation state of WT Aβ42 incubated overnight (Figure 3. 6A) to WT Aβ42 incubated at 4°C for 7 days (Figure 3. 6B) to induce a more aggregated state with more protofibrils and fibrils. We performed binding SPR experiments with immobilized Fbg (Figure 3. 6C) using the 7-day incubated WT Aβ42 peptide. Both 1- and 7-day incubations of WT Aβ42 exhibited similar K_D values, 14 ± 2.7 nM and 12 ± 7.8 nM, respectively. Thus, the more aggregated state of WT Aβ42 did not affect the binding affinity to Fbg (Figure 3. 6D). These results indicate that the aggregation state of Aβ alone does not dictate its binding affinity to Fbg. Other factors

such as changes to the physicochemical properties of Aβ due to the HCAA mutations may be significantly contributing to the strong binding affinity in Aβ-Fbg interaction.

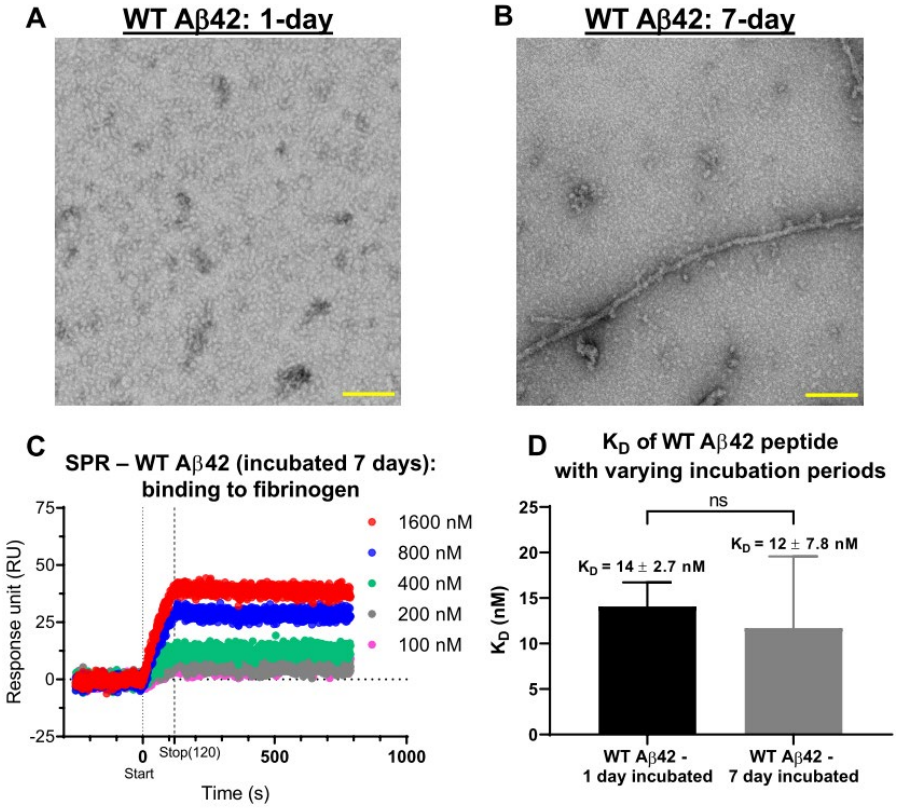

Figure 3. 6. Inducing a more aggregated state in WT Aβ42 does not affect binding affinity to Fbg.
TEM images of WT Aβ42 peptide, prepared in the same manner as for all *in vitro* experiments, incubated overnight (A) and for 7 days (B) at 4^0C and subsequently used for (C,D) SPR assays with immobilized Fbg as the ligand. Representative TEM images of (B) 7-day incubated WT Aβ42 shows more fibrillar and proto-fibrillar structures compared to (A) 1-day (overnight) incubated WT Aβ42.(C) Representative SPR response curve of 7-day incubated WT Aβ42 shows similar SPR association (start) and dissociation (stop) response signal as 1-day incubated WT Aβ42 as shown in Figure 1D. (D) Bar graph generated from SPR curves indicating the mean ± SEM (standard error mean). K_D shows there was no difference in binding affinity to Fbg between the more aggregated 7-day incubated WT Aβ42 and 1-day incubated WT Aβ42. Bar graph represents mean ± SEM of ≥3 separate experiments that were statistically analyzed by performing a two-tailed unpaired t-test. ns (not significant) =p>0.05. Scale bar is 100 nm.

3.5. HCAA Aβs lead to further alterations to fibrin architecture relative to WT Aβ

Given that WT Aβ42 leads to an altered fibrin architecture (66), the stronger binding affinity between HCAA Aβ and fibrin(ogen (Figure 3.2) may have further aggravating effects on fibrin clot structure. To determine the structural effects of HCAA Aβ on *in vitro* fibrin clot formation, clots were formed using purified human Fbg in the absence of Aβ (Figure 3.7) or incubated with the Aβ42 peptides (Figure 3.7D) and the Aβ40 peptides

(Figure 3.7E-G)(66). Figure 3.7 shows representative scanning electron microscope (ScEM) images of the various clots (Figure 3.7A-G) that were acquired and analyzed for fiber thickness (Figure 3.7H,I) and number of aggregated clot aggregates or clumps (Figure 3.7J,K). Normal fibrin clots incubated in the absence of Aβ (Figure 3.7A) demonstrated a homogenous area of normal clot mesh consisting of fibrin fibers that averaged 84±3.0 nm (mean ± SEM (standard error mean)) in thickness and revealed nearly no amorphous clumps or fiber aggregates. When clots were formed in the presence of WT Aβ42 (Figure 3.7B), thinner clot fibers formed with a mean thickness of 56±2.0 nm along with the presence of aggregated fibrin clumps (indicated by the red asterisks), as previously reported (64, 66, 111). Compared to WT Aβ42, fibrin clots in the presence of Dutch Aβ42 (Figure 3.7C) showed signs of greater alteration of the fibrin network with thinner fibers with a mean thickness of 40±1.5 nm (Figure 3.7H) and more aggregates compared to WT Aβ42 (Figure 3.7J), while Iowa Aβ42 (Figure 3.7D) led to even thinner fibers with a mean thickness of 33±1.1 nm, and an increased trend of fibrin clumps (Figure 3.7J). HCAA mutant Aβ40 peptides also led to more dramatic structural changes to fibrin clots fibers compared to their WT Aβ40 counterpart (Figure 3.7E). Fibrin fibers formed in the presence of Dutch (Figure 3.7F) or Iowa Aβ40 (Figure 3.7G) were thinner and more tortuous (mean fiber thickness of 29±1.0 nm and 57± 2.5nm, respectively) (Figure 3.7I), with more fiber clumps (Figure 3.7K). WT Aβ40-induced clots did not lead to structural changes to clot formation compared to fibrin clots formed in the absence of Aβ, which correlates with its weaker binding affinity for Fbg, K_D of 340 ± 86 nM, in SPR analysis (Figure 3.2H). These results indicate that the Dutch and Iowa HCAA Aβ mutations enhance Aβ's perturbation of fibrin clots, which was especially dramatic with the HCAA Aβ40 peptides. Thus, the alterations of HCAA Aβs to clot architecture correlate with their stronger Fbg binding affinity.

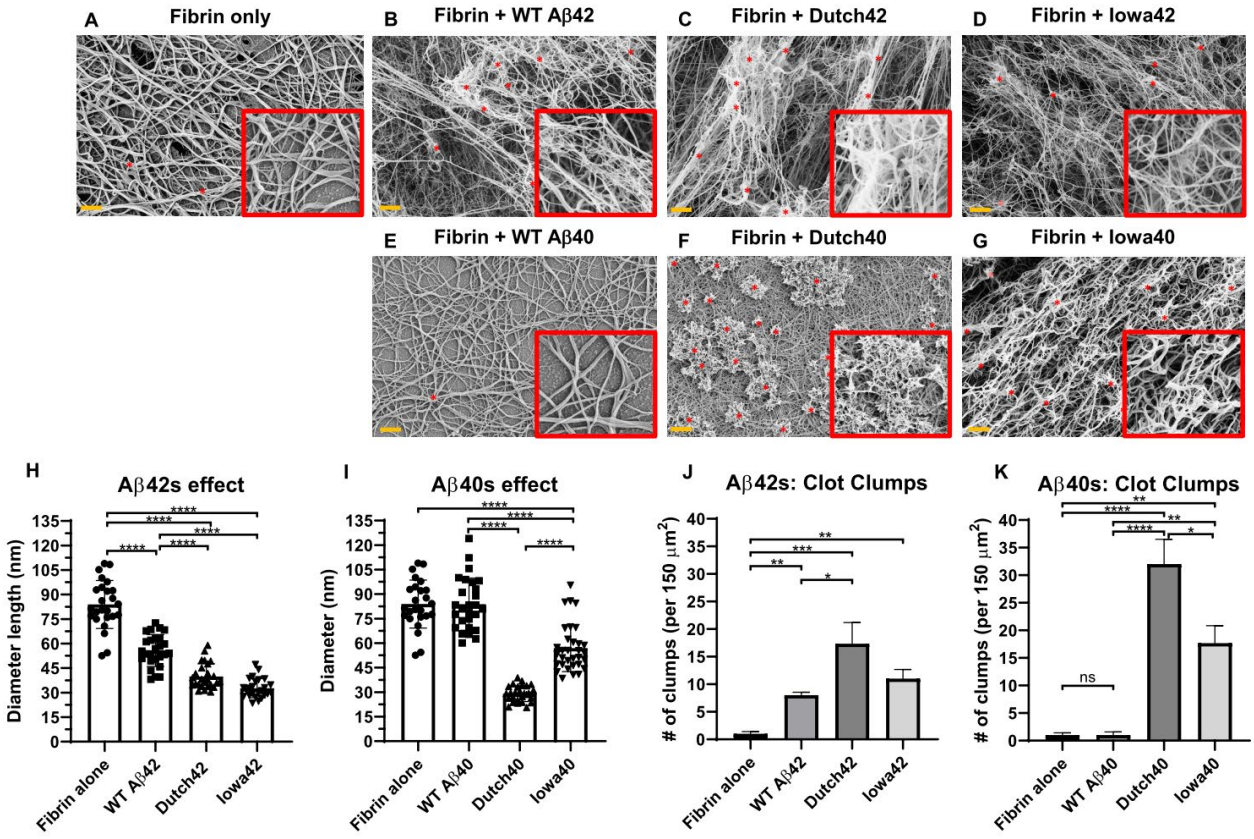

Figure 3.7. HCAA Aβ-induced fibrin clots demonstrate greater structural alterations than WT Aβ-induced clots.
Scanning electron microscopy (ScEM) analysis of clots formed in the presence of (A) no Aβ (control), (B) WT Aβ42, (C) Dutch Aβ42, (D) Iowa Aβ42, (E) WT Aβ40, (F) Dutch Aβ40, and (G) Iowa Aβ40. Fibrin clots were prepared using human fibrinogen (1.5 μM), in the absence or presence of Aβ peptides (3.0 μM). (H-K) Quantification of clot fiber diameter (nm) and number of aggregates/clumps. (H,J) HCAA Aβ42-induced clots show greater alteration in fibrin clot structure with thinner fibers and clumps compared to WT Aβ42. (I,K) HCAA Aβ40-induced clots also led to fibrin clot with a smaller fiber diameter and increased clumps relative to WT Aβ40. Uniquely, WT Aβ40 did not have gross effect on fibrin structure (E), fiber thickness (I), and aggregates (K) compared to control clots made without Aβ (A). Red box inserts display clots at higher magnification. Red asterisks (*) on clot images are indicative of some of the fibrin aggregates/clumps counted per clot. Bar graphs represent mean ± SEM (standard error mean) of ≥3 separate images per clot. Statistical analyses were performed using one-way ANOVA followed by Tukey's post-hoc test. ****p<0.0001; ***p<0.001; **p<0.01; *p<0.05. ns (not significant) =p>0.05. Clots visualized via ScEM are representative of ≥3 separate experiments. Orange scale bar is 1 μm.

Given the concern that brain levels of Aβ are often reported to range from picomolar to low nanomolar concentrations, we tested if fibrin clots made with lower concentrations of WT and HCAA mutant Aβ (375 nM) would have alterations structure (Figure 3.8). The fibrinogen concentration in these clots was lowered to 1 μM, which is

the minimum concentration at which clots can be formed on glass slides for ScEM imaging. Since perturbations in clot lysis is Aβ-concentration dependent, where an Aβ concentration higher than a 1:3 Aβ:Fbg molar ratio is necessary to show the effects of Aβ in clot formation and dissolution (64), we made clots in 375 nM Aβ. The effects of lower levels of Dutch42 (Figure 3.8C) and Iowa42 (Figure 3.8D) Aβ on fibrin fiber structure are still evident with a fibrin mesh that is more irregular and aggregated compared to the WT Aβ42-induced fibrin mesh (Figure 3.8B). However, the effects are less severe at this lower HCAA Aβ concentration. These results suggest that lower Aβ concentrations still exhibit clear differences on fibrin clots between WT and HCAA Aβs.

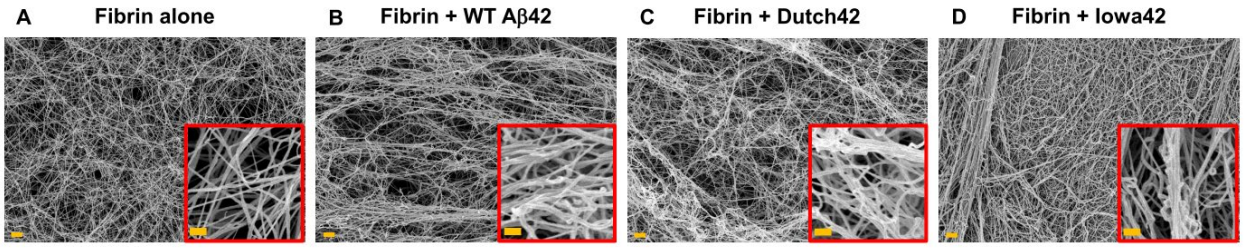

Figure 3.8. HCAA Aβ-induced fibrin clots made with nanomolar Aβ concentration still shows signs of increased structural perturbations compared WT Aβ-induced clots.
Scanning electron microscopy images of clots formed in the presence of (A) no Aβ and 375 nM (B) WT Aβ42, (C) Dutch Aβ42, (D) Iowa Aβ42. Fibrin clots made in the (A) absence of Aβ peptides consisted of a uniform fibrin mesh, while clots made in the presence of (B-D) all the Aβs tested consisted of an irregular mesh. (C,D) HCAA Aβ-induced clots show greater alterations in fibrin clot structure, including more gaps between fibrin fibers, compared to (B) WT Aβ42-induced clots, however, there were no apparent changes in fiber thickness. Red box inserts display enlarged views of clots. Orange scale bar is 1 μm.

3.6. The majority of HCAA Aβ mutants further delay *in vitro* fibrinolysis

Since the Aβ-Fbg interaction is known to delay Pn-mediated fibrinolysis (64), we tested whether the stronger interactions with fibrinogen shown by the HCAA-type Aβ peptides translated into functional consequences in clot formation and dissolution (fibrinolysis) using an *in vitro* clot turbidity assay (Figure 3.9). Turbidity assays can monitor the kinetics of the clotting process by measuring the turbidity of a solution as it increases during clot formation and decreases during clot dissolution or fibrinolysis. Fibrinolysis of the fibrin clot in the presence of Aβ42 was delayed (red line curve, Figure 3.9A) relative to the buffer control clot made without Aβ peptide (black line curve, Figure 3.9A), as previously reported (60, 64), also depicted as an increase in time to half lysis (Figure 3.9C). Fibrinolysis was further delayed in the presence of Iowa-type Aβ42 (gray line curve, Figure 3.9A) relative to WT Aβ42 (red line curve, Figure 3.9A), which resulted in a prolonged time to half lysis for Iowa42 relative to WT Aβ42 (Figure 3.9C). Under the same conditions, fibrin clot formation and dissolution in the presence of WT Aβ40 (red line curve, Figure 3.9B) showed similar kinetics to that of control buffer (black line curve, Figure 3.9B). However fibrin clots formed in the presence of Dutch Aβ40 and Iowa Aβ40 (green and gray line curves, respectively, Figure 3.9B) had prolonged fibrinolysis and an increase in time to half lysis compared to WT Aβ40 (Figure 3.9D).

These results were consistent with our ScEM images (Figure 3.7) in which the HCAA Aβ-induced clots were more structurally altered compared to WT Aβ-induced clots. These findings suggest that HCAA-type Aβs not only alter the fibrin network architecture, but also have a greater functional impact on the clotting clearance process compared to WT Aβ.

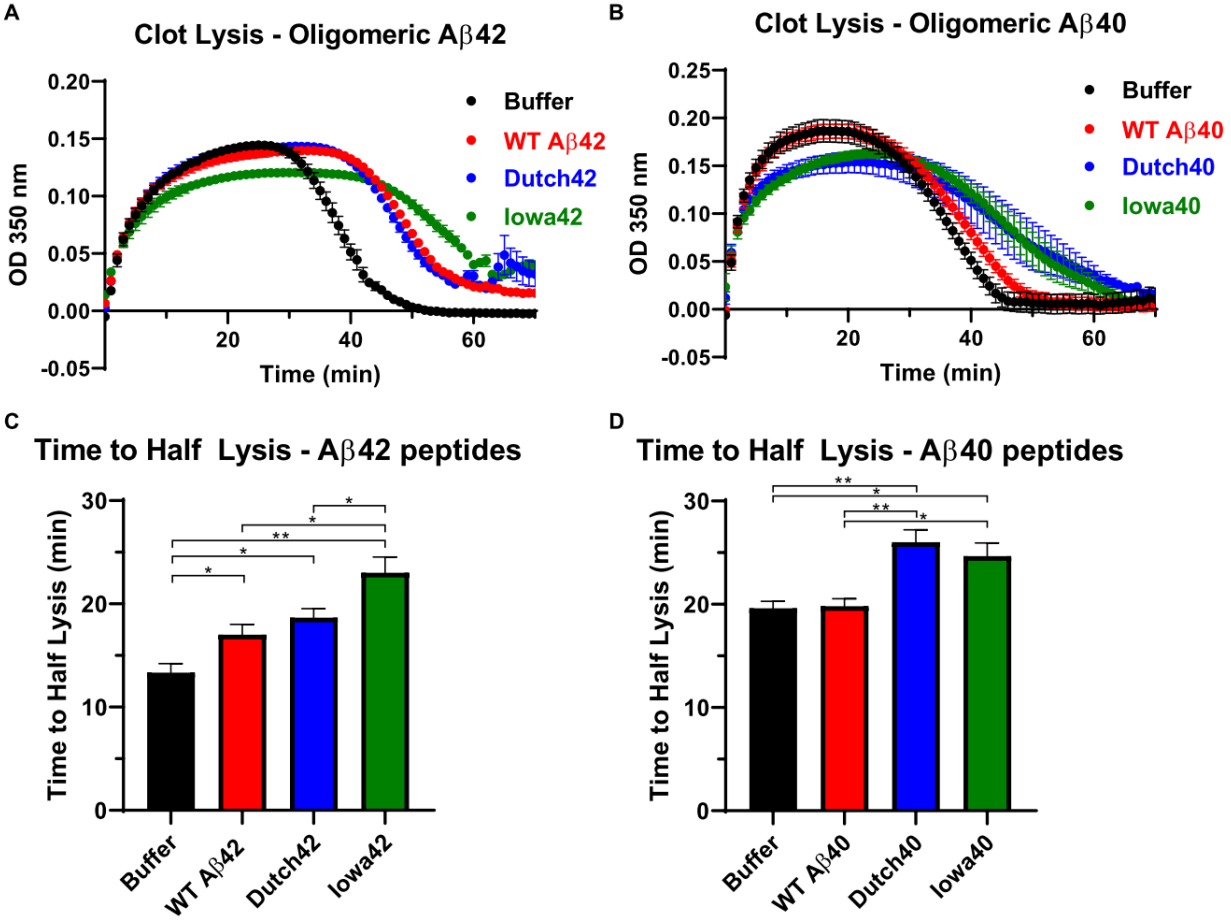

Figure 3.9. HCAA-type Aβs increase resistance to fibrinolysis.
(A and B) Fibrin clot formation and degradation were assessed by measuring time-dependent turbidity changes at 350 nm. These experiments involved incubation of Fbg, tPA, plasminogen, and the absence (black, buffer control only) or presence of WT Aβ (red) or HCAA Aβ peptides (green for Dutch, gray for Iowa). Reactions were initiated by adding thrombin. Time-dependent turbidity plots show the effect of WT Aβ42 and HCAA Aβ42 (A) and WT Aβ40 and HCAA Aβ40 (B) on thrombosis and fibrinolysis. (C) Time to half lysis times for WT Aβ42, Dutch42, and Iowa42 are prolonged compared to control. Clot lysis time of Iowa42 was significantly more delayed than WT Aβ42. (D) While WT Aβ40 did not have any effect on fibrin clot lysis, Dutch40 and Iowa40 significantly delayed fibrinolysis compared to buffer alone and WT Aβ40. (**p<0.01; *p<0.05; n=3). Statistical analyses were performed using one-way ANOVA followed by Tukey's post-hoc test. Bar graphs represent mean ± SEM (standard error mean) of ≥3 separate experiments.

To test whether lower HCAA Aβ concentrations could also delay clot lysis, we performed clot turbidity assays using lower concentrations of WT Aβ42 and Dutch42 (Figure 3.9). We measured the kinetics of clot formation and lysis of these Aβ in a dose-dependent manner (Figure 3.10A). At the highest Aβ concentration tested (3.0μM), WT Aβ42 (dark red curve, 3 μM) and Dutch42 (dark blue curve, 3 μM) further delayed clot lysis relative to respective lower concentrations. At the lowest Aβ concentration tested (0.75μM), there was the largest separation in clot lysis curves between Dutch42 (light blue curve) and WT Aβ42 (light red curve), which means that WT Aβ had a decreased ability to prolong clot lysis compared to Dutch42. For almost every concentration of Dutch42 tested, there was an increased trend in time to half lysis (Figure 3.10B), which were extrapolated from the clot turbidity kinetics. Separation of the clot turbidity experiment by different Aβ concentrations tested (Figure 3.10C-E) more easily shows the separation in clot lysis times between WT Aβ42 and Dutch42.

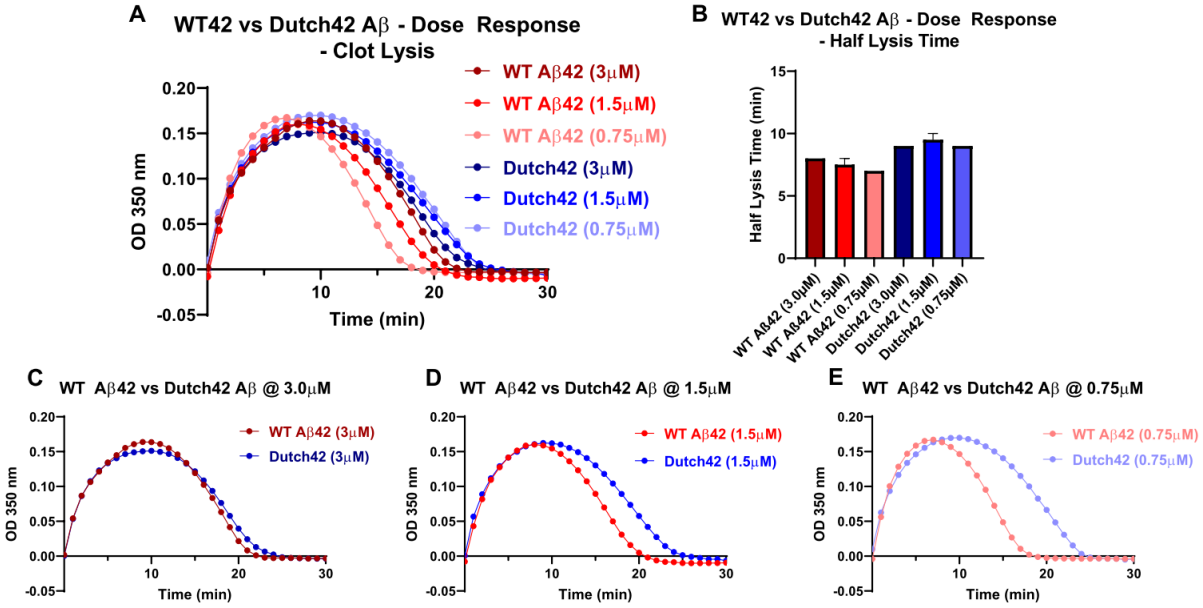

Figure 3.10. Lower Dutch42 concentrations delays clot lysis compared to WT Aβ42.
(A) Fibrin clot turbidity and fibrinolysis differences between WT Aβ42 (different shades of red) and Dutch42 (different shades of blue curves) at lower concentrations were assessed in a dose-dependent manner. (B) Time to half lysis times for almost all concentrations of Dutch42 (blue bars) had an increased trend compared to WT Aβ42 (red bars). (C-E) Separation of clot turbidity and fibrinolysis kinetics by Aβ concentration tested. (E) At the lowest Aβ concentration tested, 0.75 μM, there was a large separation in clot lysis between WT Aβ42 and Dutch42. Bar graphs represent mean ± SEM (standard error mean) of ≥2 separate experiments.

Given that we observed nanomolar concentrations of Dutch42 have a trend in prolonged clot lysis compared to WT Aβ42, we tested lower nanomolar Aβ concentrations (Figure 3.10). The kinetics of the clot turbidities (Figure 3.11A) show that in a dose-dependent manner, all nanomolar concentrations of Dutch42 (different blue

curves) tested prolonged fibrinolysis and led to increases in time to half lysis compared to control buffer (black kinetic curve and bar) and WT Aβ42 separately (Figure 3.11B). In addition, the highest of Dutch42 Aβ tested lowered the maximum turbidity compared to buffer alone. At all concentrations tested, WT Aβ42 (different red curves) showed similar kinetics to that of buffer and did not delay clot lysis (Figure 3.11B).

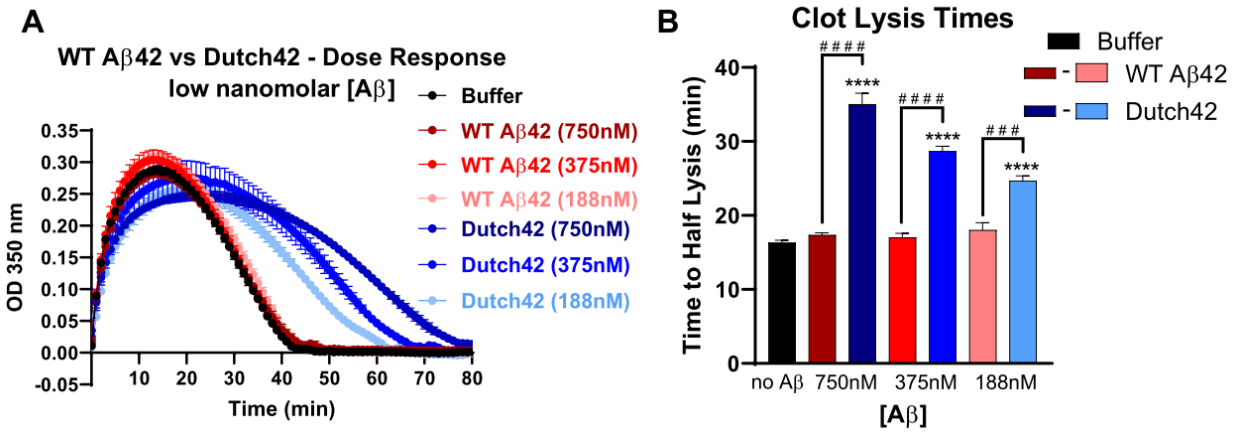

Figure 3.11. Lower nanomolar HCAA Aβ concentrations still perturb clot lysis. (A) Fibrin clot turbidity and fibrinolysis differences between WT Aβ42 (different shades of red) and Dutch42 (different shades of blue curves) were assessed in a dose-dependent manner at low nanomolar concentrations. (B) Time to half lysis times of all concentrations of Dutch42 were significantly higher than both control buffer (black bar, significant differences shown by *) and WT Aβ42 (red bars, significant differences shown by #). (**** or #### p<0.0001; *** or ### p<0.001; n=3). Statistical analyses were performed using one-way ANOVA followed by Tukey's post-hoc test. Bar graphs represent mean ± SEM (standard error mean) of ≥3 separate experiments.

3.7. Increased vascular Aβ and fibrino(gen) co-deposition in HCAA Dutch and Iowa patients' cerebral cortex blood vessel walls

The stronger binding affinity for Fbg and delayed fibrinolysis by HCAA Aβs (Figure 3.9) could translate to higher levels of fibrin(ogen) deposits at sites of CAA in HCAA patient's brains. To test this hypothesis, we acquired postmortem human occipital cortex brain tissue from HCAA-Dutch (n = 5) and -Iowa (n = 1) type patients, age-matched non-HCAA, early-onset AD patients (EOAD) (n = 5), and non-dementia (ND) controls (n = 7), with characteristics of patient tissue listed in Table 3.1. Of note, EOAD patients collected for our analysis do not contain any mutation within Aβ or near Aβ cleavage site as confirmed by sequencing of exon 16 and 17 of the APP gene.

Table 3.1. Characteristics of HCAA patients used in our immunofluorescence analysis of cortical fibrin(ogen), Aβ, and Aβ-Fbg co-deposition levels.

Patient Group	ID	Age	Gender	PMI or Autolysis Time (hours)	Brain section	Brain area (mm^2) evaulated per group (mean ± SD)
HCAA-Dutch	E12-82	55	F	15	Occipital Cortex	33.9 ± 5.11
HCAA-Dutch	E13-99	50	M	19	Occipital Cortex	
HCAA-Dutch	E06-004	57	M	2.5	Occipital Cortex	
HCAA-Dutch	E10-204	53	F	6	Occipital Cortex	
HCAA-Dutch	E04-019	51	M	2.5	Occipital Cortex	
HCAA-Iowa	B14	53	F	--	Occipital Cortex	25.6
EOAD (no intra-Aβ mutation)	AD-4833	59	F	19	Occipital Cortex	26.9 ± 4.98
EOAD (no intra-Aβ mutation)	AD-5854	56	F	4	Occipital Cortex	
EOAD (no intra-Aβ mutation)	2285	60	M	10	Occipital Cortex	
EOAD (no intra-Aβ mutation)	2412	59	M	11	Occipital Cortex	
EOAD (no intra-Aβ mutation)	3291	55	F	13.3	Occipital Cortex	
EOAD (no intra-Aβ mutation)	4668	57	M	14	Occipital Cortex	
ND	2546	57	M	20.3	Occipital Cortex	24.5 ± 3.20
ND	3529	58	M	9	Occipital Cortex	
ND	3558	59	F	19.5	Occipital Cortex	
ND	3839	59	M	15.8	Occipital Cortex	
ND	ND-4238	55	F	12	Occipital Cortex	
ND	ND-4324	62	F	18	Occipital Cortex	
ND	ND-6065	55	M	22	Occipital Cortex	

-- means there was no provided information for the column category from the tissue bank source.

PMI = Postmortem interval

Using these tissues, we probed for fibrin(ogen) deposits (Dako antibody) and congophillic aggregated Aβ deposits (Congo Red) and assessed their co-localization via immunofluorescence (IF) analysis (Figure 3.12). We imaged a single HCAA-Iowa patient's brain due to the limited number of HCAA-Iowa cases and did not include it into our quantification analysis. Consistent with previous findings (12, 18), our IF analysis showed that EOAD brains overall contained higher fibrin(ogen) deposition than ND brains (Figure 3.12A). They had elevated fibrin(ogen) deposition (Figure 3.12B) in and around vascular sites, often at sites of CAA-laden parenchymal vessels, which was pervasive throughout the EOAD occipital cortex samples (as depicted in Figure 3.12A, cyan, vascular Aβ deposits). HCAA-Dutch and -Iowa type patients showed more fibrin(ogen) staining especially in and around CAA-laden vessels compared to EOAD and ND brains (Figure 3.12A,B). While, HCAA-Dutch brains had an elevated amount of vascular Aβ deposits with increased sites of CAA, EOAD brains often presented with abundant CAA pathology and Aβ parenchymal plaques, which made our analysis of total Aβ deposits (Figure 3.12C) reveal no difference between HCAA-Dutch and EOAD brains.

While EOAD brains contained considerable amount of CAA pathology, confocal microscopy analysis showed that there was higher fibrin(ogen) co-localization with Aβ deposits in HCAA brains compared to EOAD brains (Figure 3.12D), at sites of parenchymal Aβ plaques and especially striking at sites of CAA pathology. Aβ deposits and fibrin(ogen) co-deposition was depicted as an overlapping merged channel (Figure 3.12A, merged, yellow). Closer examination of Congo Red-positive (CR+) CAA-laden

(CAA+) vessels, specifically, among the groups also revealed much higher levels of intra-vascular and extra-vascular fibrin(ogen) co-deposition with congophillic Aβ in the HCAA brains (Figure 3.12E). These results suggest that there is more interaction between HCAA Aβ and fibrin(ogen) in CAA+ vessels compared to EOAD patients who also have considerable amounts of CAA, which correlates with our *in vitro* Fbg binding experiments.

Figure 3.12. Increased fibrin(ogen) deposits and Aβ-fibrino(gen) co-deposition in HCAA patients' occipital cortex.
Representative 20x images of brain sections were probed with antibodies against fibrin(ogen) (Fbg, magenta), Aβ deposits using (Congo Red, cyan), and blood vessels (col IV, red). (A) Occipital cortical sections in HCAA-Dutch (n=5) and -Iowa (n=1) type patient brains shows abundant intra- and extra-vascular fibrin(ogen) deposits (magenta) and high amounts of vascular Aβ (cyan) around cerebral blood vessels (red), demarcated by basement membrane collagen IV, which frequently overlapped (Merged, yellow) at sites of CAA. (B,C) Quantification of % area of target protein reveals elevated levels of fibrin(ogen) and Aβ deposits, respectively. (D, E) Confocal analysis shows elevated co-localization between Aβ and fibrin(ogen) in HCAA-Dutch brains, with particularly higher levels of fibrin(ogen) co-deposition in CAA-laden vessels (Congo Red-positive), compared to EOAD (n=5) and ND (n=7) brains. Due to the limited amount of HCAA-Iowa (n=1) individuals available in our study, it was not included in our immunofluorescence quantification analysis. Statistical analyses were performed using one-way ANOVA followed by Tukey's post-hoc test. ****$p<0.0001$; ***$p<0.001$; **$p<0.01$; *$p<0.05$. Scale bar is 100 μm.

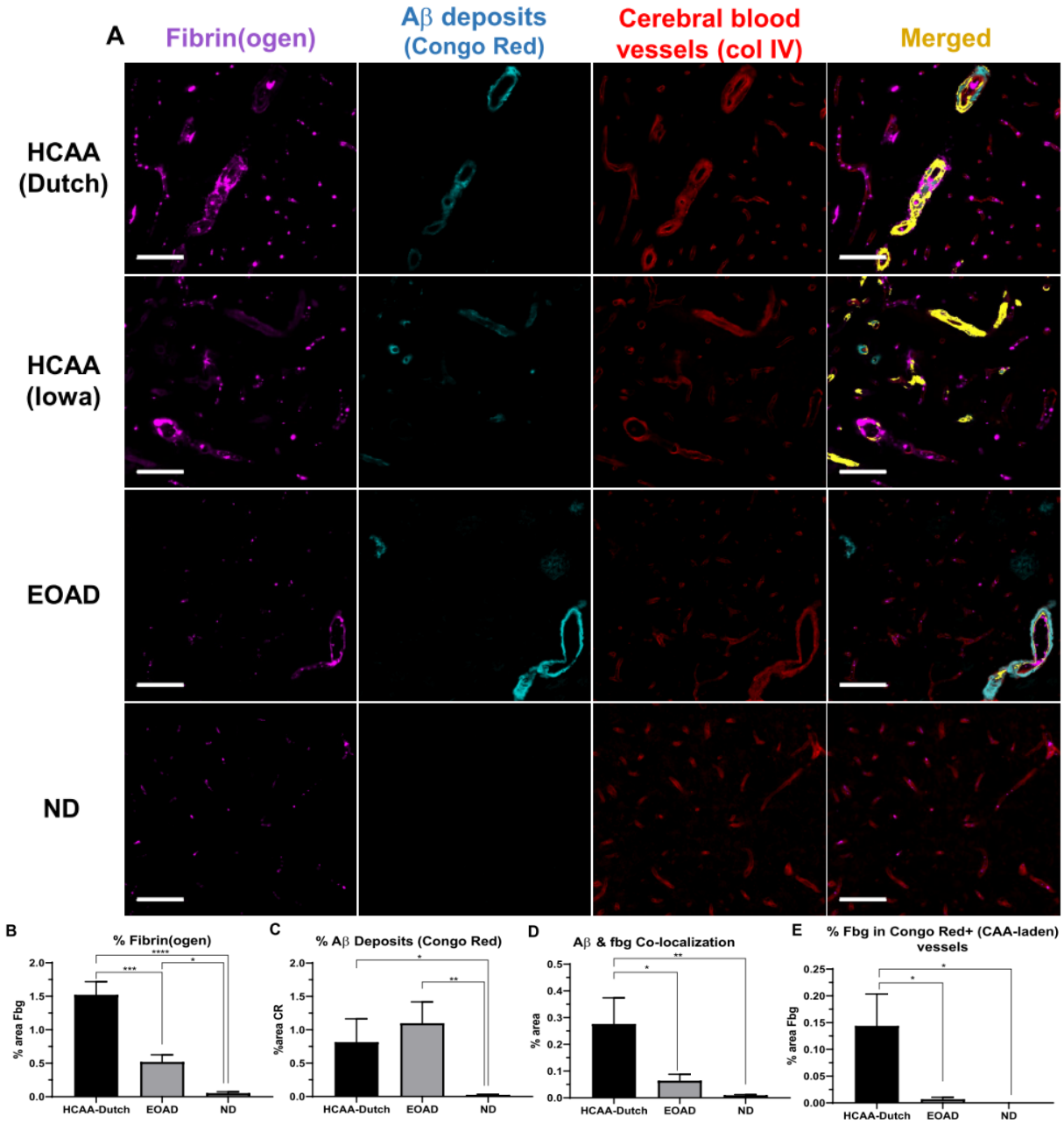
A
Fibrin(ogen)
Aβ deposits (Congo Red)
Cerebral blood vessels (col IV)
Merged
HCAA (Dutch)
HCAA (Iowa)
EOAD
ND
B
% Fibrin(ogen)
% area Fbg
HCAA-Dutch
EOAD
ND
C
% Aβ Deposits (Congo Red)
%area CR
D
Aβ & fbg Co-localization
% area
E
% Fbg in Congo Red+ (CAA-laden) vessels
% area Fbg

Oligomeric Aβ42 interacts with fibrin(ogen) with high binding affinity (15, 16, 18), more so than fibrillar Aβ42. Given the importance of soluble oligomeric Aβ in AD pathology(20-22), our SPR Fbg binding results (Figure 3.2G,H) and the clot structural effects (Figure 3.7) demonstrated by HCAA Aβ oligomers further corroborate that the oligomeric state of Aβ is important in its interaction with fibrin(ogen)(15). Therefore, we also analyzed oligomeric Aβ species in HCAA brains (Figure 3.13) using an Aβ oligomer-specific antibody (NAB61)(27). While HCAA brains exhibited higher levels of CAA pathology (Figure 3.12A), they did not exhibit higher total Aβ deposits compared to EOAD brains (Figure 3.12C), due to their abundant parenchymal Aβ plaques. However, HCAA brains contained much higher levels of vascular Aβ oligomers (Figure 3.13A, NAB61, green) compared to the EOAD brains, which was confirmed with our quantification (Figure 3.13B). Confocal imaging showed abundant fibrin(ogen) co-localized with Aβ oligomers in HCAA-Dutch and -Iowa brains, depicted as an overlapping merged channel (Figure 3.13A, merged, yellow) particularly at sites of CAA pathology. Quantification showed higher levels of Aβ oligomer-fibrin(ogen) co-localization in HCAA-Dutch brains compared to EOAD brains (Figure 3.13C). Furthermore, NAB61-positive (+) vessels also revealed much higher levels of intra- and extra-vascular fibrin(ogen) deposition in HCAA brains compared to EOAD brains (Figure 3.13D). These findings provide evidence that the vast presence of vascular Aβ in CAA pathology in HCAA brains might be composed of a mixture of highly aggregated and oligomeric Aβ, both of which may be abundantly co-depositing with fibrin(ogen) along cerebral vessels. The higher presence of Aβ oligomers at sites of CAA pathology in HCAA patients' brains compared to EOAD brains may be attributable to the stronger interaction between mutant HCAA Aβ oligomers and fibrin(ogen) compared to WT Aβ. which can greatly contribute to their vascular deposition.

To aid the visualization of the co-deposited/co-localized fibrin(ogen) and Aβ deposits (the Congo Red probe) or Aβ oligomers (the NAB61 probe) in HCAA patient brains, close-up confocal z-stacks images of CAA-laden vessels were obtained (Figure 3.14). The z-stack images were compiled into 3D movies that allow close-inspection of the vascular Aβ-Fbg co-localization. CAA-laden vessels in the HCAA-Dutch and EOAD group brains were selected by identifying vessels with abundant vessel Congo Red signal or NAB61 signal. HCAA-Dutch and -Iowa brain samples contained abundant vascular fibrin(ogen) within and around cerebral vessel walls often co-localizing and/or near aggregated Aβ (Figure 3.13A) and Aβ oligomers (Figure 3.13B) at various depths of tissue, whereas EOAD patient samples contained much less co-deposited fibrin(ogen) at sites of CAA.

Figure 3.13. Increased cerebrovascular Aβ oligomer and fibrin(ogen) co-deposition in HCAA patients' cortical blood vessels.
Representative 20x images of brain sections were probed for fibrin(ogen) (Fbg, magenta), Aβ oligomers (NAB61, green), and blood vessels (col IV, red). (A) Brain sections from HCAA-Dutch (n=5) and -Iowa (n=1) patients show extensive Aβ oligomer deposits abundantly co-localizing (merged, yellow) with intra- and extra-vascular fibrin(ogen) along cerebral blood vessel walls, most probably at sites of CAA pathology. The EOAD group demonstrated sparse NAB61 signal or Aβ oligomer deposits at sites of apparent parenchymal plaques. (B) Quantification of % area of NAB61 signal reveal significantly elevated levels of Aβ oligomer deposition, in HCAA-Dutch brain compared to EOAD (n=5) and ND (n=5) brains. (C, D) Co-localization analysis of the same tissue sections using confocal microscopy reveal dramatic co-localization between Aβ oligomers and intra- and extra-vascular fibrin(ogen) in HCAA-Dutch brains compared to the EOAD and ND groups, which was particularly prominent along cerebral vessel walls. There was almost no co-localization between fibrin(ogen) and Aβ oligomers at sites of parenchymal plaques throughout the three patient groups. Due to the limited amount of HCAA-Iowa (n=1) individuals available in our study, it was not included in our immunofluorescence quantification analysis. Statistical analyses were performed using one-way ANOVA followed by Tukey's post-hoc test. ****$p<0.0001$; **$p<0.01$. Scale bar is 100 μm.

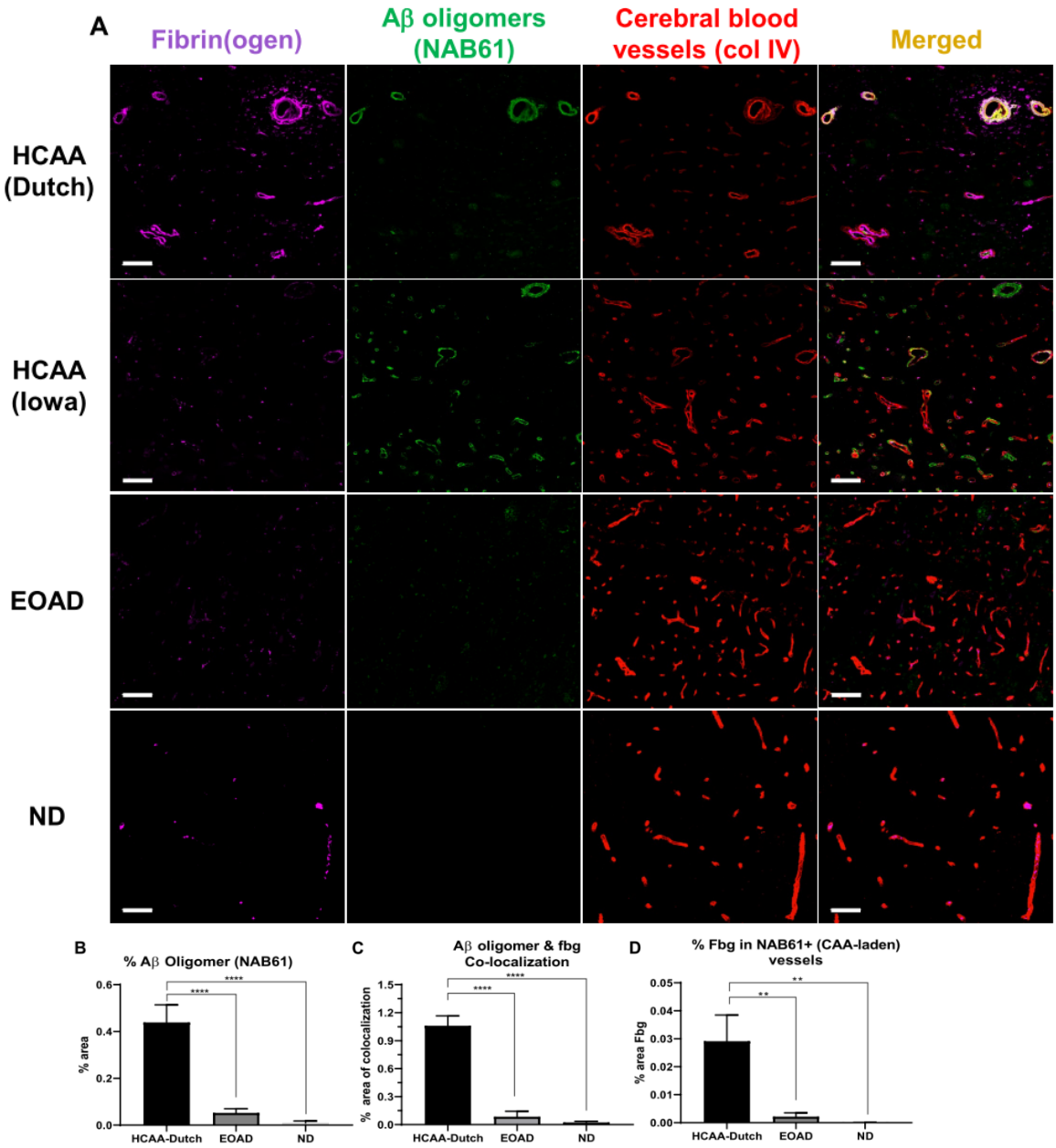
A
Fibrin(ogen)
Aβ oligomers (NAB61)
Cerebral blood vessels (col IV)
Merged
HCAA (Dutch)
HCAA (Iowa)
EOAD
ND
B
% Aβ Oligomer (NAB61)
% area
HCAA-Dutch
EOAD
ND
C
Aβ oligomer & fbg Co-localization
% area of colocalization
D
% Fbg in NAB61+ (CAA-laden) vessels
% area Fbg

Figure 3.14. Abundant Aβ deposit/oligomer-fibrino(gen) co-deposition in HCAA patients' occipital cortical CAA-laden vessels.
Representative close-up 63x confocal z-stacks images of cortical brain sections brain sections probed for cerebral blood vessels (collagen IV, red), Aβ deposits (Congo Red, cyan), Aβ oligomers (NAB61, cyan), and Fbg (green). CAA-laden vessels in the HCAA-Dutch, HCAA-Iowa, and EOAD brains that showed significant amounts of (A) Aβ-deposits (Congo Red) and (B) NAB61 (Aβ oligomer) signal were selected for imaging. Z-stacks consisted of 16 z-planes, 0.5 um apart, which were then reconstructed into a 3D movie composite with all three probes merged. (A) HCAA-Dutch and -Iowa brains show extensive Aβ deposits and Aβ oligomers (B) co-localized with vascular fibrin(ogen) along cerebral blood vessel walls at various depths of tissue. EOAD brains often consisted of abundant vascular Aβ deposits and Aβ oligomers but lacked abundant fibrin(ogen) co-deposition along vessel walls. ND brains contained marginal levels of intravascular fibrin(ogen) within the confines of the cerebral vessels imaged but did not have vascular Aβ deposition. Scale bar is 20 μm.

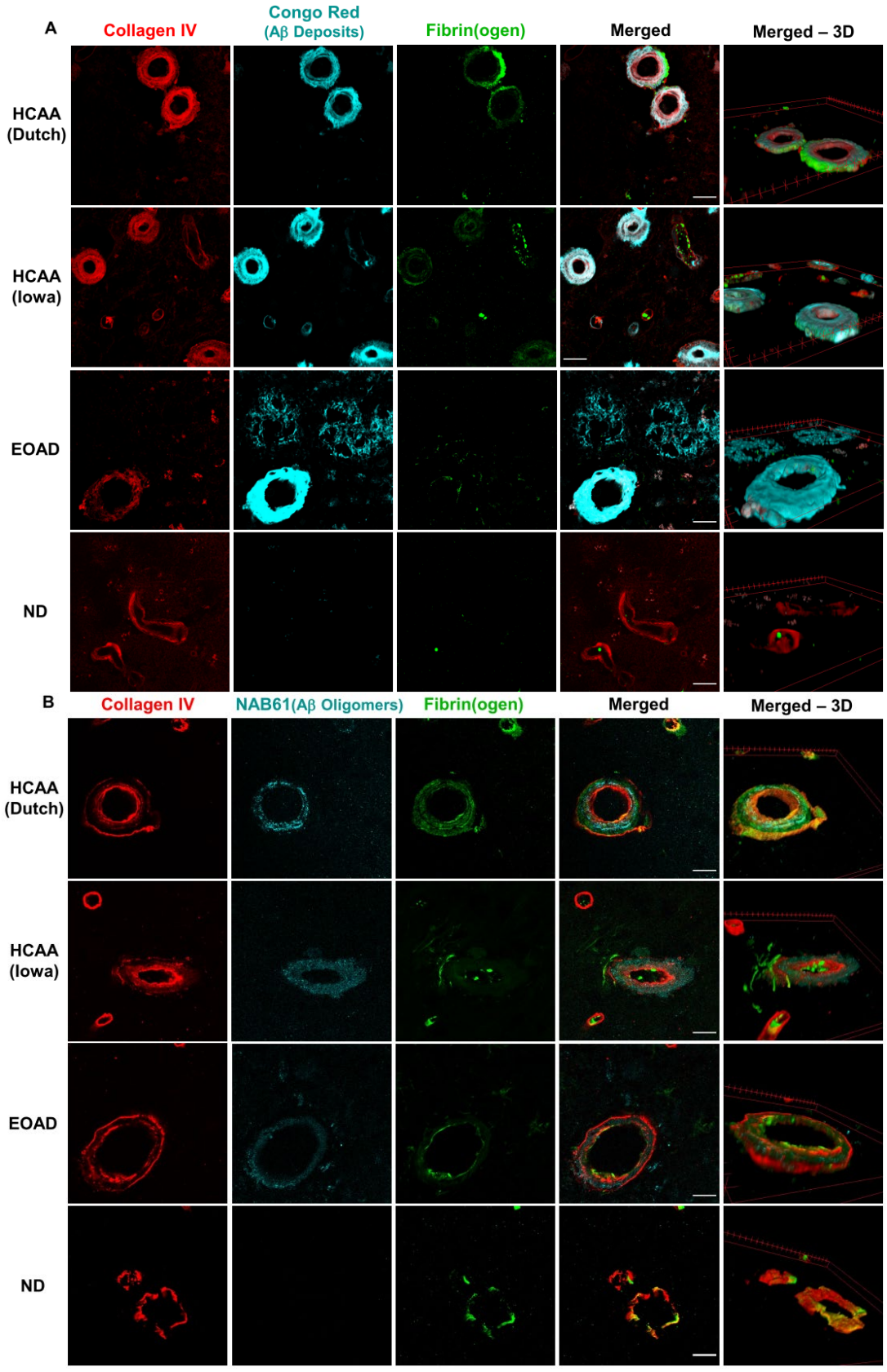
A
Collagen IV
Congo Red
(Aβ Deposits)
Fibrin(ogen)
Merged
Merged – 3D
HCAA
(Dutch)
HCAA
(Iowa)
EOAD
ND
B
Collagen IV
NAB61(Aβ Oligomers)
Fibrin(ogen)
Merged
Merged – 3D
HCAA
(Dutch)
HCAA
(Iowa)
EOAD
ND

To ensure we were assessing vascular Aβ and fibrin(ogen) across similarly sized vessels in HCAA-Dutch, EOAD, and ND brains, we further stratified our IF analyses of levels of fibrin(ogen), congophillic Aβ and Aβ oligomer by separate vessel sizes (Figure 3.15). We quantified the % area of target protein contained in the vessel walls of larger vessels, which included medium to larger arterioles, and smaller vessels, consisting of arterioles, capillaries, and venules. In HCAA-Dutch brains, larger vessels had increased levels of vascular fibrin(ogen) (Figure 3.15A), Aβ oligomer deposits (Figure 3.15C), and fibrin(ogen) co-localization with congophillic Aβ (Figure 3.15D) and Aβ oligomers (Figure 3.15E) compared to in EOAD. HCAA-Dutch brain small vessels also contained higher levels of fibrin(ogen) deposits (Figure 3.15F), Aβ oligomers (Figure 3.15H), and Aβ oligomers-Fbg co-localization (Figure 3.15J). We excluded quantification of large blood vessels, including small arteries, greater than 250 μm in diameter because large blood vessels were unevenly distributed between samples.

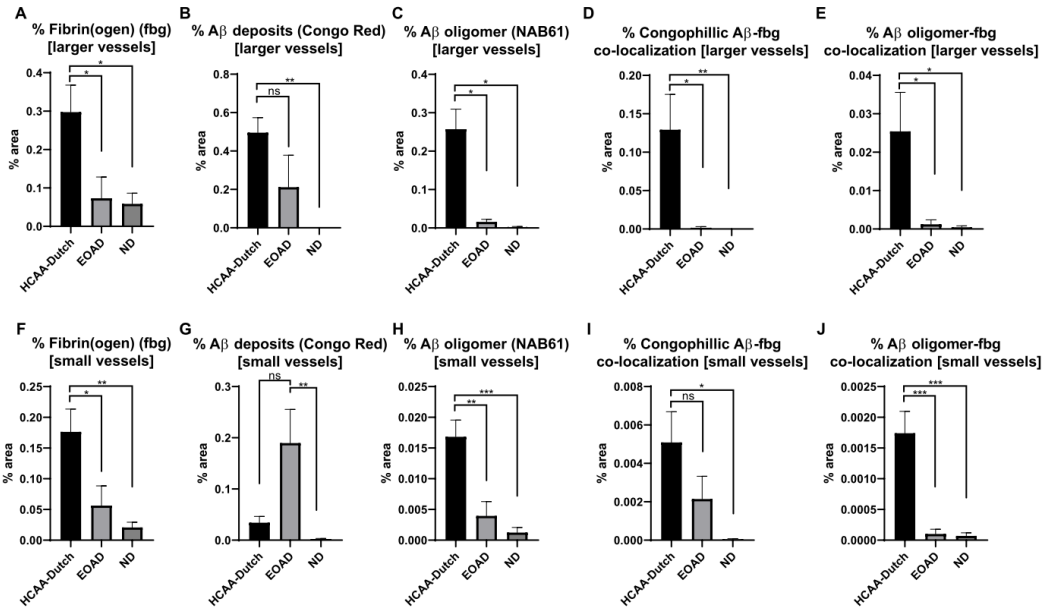

Figure 3.15. Increased Aβ deposits/oligomer-fibrin(ogen) co-deposition across small and large HCAA patients' cortical blood vessels.
Quantification of % area of target protein in larger (A-E) and smaller vessels(F-J). HCAA-Dutch brains' (n=5) larger vessels showed increased vascular (A) fibrin(ogen) deposits and (C) Aβ oligomers deposits with higher levels of fibrin(ogen) co-localized with (D) congophillic aggregated Aβ deposits and (E) Aβ oligomers compared to EOAD (n=5) and ND (n=7) brains. (B) HCAA-Dutch and EOAD brains contained abundant CAA-laden larger vessels, which resulted in elevated levels of vascular Aβ deposits. Although, smaller vessels in HCAA-Dutch brains showed abundant vascular (F) fibrin(ogen) and (H) Aβ oligomer deposits, there was lower (G) congophillic aggregated Aβ deposits compared to EOAD brains. Regardless, small vessels in HCAA brains demonstrated high co-localization between fibrin(ogen) and (I) congophillic Aβ-deposits, as well as with (J) Aβ oligomers. HCAA-Iowa (n=1) was not included in immunofluorescence quantification analysis. Statistical analyses were performed using one-way ANOVA followed by Tukey's post-hoc test. ***p<0.001; **p<0.01; *p<0.05. ns(not significant) =p>0.05.

To further examine possible differences in vessel distribution in the patient brain samples, we analyzed vessel density (vessel count per mm2) (Figure 3.16A) and % collagen IV (Figure 3.16B) area, an indicator of vessel sizes. There was no statistical difference in vessel density among the three patient groups, although EOAD and ND brains trended higher in density. There was also no statistical difference in vessel area or sizes (% collagen IV) among the groups, although HCAA-Dutch brain samples trended higher with frequent larger caliber vessels.

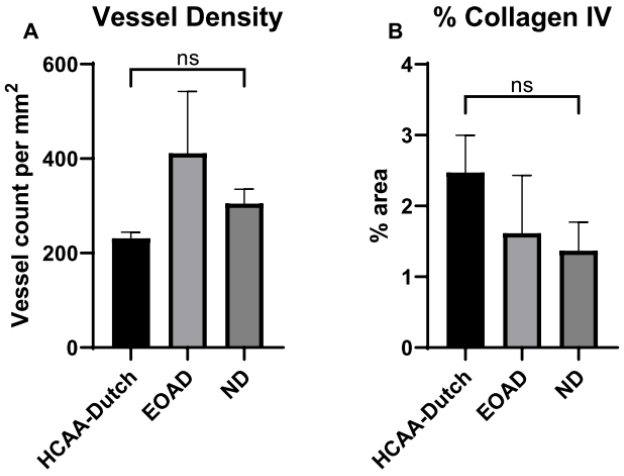

Figure 3.16. Distribution of cerebral vessels in HCAA patients' occipital cortex is not significantly different compared to EOAD and ND brains.
Quantification of collagen IV signal in immunofluorescence probe of HCAA brains. (A) EOAD brains (n=5) had a higher trend in vessel density but vessel count per mm2 was not significantly different compared to HCAA-Dutch (n=5) and ND (n=7) brains. (B) HCAA-Dutch brains had a higher trend in % collagen IV area indicative of the frequent larger vessels in Dutch brain sections. However, there was no statistical differences among the 3 patient groups. HCAA-Iowa (n=1) was not included in collagen IV signal quantification analysis. Statistical analyses were performed using one-way ANOVA followed by Tukey's post-hoc test. ns(not significant) =p>0.05.

3.8. Probe of other HCAA-linked Aβs' interaction with Fbg

We also investigated the interactions between Fbg and HCAA Arctic (E22G) and -Italian (E22K) Aβs. Italian-carrier patients are also afflicted by severe CAA with ICH. However, while this HCAA variant has been less studied than other variants, its neuropathological changes are similar to those found in Dutch and Iowa variants (112, 113). Italian Aβ also shows the ability to form abundant β-sheet structure and assume higher order aggregated states (114, 115). In HCAA Arctic uniquely stands from the rest of the HCAA variants because although carriers of the Arctic-mutation are afflicted by severe CAA pathology, unlike Dutch-, Iowa-, and Italian-mutation carriers, these patients do not present with ICH. Interestingly, similar to Dutch, Iowa, and Italian Aβ, Arctic Aβ also demonstrates increased protofibril formation compared to WT Aβ, which may increase its insolubility and lead to its accumulation in the cerebrovasculature in the form of CAA (89).

3.8.1. HCAA-linked Arctic Aβ has increased binding to Fbg

Under similar conditions as in Figure 3.1, the specific binding affinity of Arctic42 for Fbg was assessed using SPR analysis where Fbg was immobilized to interact with infused Aβ peptides in a dose-dependent manner. WT Aβ42 (Figure 3.17A) exhibited slightly higher SPR association response signal curves compared to Arctic42 (Figure 3.17B) although at the highest Arctic42 concentration (5000 nM) the response curve was saturated. K_D values were calculated from the association (from 0 – 120 seconds) and dissociation (120 – 10,000 seconds) events between the different Aβ peptides and Fbg (Figure 3.17C). Arctic42 had lower K_D values with Fbg compared to WT Aβ42, indicating ~2 times stronger binding affinity. Comparison of the Fbg binding K_D values (mean ± SEM) of the of all the WT and HCAA Aβ peptides tested in all of our *in vitro* experiments were plotted in bar graph (Figure 3.17D) and tabulated (Figure 3.17E). Overall, all HCAA Aβ peptides tested exhibited stronger Fbg binding affinities compared to WT Aβ42/40. For example, Dutch42, Iowa42, and Arctic42 had significantly stronger binding affinities (denoted by lower K_D values) for Fbg compared to WT Aβ42.

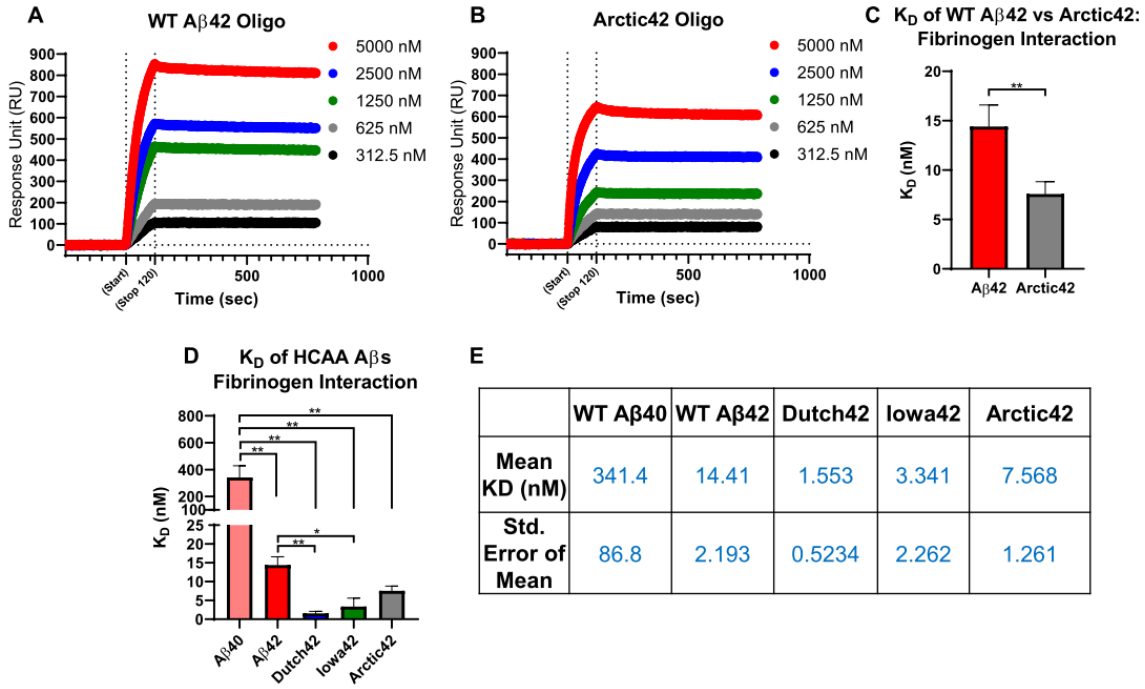

	WT Aβ40	WT Aβ42	Dutch42	Iowa42	Arctic42
Mean KD (nM)	341.4	14.41	1.553	3.341	7.568
Std. Error of Mean	86.8	2.193	0.5234	2.262	1.261

Figure 3.17. HCAA-type mutant Arctic Aβ has increased binding affinity for Fbg. (A, B) Representative SPR response curves of WT Aβ42 (A) and Arctic42 (B) peptides respectively, that were incubated into an oligomeric state overnight at 4^0C. Aβ peptides were infused over immobilized Fbg in a dose dependent manner. Arctic42 exhibited slightly lower SPR association response signal curves compared to WT Aβ42. (C) Bar graphs generated from SPR curves show that binding affinity (K_D) for Fbg of Arctic42 was stronger than the binding affinity of WT Aβ42. (E, F) Comparison of all K_D values of all HCAA Aβ peptides tested in SPR Fbg binding experiments. (***p<0.001; **p<0.01, *p<0.05. n = 3-6). Bar graphs represent mean ± SEM (standard error mean) of ≥3 separate experiments. Statistical analyses were performed using two-tailed unpaired t test and one-way ANOVA followed by Tukey's post-hoc test.

3.8.2. HCAA-linked Italian Aβ further delays fibrinolysis compared to WT Aβ40

In order to explore whether the stronger Aβ-Fbg binding exhibited by Arctic40 Aβ also lead to functional effects on fibrin formation and dissolution, similar to Dutch40 and Iowa40, we carried out clot turbidity assays using Arctic40 (Figure 3.18). We also included Italian40 Aβ peptides in this analysis. Fibrinolysis of clots in the presence of Dutch40 (Figure 3.18A, green curve), as seen before in Figure 3.9, and Italian40 (Figure 3.18B, magenta curve) was delayed relative to the buffer control clots (no Aβ, black curves) and WT Aβ40 (red curves), which resulted in their prolonged time to half lysis (Figure 3.18C). However, unlike previous clot lysis kinetics of Dutch40 & Iowa40 (Figure 3.9B), clot formation and dissolution in the presence of Arctic40 (Figure 3.18A, blue curve) did not delay clot lysis and did not lead to prolonged time to half lysis. The maximum turbidity or optical density (OD) during clot formation in the presence of Arctic40 was decreased, relative to control clots, similar to Dutch40. These findings suggest that Italian40, like Dutch40, can have a functional impact on the clotting clearance process compared to WT Aβ40. In contrast, Arctic40 shows ambiguous results, where it does not delay clot lysis, but does lower the maximum OD. Based on previous studies (64, 66), the lower turbidity exhibited by clots made in the presence of Arctic40 is suggestive of a fibrin mesh that is more irregular with more gaps in between. The irregular mesh allows more light to pass through thus making the clot less turbid, lowering the maximum OD. These results highlight the possibility that Arctic40, which may be the principal component of vascular amyloid in HCAA-Arctic patients, can alter structure and yet not affect fibrinolysis, contrary to other HCAA Aβ variants.

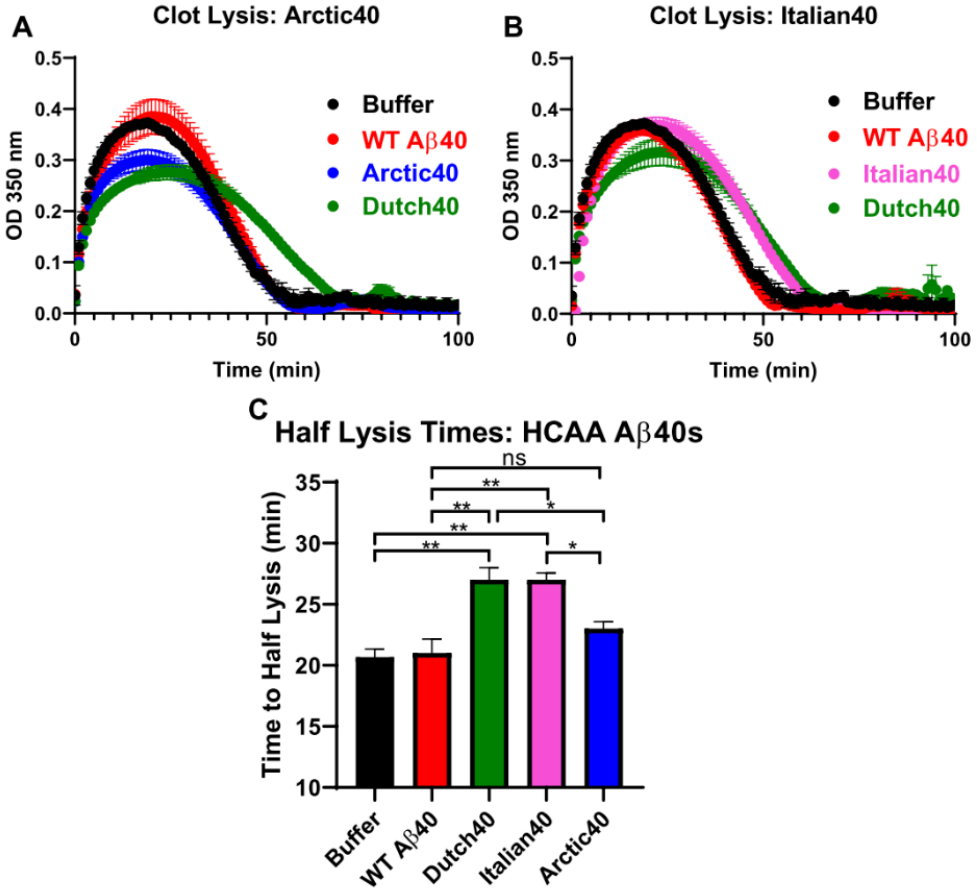

Figure 3.18. HCAA-type Italian Aβ40 increases resistance to fibrinolysis, while Arctic Aβ40 lowers maximum clot turbidity.
(A, B) Fibrin clot turbidity and fibrinolysis differences between WT Aβ40 (red curves), Dutch40 (green curves), and Italian40 (magenta curve). (A) Dutch40 and (B) Italian40 similarly delayed clot lysis relative to WT Aβ40 and control buffer clots (black curves). Both Dutch40- and Arctic40-induced clots had lower maximum OD values. (C) Time to half lysis times of Italian40 (magenta bar) and Dutch40 (green bar) were significantly higher than both control buffer (black bar) and WT Aβ40 (red bar). (**p<0.01; *p<0.05; n=3). ns (not significant) =p>0.05. Statistical analyses were performed using one-way ANOVA followed by Tukey's post-hoc test. Bar graphs represent mean ± SEM (standard error mean) of ≥3 separate experiments.

3.9. Longer length Aβs (>Aβ42) & Fbg

We investigated the fibrin(ogen) interactions of long Aβ species (≥ Aβ43) because recent studies have highlighted their involvement in parenchymal (105) and vascular Aβ deposits (106) in AD brains. We evaluated the effects of longer Aβ peptides in fibrin(ogen) interaction and compared them with shorter Aβ peptides (Aβ38, Aβ40 and Aβ42).

3.9.1. Profiling longer length Aβ peptides aggregation propensity via EM

We first acquired TEM images of different length Aβs [Aβ (1-n)] peptides (Figure 3.19) in order to assess their aggregations state and fibrillization capacity, which could influence their interaction with fibrin(ogen). Aβ42 and Aβ40 formed the least amounts of fibrillar structures. Aβ40, as seen in Figure 3.4, was seen to rarely aggregate or form circular white-dot structures, indicative of oligomeric aggregates. Aβ38 showed long straight protofibrils/fibrils that are similar in morphology to what has been reported in the literature (113). Aβ43 exhibited abundant oligomer formation (white circular structures), while Aβ46 demonstrated the most extensive oligomer formation with branching and aggregated protofibrils/fibrils compared to the shorter Aβs. We did not observe a clear trend in fibrillization capacity of longer length Aβs compared to shorter ones, since Aβ38 peptide showed increased peptide aggregation.

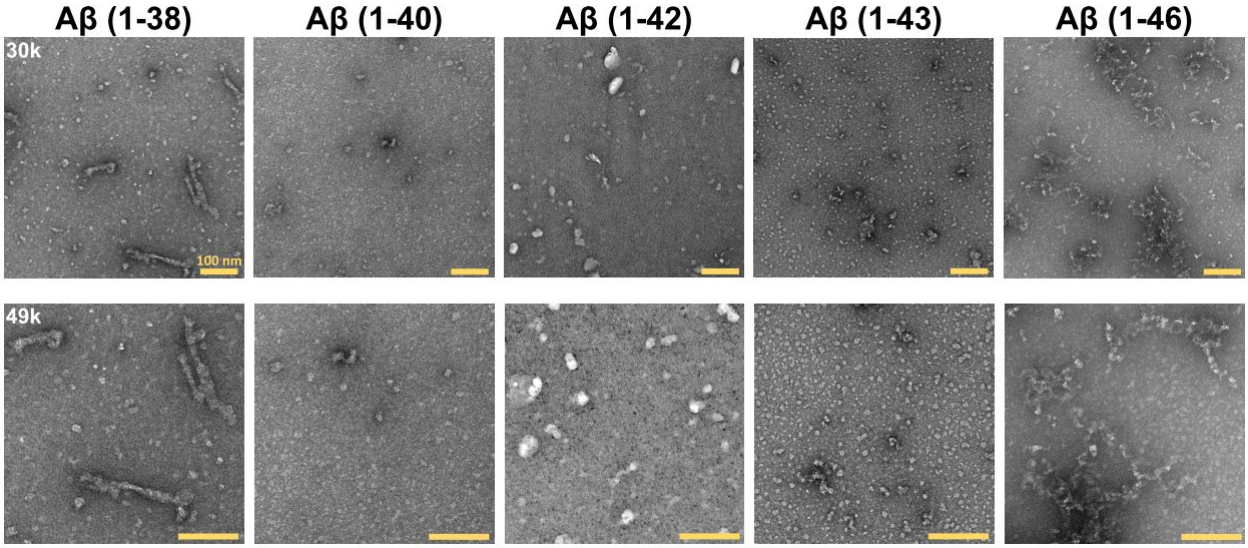

Figure 3.19. TEM analysis of different length Aβ (1-n) peptides.
The Aβ (1-n) peptides used for the *in vitro* experiments were initially monomerized with hexafluoroisopropanol (HFIP), then allowed to oligomerize overnight at 4°C, and subsequently placed on carbon grids TEM imaging. Representative TEM images of Aβ38, 40, 42, 43, and 46 are shown at 30k and 49k magnification. Aβ38 and Aβ46 showed the most extensive aggregation and protofibril/fibril formation compared to WT Aβ42. The Aβ38 rod-like morphology resembles previously reported structures for Aβ38. Aβ40 showed the least amount of oligomer structure or formation. Yellow scale bar is 100 nm.

3.9.2. Probing the binding affinity for Fbg of longer length Aβs

To evaluate how the strength of Fbg binding compared amongst the different length Aβs, under similar conditions as in Figure 3.1, the binding affinity of Aβ38, 40, 42, 43, and 46 for Fbg was assessed using SPR analysis. Fbg was immobilized to interact with infused Aβ peptides in a dose-dependent manner (Figure 3.20). Aβ38 (Figure 3.20A) and Aβ42 (Figure 3.20B) showed similarly elevated SPR association response curves across all Aβ concentrations, however, their binding affinities (K_D) for Fbg (Figure 3.20E) were different. The association (ka) rate constants for Aβ42 were higher (data

not shown), consequently its K_D, calculated from ka and dissociation (kd) rate constants, was lower than Aβ38, indicative of higher binding affinity. Aβ43 (Figure 3.20C) and Aβ46 (Figure 3.20D) had lower SPR response curve and consequently had much weaker Fbg binding affinity compared to Aβ38 and Aβ42. Aβ43 had a stronger Fbg binding affinity than Aβ46. Aβ40's binding affinity for Fbg, previously obtained from experiments in Figure 3.2, were also plotted in the bar graph for comparison (Figure 3.20E). Comparison of the Fbg binding K_D values (mean ± SEM) of the of all the Aβ (1-n) peptides tested were tabulated (Figure 3.20F). Overall, Aβ40 has the weakest binding affinity (highest value K_D) compared to all other length Aβ (1-n) tested. Among the Aβs (1-n) tested, the intermediate length Aβ42 peptide had the strongest binding affinity compared to the shortest and longest Aβ. Linear regression analysis revealed that there was low correlation ($r^2 = 0.086$) between Fbg binding affinity and length of Aβ when comparing Aβ lengths 38 through 46 (Figure 3.20G). However, I observed a strong correlation ($r^2 = 0.999$) when isolating Aβ lengths ≥ 42 (Figure 3.20H), which included Aβ43 and Aβ46. The fitted regression line with a r^2 value close to 1 indicates that there is strong evidence that Fbg binding of Aβ peptides longer than Aβ42 have higher K_D values meaning that their Fbg binding affinities are weaker. Due to limitations in the commercial availability of other Aβ variant lengths from the same Aβ peptide vendors as the rest (Bachem), we did not obtain and analyze Aβ45 and Aβ49 variants.

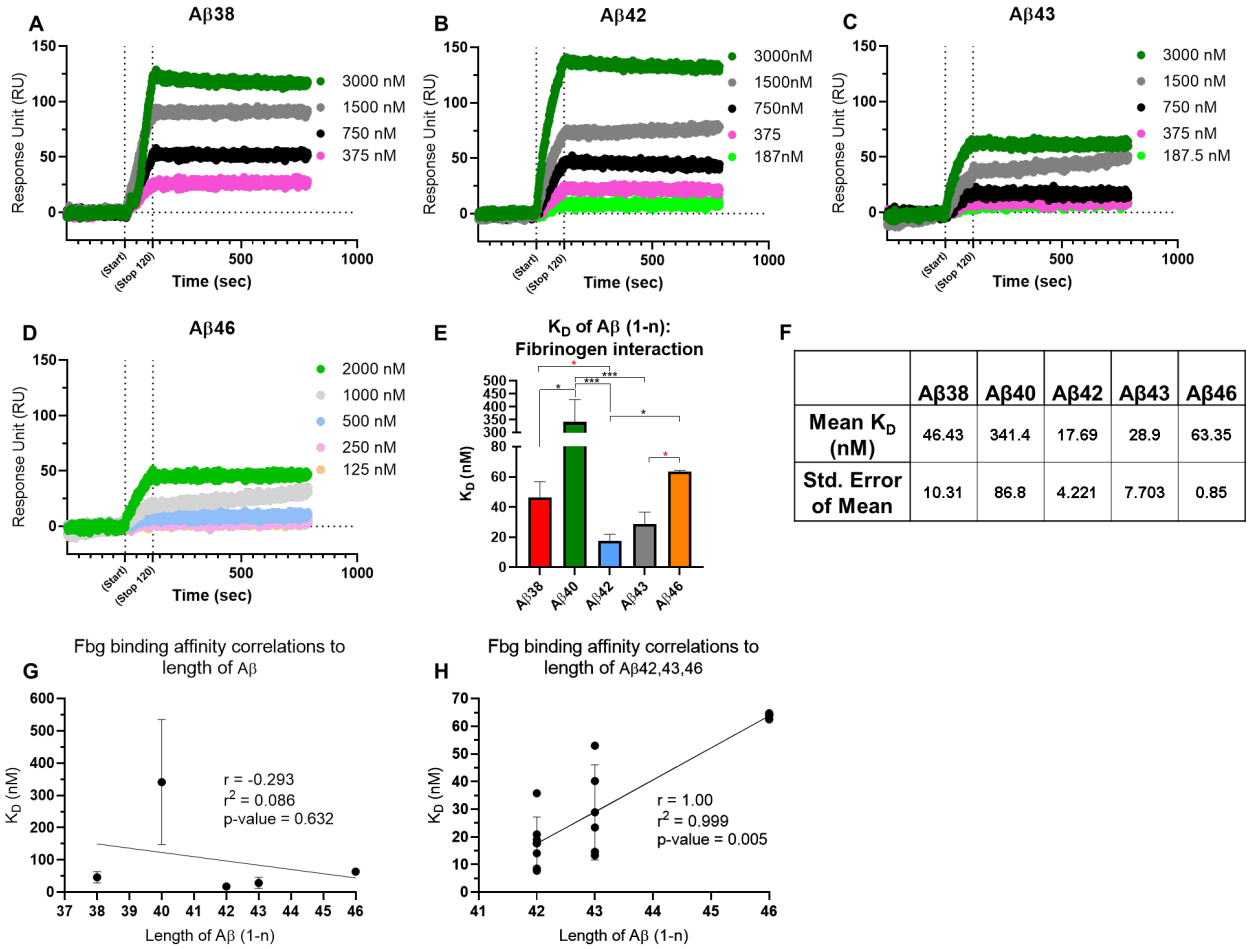

	Aβ38	Aβ40	Aβ42	Aβ43	Aβ46
Mean K_D (nM)	46.43	341.4	17.69	28.9	63.35
Std. Error of Mean	10.31	86.8	4.221	7.703	0.85

Figure 3.20. Assessing the increased binding affinity for Fbg of Aβs (1-n). (A-D) Representative SPR response curves of (A) Aβ38, (B) Aβ42, (C) Aβ43, and (D) Aβ46 peptides that were incubated into an oligomeric state overnight at 4^0C. Aβ peptides were infused over immobilized Fbg in a dose dependent manner. Aβ38 and Aβ42 showed similar SPR association response curves across all Aβ concentrations. However, bar graphs (E) generated from SPR curves show that Fbg binding affinity (as measured by K_D) was strongest for Aβ42 and weakest for Aβ40 and Aβ46. (F) Tabulation of all mean ± SEM K_D values of all Aβ (1-n) peptides tested in SPR Fbg binding experiments. (G, H) Linear regression analysis of Fbg binding affinity K_D values and length of Aβs tested. (G) The fitted regression line shows no correlation when considering Aβ lengths 38-46. (H) However, when considering only the long Aβs (≥42) tested, the fitted linear regression was excellent ($r^2 = 0.999$) and showed a positive strong Pearson correlation (r = 1) between length of Aβ and higher Fbg binding K_D values. Bar graphs represent mean ± SEM (standard error mean) of ≥3 separate experiments. (***p<0.001; *p<0.05, statistical analysis by one-way ANOVA followed by Tukey's post-hoc test). *p<0.05, statistical analysis by two-tailed unpaired t test.

3.10. Longer length Aβs alterations to fibrin architecture

Given that we did not observe a trend between Fbg binding strength and length of Aβ, we decided to assess if and how Aβ (1-n) altered fibrin architecture differently. We

captured ScEM images to observe the structural effects of Aβ38, 40, 42, 43, and 46 on *in vitro* fibrin clot formation. The clots were formed in the absence or presence of these Aβ (1-n) peptides (Figure 3.21). Aβ42-, Aβ43-, and Aβ46-induced clots were marginally impacted and exhibited a slightly more irregular mesh compared to the normal fibrin mesh found in control fibrin clots (without Aβ). Aβ42-induced clots showed the most irregular mesh followed by Aβ43, then Aβ46. In addition, Aβ42-clots showed areas of fibrin aggregations or clumps that were not found in the other length Aβ-induced clots. Aβ38- and Aβ40-induced clots showed no structural effect on clot fiber thickness or the presence of fibrin clumps. In summation, like our SPR Fbg binding experiment results, our ScEM results did not show a trend between length of the Aβ peptide and degree of structural perturbation in fibrin clot formation. However, our SPR and ScEM results appear to complement each other by indicating that Aβ42 has the highest Fbg binding affinity and also perturbs clot structure the most, followed by Aβ43.

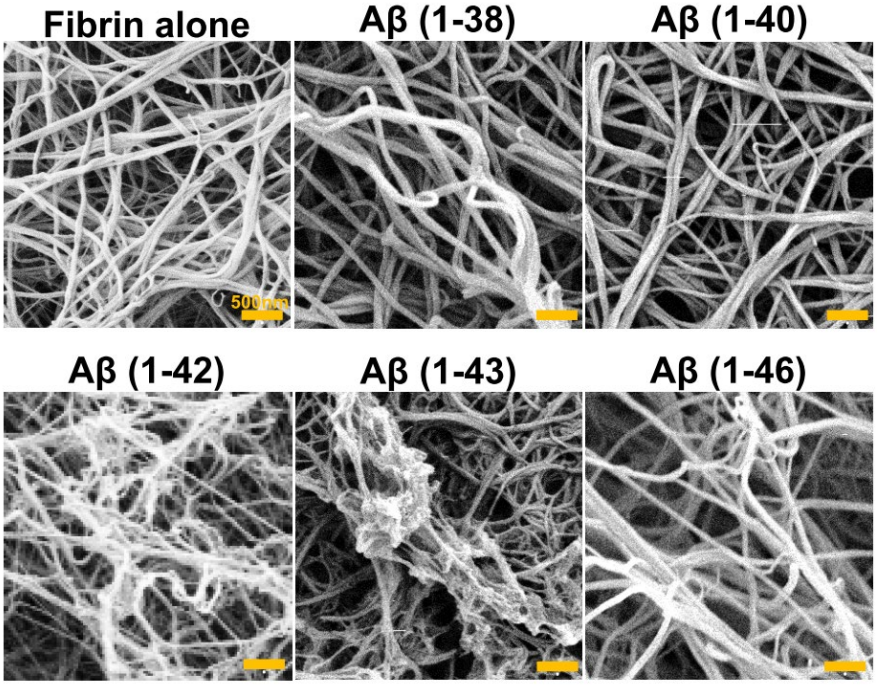

Figure 3.21. ScEM analysis of Aβ (1-n)-induced fibrin clots.
Scanning electron microscopy images of clots formed in the presence of fibrin alone (no Aβ), Aβ38, Aβ42, Aβ43, and Aβ46. Fibrin clots made in the absence of Aβ consisted of a uniform fibrin mesh as seen in previous ScEM fibrin clot analyses. Clots made in the presence of Aβ42, Aβ43, and Aβ46 consisted of a marginally irregular mesh. Degree of qualitative perturbations varied amongst these Aβ (Aβ42 > Aβ43 > Aβ46). Aβ38- and Aβ40-induced clots showed no apparent changes to fibrin mesh and/or fiber thickness. Yellow scale bar is 500nm.

3.10.1. Longer length Aβs effect on *in vitro* fibrinolysis

In lieu of clear trends in Fbg binding strength and structural effects to fibrin exhibited by Aβ (1-n), we carried out clot turbidity assays to observe if there were any trends in functional effects on fibrinolysis dependent on Aβ length (Figure 3.22). The kinetics of *in vitro* fibrinolysis of clots in the presence of Aβ (1-n) were monitored (Figure 3.22A) and showed that Aβ42 (grey curve), Aβ43 (light blue curve), and Aβ46 (orange curve)

delayed fibrinolysis relative to control buffer clots (black curve), which led to prolonged time to half lysis times (Figure 3.22B). However, there was no difference in time to half lysis times between Aβ42 and Aβ43. Aβ46 led to the significantly longest clot lysis time and time to half lysis than the shorter Aβs tested.

Clot formation/dissolution in the presence of Aβ42 and Aβ38 showed the lowest maximum turbidity or OD value (Figure 3.22C,D), yet had different degrees of shifting the turbidity curve to the right. The kinetics of clot formation & dissolution in the presence of Aβ38 showed increased variance, which may have contributed to its increased time to half lysis in our calculations. The clot kinetics exhibited by Aβ40 were similar to that of control clots and therefore did not feature increases in time to half lysis. All different length Aβs tested led to significantly lower maximum turbidity values and percent changes in maximum turbidity relative to control clots (Figure 3.22D). Overall, there was no clear trend in the length of the Aβ peptide and the degree of its delay to clot lysis/fibrinolysis. However, interestingly, our results showed that Aβ46 prolonged fibrinolysis leading to the highest time to half lysis. This result highlight the possibility of new roles for Aβ46 in cerebrovascular pathology in AD, particularly in further perturbing normal fibrinolysis at sites of CAA. Our Aβ TEM image (Figure 3.19) results indicated that both Aβ43 and Aβ46 formed more fibrillar and oligomeric structures, which may help explain their role in delaying clot lysis. Accurate amounts of Aβ43 and Aβ46 in parenchymal and vascular Aβ plaques are often not measured in cerebral histological examinations of human AD brains due to poor solubility of these longer Aβs and difficult extraction methods. It is possible that the Aβ-Fbg interaction of these longer length Aβs may play a different, but more significant role in cerebrovascular pathology in AD relative to the conventionally studied Aβ42 and Aβ40 lengths.

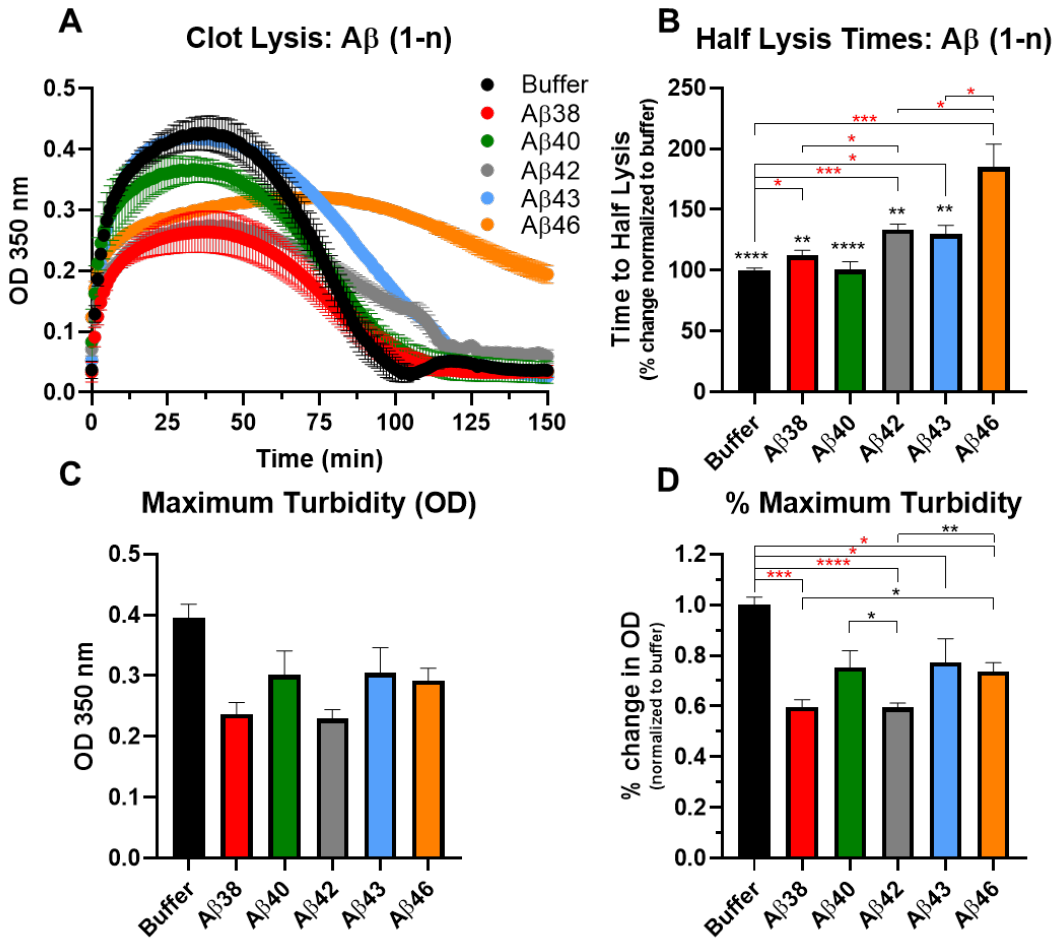

Figure 3.22. Longer length Aβs also prolong in vitro fibrinolysis.
(A) Fibrin clot turbidity and fibrinolysis differences between the various Aβ (1-n) peptides, Aβ38 (red curve), Aβ40 (green curve), Aβ42 (gray curve), Aβ43 (light blue curve), and Aβ46 (orange curve). Aβ42 and Aβ43 similarly delayed fibrinolysis shown by shifting the turbidity kinetic curve to the right compared to control buffer (no Aβ, black curve), producing (B) similar time to half lysis times. Aβ46 delayed fibrinolysis the most and had the longest time to full clot dissolution beyond the time captured in turbidity assays. Aβ46 had higher to time to half lysis than Aβ42, Aβ43, and control. (C) Maximum turbidity or optical density (OD) for clot turbidity kinetic curves for Aβ (1-n) peptides. (D) Percent change in maximum turbidity, relative to control. Aβ38- and Aβ42-induced clots had the lowest maximum turbidity values. ****p<0.0001; **p<0.01; with statistical analyses using one-way ANOVA followed by Tukey's post-hoc test. * using lines above bars, ****p<0.0001; ***p<0.01, *p<0.05; with statistical analysis using unpaired two-tailed t-test. Bar graphs represent mean ± SEM (standard error mean) of ≥3 separate experiments.

CHAPTER 4: Aβ VARIANTS FEATURE DIFFERENTIAL ACTIVATION OF tPA-MEDIATED PLASMINOGEN ACTIVATION

As mentioned in Chapter 1.5, Aβ and fibrin(ogen) can bind, stimulate tPA (94, 96), and enhance tPA-Plg activation, which, in the context of deposited vascular amyloid, could be of detriment to the integrity of cerebral vessels. Since HCAA patients are afflicted by extensive cerebrovascular pathology including severe CAA, which contains an extraordinary amount of co-deposited Aβ-Fbg in HCAA-Dutch and -Iowa brains as shown in Chapter 3.7, we tested the ability of these HCAA Aβ to enhance mediators of the proteolytic system involved in fibrinolysis. In addition, previous studies have shown that more aggregated Aβ lead to higher *in vitro* tPA-Plg activation relative to unaggregated Aβ (97).These studies could help uncover the pathogenesis intracerebral hemorrhages (ICH) in HCAA, which is the most lethal clinical feature in most HCAA disease variants.

4.1. Most HCAA Aβ mutant variants greatly stimulate and enhance Plg activation

We examined the effect of WT and HCAA-Dutch, -Iowa, and -Arctic HCAA Aβ peptides on *in vitro* tPA-mediated Plg (tPA-Plg) activation (Figure 4.1) in order to better understand how these mutant Aβ may lead to ICH. We used the same Aβ peptides as in Chapter 3 and any additional peptides (ex. Dutch-Iowa40) in this chapter (Chapter 4) were prepared using the same methods as in Chapter 2.1. All Aβ peptides were initially monomerized using HFIP and then reconstituted in 5% DMSO-Tris pH 7.4, followed by an overnight incubation at 4^0C to allow the peptides to steadily oligomerize.

To monitor tPA-Plg activation (or generation), I used enzymatic assays using a chromogenic Pn-specific substrate Pefa-5264. As shown in Figure 4.1A, Dutch42 and Iowa42 led to elevated tPA-Plg activation relative to WT Aβ42 and control buffer only (no Aβ), which can also be viewed as an increased slope/rate (Vmax) of the activity curve (Figure 4.1B). As previously reported (93, 94, 97), WT Aβ42 led to higher tPA-Plg activation compared to buffer. Iowa42 led to the highest rate of Plg activation, followed by Dutch42, and finally by WT Aβ42. When considering the Aβ40 peptides (Figure 4.1C), both HCAA Aβ40 peptides led to strikingly higher rates of tPA-Plg activation compared to WT Aβ40 (Figure 4.1D).

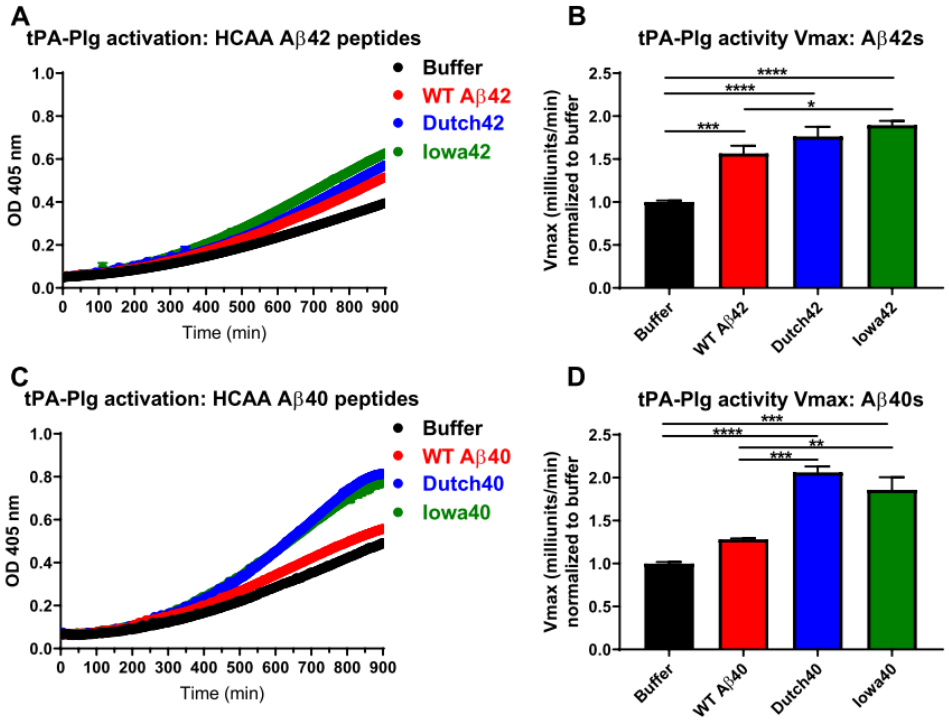

Figure 4.1. HCAA Aβ42 and Aβ40 mutant peptides further enhance tPA-Plg activation.
(A-D) tPA-mediated Plg activation were performed by mixing the various (A) Aβ42 and (C) Aβ40 (1μM) peptides or vehicle control buffer (5% DMSO-Tris), tPA (125pM), Plg (250nM), and Pn-specific chromogenic substrate Pefa-5264 (200μM). Pn generation and activity was assessed by measuring time-dependent changes in absorbance at 405 nm. (A) Dutch42 and Iowa42 had increased stimulation of tPA-Plg activation relative to WT Aβ42, also shown as an (B) increased rate of activity or Vmax for Iowa42. (C) Dutch40 and Iowa40 had strikingly increased stimulation of tPA-Plg activation relative to WT Aβ40 and (D) significantly increased activity Vmax. (****p<0.0001; ***p<0.001; **p<0.01; *p<0.05; n=3/group). Statistical analyses were performed using one-way ANOVA followed by Tukey's post-hoc test. Bar graphs represent mean ± SEM (standard error mean) of ≥3 separate experiments.

Aβ can bind and enhance tPA activity, which can lead to increased tPA-Plg activation. To further understand how Aβ is stimulating this activation, I assessed the direct effects of HCAA Aβ on individual fibrinolytic enzyme activities. I compared the effects of HCAA Aβ on the activities of Pn and tPA, using Pn specific-Pefa-5264 and tPA-specific S-2238 chromogenic substrates, respectively (Figure 4.2). Dutch42 and Iowa42 led to marginally higher tPA activity relative to WT Aβ42 (Figure 4.2A) and approximately the same rate of activity (Figure 4.2B), whereas, Dutch40 and Iowa40 led to much higher rates of tPA activity relative to WT Aβ40 (Figure 4.2C,D).

Considering the effects of HCAA Aβ on Pn activity, I observed that both Aβ42 and Aβ40 versions of Dutch and Iowa Aβ led to much higher activity (Figure 4.2E,G) and quantitatively higher rates of Pn activity (Figure 4.2F,H). In summation, our data shows that HCAA Aβs enhance tPA-Plg activation, which could be partially explained by their

influence in increasing the activity of the fibrinolytic enzymes tPA and Pn. Given the predominance of Aβ40 in vascular Aβ amyloid deposition in CAA, our results indicating that HCAA Aβ40s, Dutch40 and Iowa40, showed clear enhancements to tPA and Pn activity may have more relevance to HCAA disease pathogenesis. Overall, our data in Figure 4.1 and Figure 4.2, placed in the context of our HCAA Aβ clots lysis results (Figure 3.9), indicate that in a contradictory manner, HCAA Aβ simultaneously inhibit tPA- and Pn-mediated fibrinolysis and enhance the proteolytic activity of the same fibrinolytic enzymes in solution (tPA-Plg activation and tPA and Pn activities).

Figure 4.2. Components of the fibrinolytic system are enhanced by HCAA Aβ. The various Aβ42 and Aβ40 (1μM) peptides or vehicle control buffer (5% DMSO-Tris) were combined with (A-D) tPA (12.5nM) and the chromogenic substrate S-2288 (210μM) to monitor tPA activity; (E-H) plasmin (110nM) and the chromogenic substrate Pefa-5264 (200μM) to monitor plasmin activity. tPA and plasmin activity were assessed by measuring time-dependent changes in absorbance at 405 nm. (A,B) Dutch42 and Iowa42 led to marginal increases to tPA activity relative to WT Aβ42, while their Aβ40 counterparts, (C,D) Dutch40 and Iowa40 led to vast increases in tPA activity compared to WT Aβ40. (E-G) Both Aβ42 and Aβ40 variants of Dutch and Iowa Aβ led to significant increases to plasmin activity relative to their WT Aβ counterpart. (****$p<0.0001$; ***$p<0.001$; **$p<0.01$; *$p<0.05$; n=3). Statistical analyses were performed using one-way ANOVA followed by Tukey's post-hoc test. Bar graphs represent mean ± SEM (standard error mean) of ≥3 separate experiments.

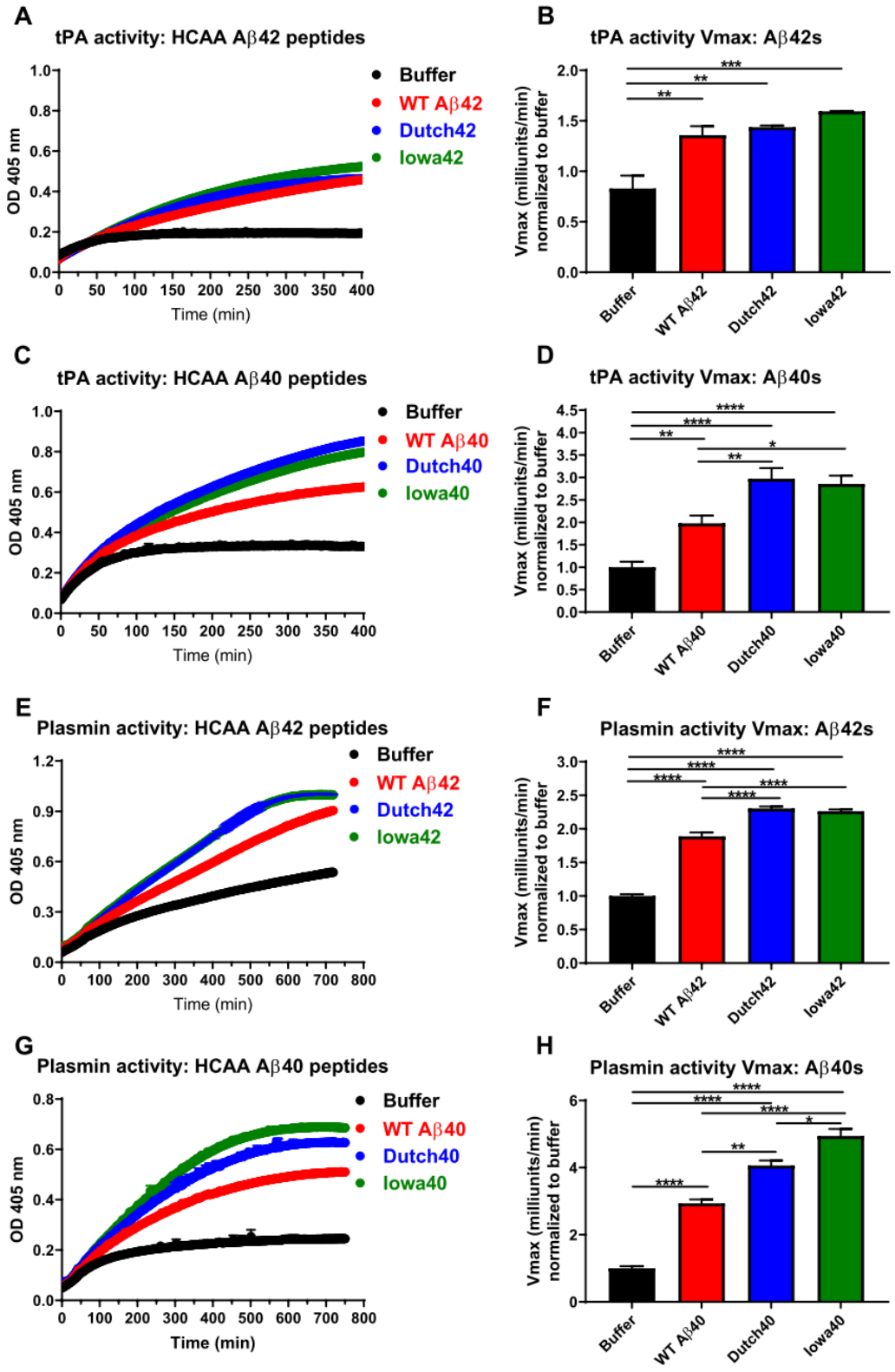
A
tPA activity: HCAA Aβ42 peptides
OD 405 nm
Time (min)
Buffer
WT Aβ42
Dutch42
Iowa42
B
tPA activity Vmax: Aβ42s
Vmax (milliunits/min) normalized to buffer
C
tPA activity: HCAA Aβ40 peptides
WT Aβ40
Dutch40
Iowa40
D
tPA activity Vmax: Aβ40s
E
Plasmin activity: HCAA Aβ42 peptides
F
Plasmin activity Vmax: Aβ42s
G
Plasmin activity: HCAA Aβ40 peptides
H
Plasmin activity Vmax: Aβ40s

I also explored the effects of HCAA Arctic (E22G) and Italian (E22K) Aβ40s on fibrinolytic enzyme activity. Although these HCAA variants have not been studied as extensively as the HCAA-Dutch and -Iowa, it is important to study these variants because they may help clarify the general trends HCAA Aβ have on delaying fibrinolysis and/or stimulating the fibrinolytic/proteolytic system. As mentioned before, the clinical features of HCAA Arctic disease stands apart from HCAA-Dutch, -Iowa, and -Italian because Arctic-carriers do not present with ICH. Like most HCAA Aβ, Arctic and Italian Aβ also demonstrate increased fibrillization propensity with enhanced protofibril formation(89, 115), which could contribute to increased stimulation of the tPA-Plg fibrinolytic system. I also decided to analyze a double mutant Aβ40 peptide containing both Dutch- and Iowa-specific amino acid substitutions (Dutch-Iowa40) since I previously observed that Dutch and Iowa40 lead to striking stimulation of fibrinolytic enzymatic activity. Clot turbidity analysis also showed that Dutch-Iowa40 delays fibrinolysis (data not shown).

I monitored the effects of Arctic40 and Italian40 on tPA-Plg activation/generation, Pn activity, and tPA activity (Figure 4.3). Dutch40 led to the higher tPA-Plg activation, followed by the double mutant peptide, Dutch-Iowa40 (Figure 4.3A). Arctic40, WT Aβ40, and Italian40 similarly enhanced tPA-Plg activation. All Aβ40 peptides tested led to significantly increased tPA-Plg activation compared to control buffer (no Aβ). Considering the effects on Pn activity (Figure 4.3B), Dutch-Iowa40 led to the highest activity followed by Arctic40 and Italian40. Dutch40 and Iowa40 had similar effects on Pn activity. WT Aβ40 had the smallest effect on Pn activity, which was still higher than control buffer only. Considering the effects on tPA activity, Italian40 had the highest effect on tPA activity, followed by Dutch-Iowa40 (Figure 4.3C). Both Dutch40 and Iowa40 had similar effects on tPA activity. Arctic40 and WT Aβ40 had the smallest effect on tPA activity compared to the rest of the Aβs tested. These results indicate that Dutch40 lead to increased tPA-Plg activation, consistent with my previous observation in Figure 4.1, and enhanced stimulation of the fibrinolytic enzyme activity relative to WT Aβ40. However, Arctic40 and Italian40 exhibit differential effects: Arctic40 has increased effects on Pn activity only, Italian40 has increased effects on both Pn/tPA activity, yet both Aβs do not increase tPA-Plg activation relative to WT Aβ40.

These findings suggest that the lower effects on fibrinolytic enzyme activity featured by Arctic40 may the basis of understanding why there is a lack of ICH in Arctic-carrier patients. One confounding finding was that Italian40 exhibited a lack of increased *in vitro* tPA-Plg activation because the clinical features of HCAA-Italian disease includes frequent small- and large-scale ICH. The limitation of these *in vitro* enzymatic assays using purified protein and enzymes may be masking the physiological role these mutant HCAA Aβ40 peptides have on fibrinolytic enzyme activity.

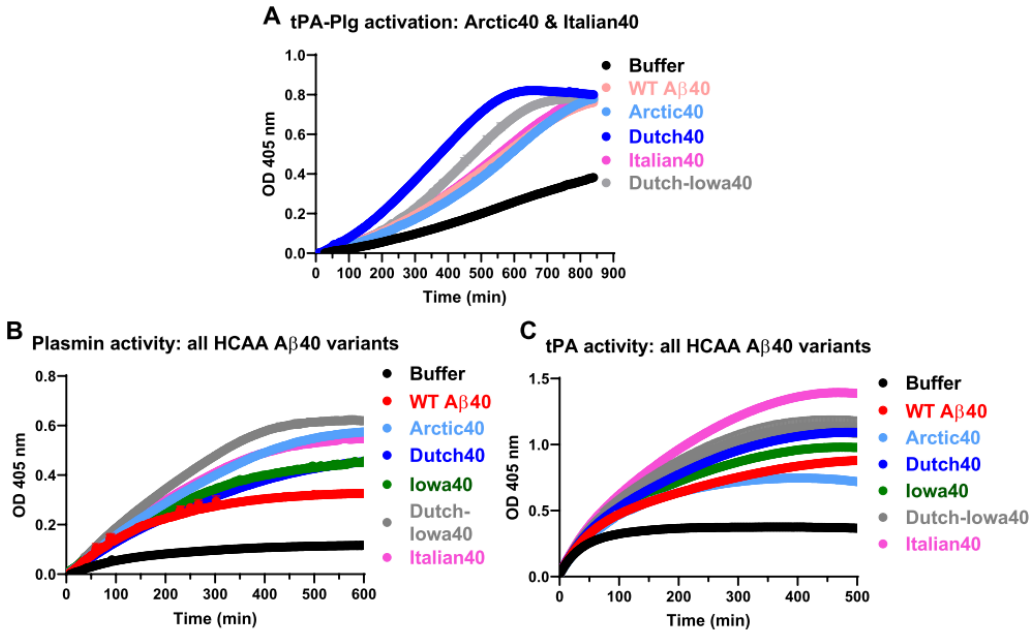

Figure 4.3. A few HCAA Aβ40 variants exhibit differential effects on fibrinolytic enzymatic activity.
The various HCAA Aβ40 (1μM) peptides or vehicle control buffer (5% DMSO-Tris) were combined with either (A) tPA (125pM), Plg (250nM), and Pn-specific chromogenic substrate Pefa-5264 (200μM) to monitor Plg generation; (B) plasmin (110nM) and Pefa-5264 (200μM); (C) tPA (12.5nM) and the chromogenic substrate S-2288 (210μM) to monitor tPA activity; (A) Dutch40 and the double-mutant peptide Dutch-Iowa40 led to increases in tPA-Plg activation and/or plasmin generation relative to WT Aβ40. Arctic40, Italian40, and WT Aβ40 had similar levels of tPA-Plg activation, which was still elevated compared to control buffer only. (B) Most HCAA Aβ40 peptide variants led to increases to plasmin activity compared to WT Aβ40. (C) Excluding Arctic40, most HCAA Aβ40 peptides led to higher tPA activity relative to WT Aβ40. Kinetic graphs showing enzyme activity represent mean ± SEM (standard error mean) bars of ≥3 separate experiments.

4.2. HCAA Dutch and Iowa Aβ lead to more Plg activation in healthy control human plasma

Due the observed varied differential effects of Arctic40 and Italian40 on fibrinolytic enzyme activity (Figure 4.3) that did not follow the trends established by Dutch40, Iowa40, and the Dutch-Iowa40 peptides and the possible limitation of the *in vitro* tPA/Pn/tPA-Plg enzymatic assays, I decided to use a more physiologically method to assess fibrinolytic enzyme activity. I quantified the amount of Plg activation by SDS-PAGE and Western blot (WB) analysis using control sodium-citrated healthy human plasma (Figure 4.4) incubated in the absence or in the presence of the various HCAA Aβ40s for different lengths of time. I probed for the Plg band (~100 kDa) using a Plg-specific polyclonal antibody (described in Chapter 2.14). Our initial experimentation used plasma simply incubated with the Aβs, collected at 0- and 36-hour timepoints (Figure 4.4A). However, I noticed that Aβ-incubated plasma even incubated after 36 hours did not show signs of Plg activation, which is indicated by the diminishment of the Plg band as it is converted into plasmin (~80 kDa). This might have been occurring due

to the lack of active tPA, which may have been affected by the sodium citrate anti-coagulant in solution and plasma freeze-thaw cycle. Therefore, in order to restore tPA activity in the human plasma, I proceeded to add exogenous purified human tPA to Aβ-incubated plasma and collected various timepoints (0-hr, 12-hr, and 36-hrs), which I then analyzed by WB (Figure 4.4B). I used 3 different human healthy control plasma for each Aβ. At the 0-hr (top half of Figure 4.4B) and 12-hr (data not shown) timepoints of collection, all the various Aβ-incubated plasmas showed similar levels of intact Plg, which is a proxy for the level of Plg activation. Differences in levels of Plg present, was observed at the 36-hr timepoint (bottom half Figure 4.4B) and was quantified in the bar plot in Figure 4.4C. WT Aβ40 and Arctic40 led to minimal changes to Plg levels, indicating that they led to minimal Plg activation, which were similar to control buffer (no Aβ). However, Dutch40, Iowa40, Dutch-Iowa40, and Italian40 peptides led to more diminishment of the Plg band in our blot, indicative of more Plg activation or Pn generation relative to WT Aβ40. Dutch-Iowa40 led to the highest enhancement of plasma tPA-Plg activation. The order of Aβ that led to the most to least enhancement of tPA-Plg activation in human plasma is as follows: (Dutch-Iowa40 > Iowa40 > Italian40 > Dutch40 > Arctic40 ≥ WT Aβ40). Pn, the lower molecular weight band (~80 kDa) in our Plg-probe, was also present at the 36-hr timepoint across all groups (Figure 4.4B), but was highest for Aβ groups that led to more tPA-Plg activation. However, levels of the Pn band did not correlate precisely with the degree of Plg band diminishment (Plg activation), therefore, it was not quantified. Our results indicate that Dutch-Iowa40 and Iowa40 led to significantly higher tPA-Plg activation compared to WT Aβ40 and Arctic40.

Due to the variances in Plg activation among the 3 different human control plasmas, our one-way ANOVA analysis (Figure 4.4C) may have not shown statistical differences among specific Aβ40 groups. In order to address this, I also compared various Aβ40s to Arctic40 using two-tailed unpaired t test statistical analysis (Figure 4.4D). Dutch40 and Italian40 demonstrated an increased trend in Plg activation compared to Arctic40. Overall, our results point to most HCAA Aβ40 peptides further stimulating and enhancing tPA-Plg activation in human plasma. Arctic40 appears to be an exception to this trend, where it minimally affects tPa-Plg activation. In this manner, these results may be more physiologically relevant than the results obtained using only *in vitro* enzymatic assays with purified proteins (Figure 4.3).

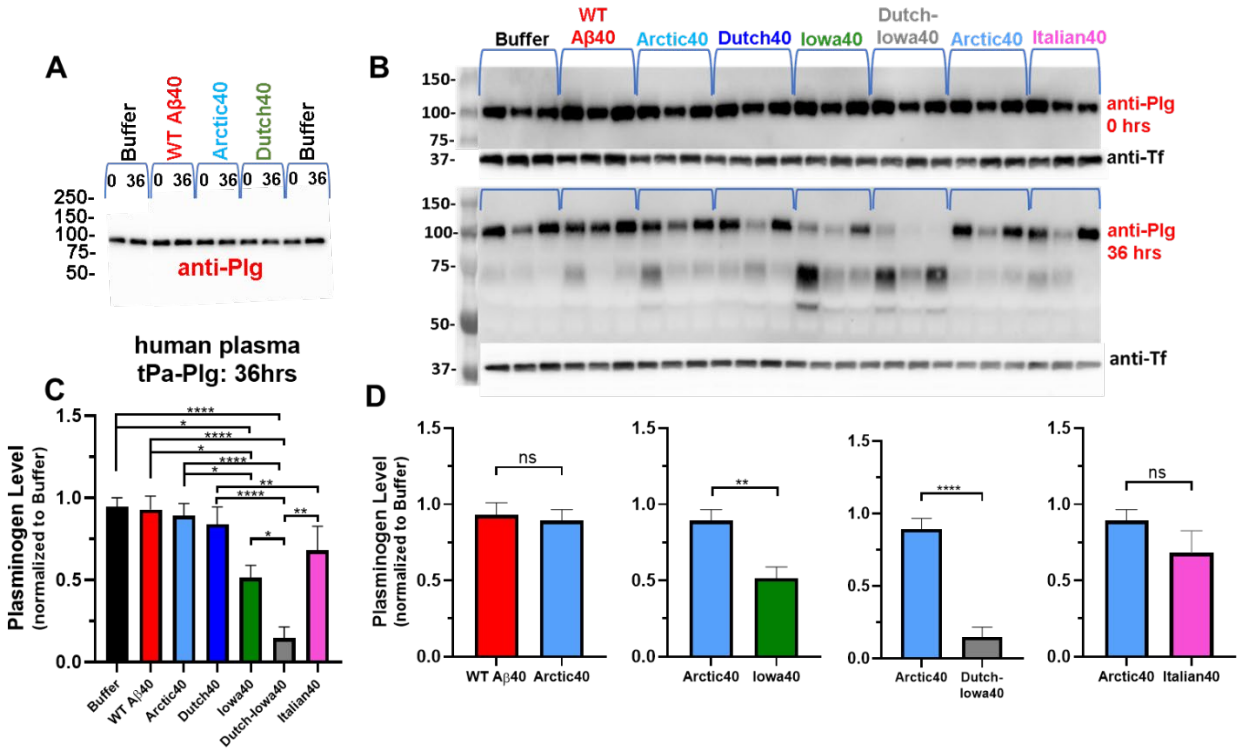

Figure 4.4. Most HCAA Aβ40 mutant peptides demonstrate higher tPA-Plg activation in normal human plasma relative to WT Aβ40.
The various HCAA Aβ40 (4μM) peptides or vehicle control buffer (5% DMSO-Tris) were mixed, incubated in 20-fold diluted sodium-citrated-treated human plasma of 3 different healthy control individuals (A) without exogenous tPA or (B) with exogenous tPA (125pM) in order to assess tPA-mediated Plg activation. 0-hr (no incubation), 12-hr, and 36-hr timepoints were collected deactivated & denatured and analyzed by SDS-PAGE and WB analysis probing for plasminogen (~100 kDa) using a Plg-specific antibody (anti-Plg). (A) WB analysis of Aβ-incubated plasma without exogenously added tPA did not show changes to Plg levels (~100 kDa band) even after 36 hours of incubation. (B) WB analysis of Aβ-incubated plasma with exogenously added tPA; Dutch-Iowa40, Iowa40, Italian40, and Dutch40 led to further decreases in intact Plg, an indicator of Plg activation, and increases in plasmin generation (~80 kDa). (C) Intact Plg quantification of 36-hr Aβ-incubated plasmas (normalized to transferrin and control buffer group) showed that Dutch-Iowa40, Iowa40, and Italian40 had the lowest amount of intact Plg relative to WT Aβ40 and Arctic40. (D) Comparison of the effects of various Aβ40s to Arctic40 via two-tailed unpaired t-tests showed that, unlike the other HCAA Aβ40s, Arctic40 did not lead to more tPA-Plg activation in human plasma. (****p<0.0001; ***p<0.001; **p<0.01; *p<0.05; n=3). ns (not significant) =p>0.05. Statistical analyses were performed using one-way ANOVA followed by Tukey's post-hoc test and two-tailed unpaired t-tests. Bar graphs represent mean ± SEM (standard error mean).

4.3. Longer length Aβs enhance tPA-Plg activation, Pn activity, and tPA activity

I also explored the connection between the length of the Aβ peptide and the ability to stimulate the fibrinolytic/proteolytic system. I examined the effects of Aβ (1-n), including Aβ38, Aβ40, Aβ42, Aβ43, and Aβ46 on *in vitro* tPA-Plg activation (Figure 4.5A,B) and

direct effects on Pn (Figure 4.5C,D) and tPA (Figure 4.5E,F) enzyme activity using enzymatic chromogenic assays as employed in Figure 4.1. Most of the Aβs tested led to stimulation of tPa-Plg activation compared to control buffer only (no Aβ present). However, Aβ38 and Aβ46 led to the highest tPA-Plg activation and highest rate of tPA-Plg activation (Figure 4.5B). Aβ43 and Aβ42 led to similar enhanced tPA-Plg activation. Aβ40 did not lead to enhancements in tPA-Plg activation compared to control buffer. The order of Aβ length, from highest to lowest enhancements of tPA-Plg activation: (Aβ38>Aβ46>Aβ43>Aβ42> Aβ40).

Considering the effects on Pn activity, Aβ42 led to the highest activity followed by Aβ43 and Aβ46. There were significant differences in rates of Pn activity between most Aβs, except a few Aβ peptide pairs (demonstrated in bar plot as not significant (ns) (Figure 4.5D)). Aβ40 did not increase Pn activity relative to buffer. Dutch40 and Iowa40 had similar effects on Pn activity. The order of Aβ length, from highest to lowest enhancements to Pn activity: (Aβ42>Aβ43≥Aβ46>Aβ38> Aβ40).

All the Aβs tested led to enhancements to tPA activity (Figure 4.5E). Aβ46, Aβ43, and Aβ42 similar higher activity compared to the shorter Aβs. Similar to the effects on Pn activity, there were significant differences in rates of tPA activity between most Aβs, except a few Aβ peptide pairs (demonstrated in bar plot as not significant (ns) (Figure 4.5F)). Although Aβ42 led to similar rates of tPA activity as Aβ43 and Aβ46, its initial tPA activity curve had a higher slope or Vmax. WT Aβ38 and Aβ40 had the smallest effect on tPA activity, which was still higher than control buffer only The order of Aβ length, from highest to lowest enhancements to tPA activity: (Aβ42>Aβ43≥Aβ46>Aβ38> Aβ40).

These results show that there is not a clear trend between length of Aβ and degree of enhancements to tPA-Plg activation and fibrinolytic enzyme activity. However, it was interesting to observe that Aβ38 led to much higher tPA-Plg activation followed by Aβ46. This pattern resembles their peptide aggregation profile qualitatively assessed by TEM imaging (Figure 3.19), which showed that Aβ38 and Aβ46 peptides had increased protofibrillar and oligomeric structures compared to Aβ42 and Aβ43. Their increased fibrillization capacity suggest there is more β-sheet formation, which may enhance their binding and activation of both tPA and Plg in a concerted manner. This may explain why relative to Aβ42, Aβ38 and Aβ46 led to clear increases in stimulation of tPA-Plg, but not Pn or tPA activity independently.

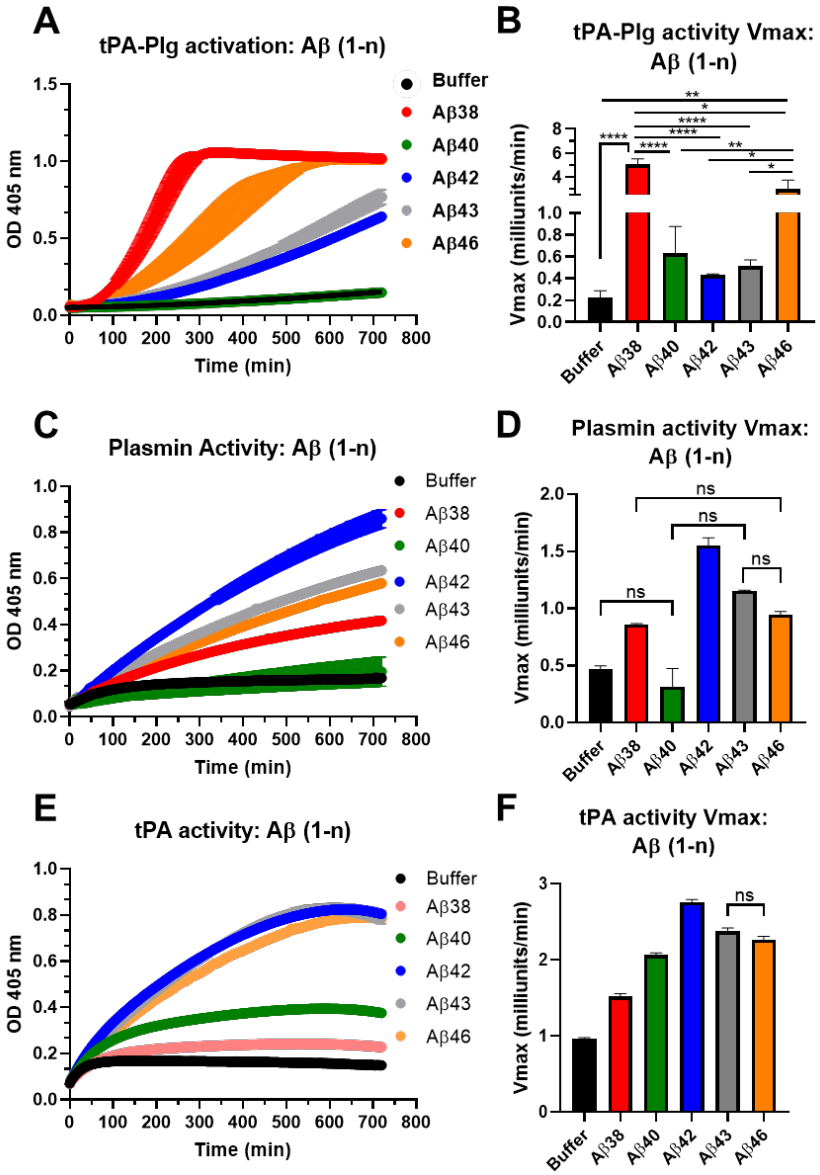

Figure 4.5. Differential effects of Aβ (1-n) on fibrinolytic enzymatic activity. The various Aβ (1-n) (1μM) peptides or vehicle control buffer (5% DMSO-Tris) were combined with either (A,B) tPA (125pM), Plg (250nM), and Pn-specific chromogenic substrate Pefa-5264 (200μM) to monitor Plg generation; (C,D) plasmin (110nM) and Pefa-5264 (200μM); (E,F) tPA (12.5nM) and the chromogenic substrate S-2288 (210μM) to monitor tPA activity; (A) Aβ38 and Aβ46 led to increases in tPA-Plg activation and (B) increased rates of activity or Vmax relative to the other length Aβs. Aβ42 and Aβ43 has similar effects on tPA-Plg activation. (C) Aβ42 led to highest Pn activity, also shown as (D) a high rate of Pn activity (Vmax). (E) Aβ42, Aβ43, and Aβ46 led to similarly elevated tPA activity and led to (F) approximately equal rates of tPA activity (Vmax). Aβ40 had the lowest stimulatory effect across the 3 fibrinolytic enzyme activity assessments (tPA-Plg activation, Pn activity, and tPA activity). (****$p<0.0001$; **$p<0.01$; *$p<0.05$; n=3). ns (not significant) =$p>0.05$. Statistical analyses were performed using one-way ANOVA followed by Tukey's post-hoc test. Bar graphs represent mean ± SEM (standard error mean) of ≥3 separate experiments.

I also assessed the ability of Aβ (1-n) to stimulate tPA-Plg activation using normal human plasma using the same methods as in Figure 4.4. Exogenous tPA was added to plasma, which was then incubated in the absence of Aβ or in the presence of the various Aβ (1-n) peptides for different lengths of time. 0-hr, 12-hr, and 36-hr timepoints were collected and analyzed by SDS-PAGE and WB analysis (Figure 4.6A). We quantified the levels of intact Plg (~100 kDa), as an indicator of Plg activation (Figure 4.6B). Lower levels of intact Plg would be indicative of more Plg activation. Aβ46-incubated plasma collected at the 36-hr timepoint had the lowest intact Plg (Figure 4.6A), therefore had the highest tPA-Plg activation in human plasma (Figure 4.6B), followed by Aβ38. Aβ42 and Aβ43 had marginally more plasma Plg activation compared to control buffer alone (no Aβ). Curiously, Aβ40 had the most intact Plg, suggesting that the buffer alone was able to stimulate tPA-Plg activation in human plasma compared to the Aβ40 peptide, which is reconstituted in the same buffer (5% DMSO-Tris, pH 7.4). Our results indicate that Aβ46 and Aβ38 led to increased stimulation of tPA-Plg both in our purified enzymatic chromogenic assays (Figure 4.5) and in human plasma, which is more physiologically relevant.

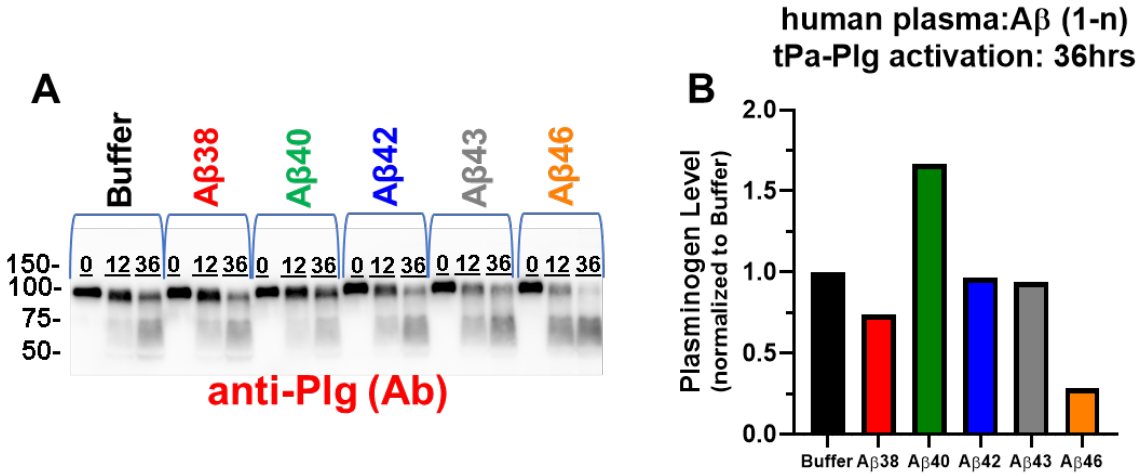

Figure 4.6. Longer length Aβ46 featured a higher trend in tPA-Plg activation in normal human plasma.
The various Aβ (1-n) (4μM) peptides or vehicle control buffer (5% DMSO-Tris) were mixed, incubated in 20-fold diluted human sodium-citrated plasma exogenous tPA (125pM) in order to assess tPA-mediated Plg activation. 0-hr (no incubation), 12-hr, and 36-hr timepoints were collected deactivated & denatured and analyzed by SDS-PAGE and WB analysis probing for plasminogen (~100 kDa). (A) Aβ46 further decreased intact Plg and increased plasmin generation (~80 kDa), followed by Aβ43 and Aβ38. (B) Intact Plg quantification (normalized to control buffer group) of 36-hr Aβ-incubated plasmas showed that Aβ46 had the lowest amount of intact Plg, while Aβ38, Aβ42, and Aβ43 showed similar levels. Aβ40 demonstrated much higher levels of intact Plg, even more than control buffer.

4.4. Aβs' role in "enzymatic approximation effect" in tPA-Plg activation

As mentioned in Chapter 1.5, Aβ can have functional mimicry to replace fibrin, bind, stimulate tPA (94, 96), and enhance the catalysis tPA-Plg activation. Akin to fibrin, Aβ's β-sheet structure in its oligomeric and/or aggregated state may be functioning as a

network of fibrin fibers, which can also act as a scaffolding template onto which tPA and Plg bind and co-localize. Consequently, the catalysis of tPA's conversion of Plg into Pn is enhanced due to Aβ's ability to bring these enzymes closer together. This effect is known as catalysis by approximation or enzymatic approximation effect (95). In order to better understand how the Aβs tested in this thesis led to increases in tPA-Plg activation, I carried out *in vitro* tPA-Plg activation enzymatic assays using various concentrations of Plg (Figure 4.7). I tested tPA-Plg activation in the presence or absence of WT Aβ42 at increasing concentrations of Plg (Figure 4.7B-F). At the lowest Plg concentration, tPA-Plg activation in the presence of Aβ42 is much higher than control buffer (no Aβ), whereas the difference between WT Aβ42 and buffer gradually diminishes as Plg concentration increases and is completely abolished at the highest Plg concentration tested, 4000 nM (Figure 4.7F). These results suggest that by increasing Plg's concentration, we are eliminating the necessary scaffolding template effect Aβ42 is providing to bring tPA and Plg closer together to enhance tPA's catalysis of conversion of Plg into Pn. Therefore, it is likely that the Aβs tested in *in vitro* tPA-Plg activation assays potentiate Pn generation via enzymatic approximation effect.

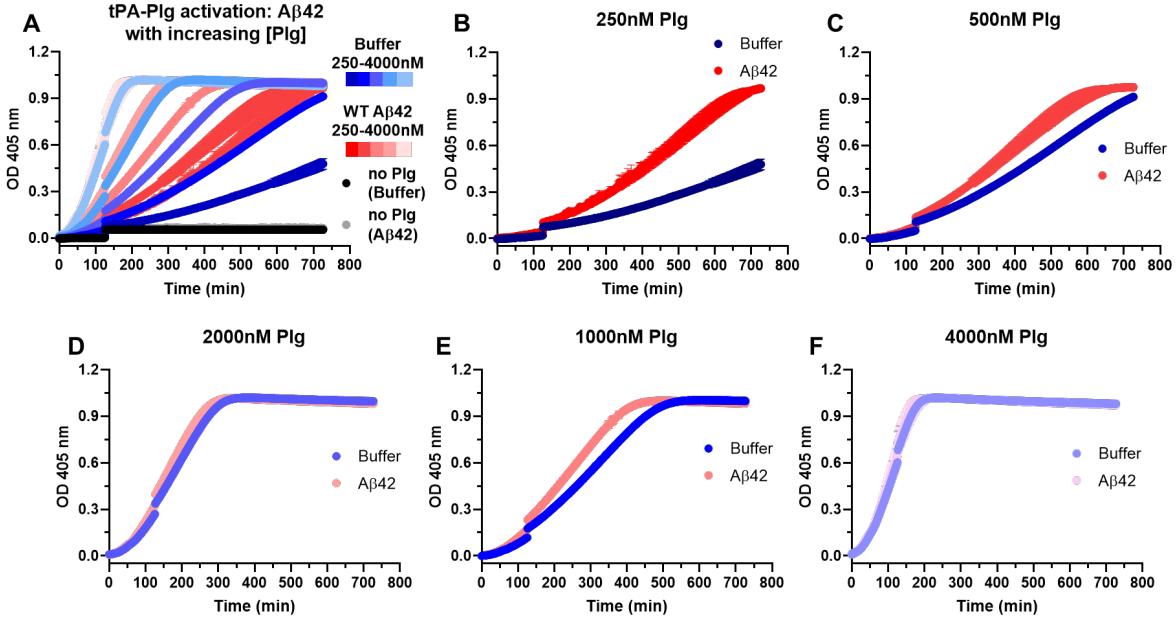

Figure 4.7. Increasing Plg concentration abolishes WT Aβ42-induced stimulation of in vitro tPA-Plg activation.
(A) In dose-dependent manner, various concentrations of purified human Plg (250-4000nM) were mixed with either WT Aβ42 (1μM) peptide or vehicle control buffer (5% DMSO-Tris) in solution with tPA (125pM) and Pn-specific chromogenic substrate Pefa-5264 (200μM) to monitor Pn generation. Overall, across the Plg concentrations used, WT Aβ42 (shades of red curves) led to higher tPA-Plg activation compared to control buffer only (shades of blue curves). (B-F) Same data as (A) but shows tPA-Plg activation between WT Aβ42 and control buffer at single Plg concentrations. (B,C) At lower Plg concentrations, differences in tPA-Plg activation between WT Aβ42 and buffer are evident, however, at (D-F) higher Plg concentrations, this differences is abolished. tPA-Plg activation kinetic graphs represent mean ± SEM (standard error mean) bars of ≥3 separate experiments.

Our results indicate that the longer length Aβ46, and, unexpectedly, the shorter Aβ38 lead to increases in tPA-Plg activation relative to the conventionally studied “normal” length WT Aβ42. One explanation for these enhanced stimulatory effects on tPA-Plg activation could be that these Aβs have assume more aggregated states, as examined by our TEM analysis, relative to WT Aβ42. The increased aggregation state and fibrillization capacity of these peptides could be further enhancing the enzymatic approximation effect featured by Aβ.

To address this possibility, I explored if and how increasing Plg concentration would abolish enhancement of tPA-Plg activation in the presence of Aβ46 relative to shorter Aβ. I examined the effects of Aβ40 and Aβ46 on *in vitro* tPA-Plg activation using low Plg (250nM) and high Plg (2000nM) concentrations (Figure 4.8). Congruent with previously observed results, Aβ40 had minimal effects on tPA-Plg activation relative to control buffer alone (no Aβ) at low and high Plg concentrations (Figure 4.8A). As expected, Aβ46 led to higher tPA-Plg activation at lower Plg concentrations, however, at higher Plg concentrations, the difference between Aβ46 and buffer alone was insignificant (Figure 4.8A). These result suggest that Aβ46 features enhanced enzymatic approximation effect in tPA-Plg activation relative to Aβ40.

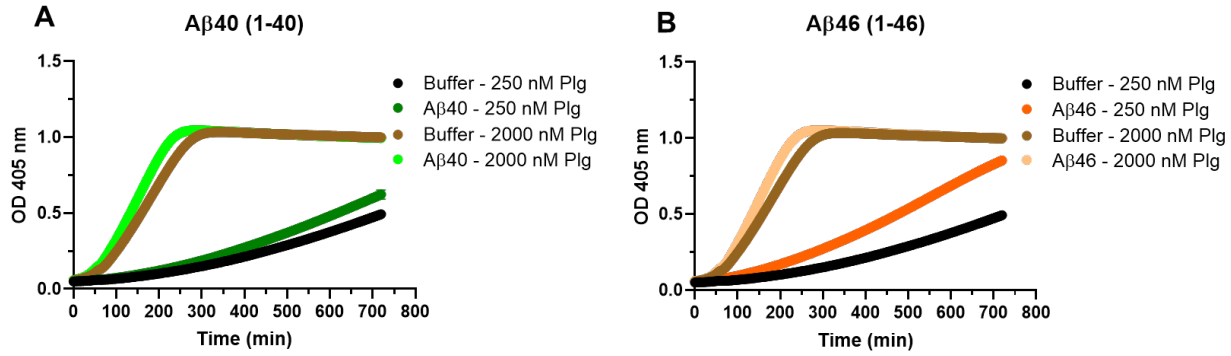

Figure 4.8. Increasing Plg concentration also abolishes the more aggregation prone WT Aβ42-induced stimulation of in vitro tPA-Plg activation.
250nM and 2000nM Plg were incorporated into reactions with either (A) Aβ40 (1μM) or (B) Aβ46 (1μM) peptide or vehicle control buffer (5% DMSO-Tris) in solution with tPA (125pM) and Pn-specific chromogenic substrate Pefa-5264 (200μM) to monitor Pn generation. (A) Aβ40 showed minimal effects in tPA-Plg activation are minimal at low (250nM) and high (2000nM) Plg concentrations relative to control buffer. (B) Aβ46 led to increased tPA-Plg activation only at low, but now high Plg concentration relative to control buffer. tPA-Plg activation kinetic graphs represent mean ± SEM (standard error mean) bars of ≥3 separate experiments.

To further test the hypothesis that an increase in the aggregation or fibrillization properties of Aβ could enhance its ability to act as a scaffolding template and bring tPA and Plg closer together for catalysis (enzymatic approximation effect), it would be crucial to test various Aβs with different aggregation profiles. Ideally, HCAA Aβ should be tested in fibrinolytic enzyme activity assays using various Plg concentrations to assess their role in increasing the enzymatic approximation effect on tPA-Plg activation.

CHAPTER 5: DISCUSSION

5.1. Overview

In this thesis, I highlighted the ability of HCAA Aβ to interact and affect the function of vital components of hemostasis, including fibrin(ogen) and fibrinolytic/proteolytic enzymes. I extended the probe of unique Aβs that may be important in the development of cerebrovascular pathology to longer length Aβs, with special emphasis on Aβ46. These findings provide an avenue through which we can better understand the etiology and pathogenesis of the main pathologies found in most HCAA disease variants, namely CAA and ICH, and CAA-related pathology in AD. The findings also underscore the new role for fibrin(ogen) in HCAA disease, which may mechanistically interconnect CAA and ICH pathophysiologies in HCAA.

5.2. HCAA-linked Aβs' strong interaction with fibrin(ogen) and alteration to fibrin(ogen) structure and function

WT Aβ-fibrin(ogen) structurally and mechanistically alter the architecture of the fibrin network and make fibrin clots Pn-resistant (64, 65). Results in Chapter 3 extend our understanding of the Aβ-fibrin(ogen) interaction by probing the interaction between HCAA Aβ and fibrin(ogen). Our *in vitro* findings show that the presence of Dutch- and Iowa-mutant Aβs lead to the formation of fibrin clots that are more structurally altered (Figure 3.7) and more resistant to Pn-mediated fibrinolysis compared to WT Aβ-induced clots (Figure 3.9). These findings may be explained by the fact that mutant Dutch- and Iowa-Aβ42 and -Aβ40 have stronger binding affinities for Fbg compared to both WT Aβ42 and WT Aβ40, respectively (Figure 3.2). While the Aβ40:Aβ42 ratio is elevated in CAA (16, 21), because there is still considerable levels of Aβ42 in CAA deposits (116, 117), we often included both HCAA Aβ variant lengths.

The increased binding affinity between HCAA Aβs (Dutch and Iowa (Figure 3.4) and Arctic Aβ (Figure 3.17)) and Fbg may be explained by the increased aggregation propensity featured by the mutant Aβs reported in the literature (89) and as seen in our TEM analysis of Aβ peptides (Figure 3.4). Our assessment whether an increased aggregated state in Aβ would increase its binding for Fbg (Figure 3. 6) indicated that an aggregated Aβ42 peptide with a more proto-fibrillar structure did not have an increased binding affinity to Fbg compared to less aggregated Aβ42. In addition, our SPR Fbg binding results for Dutch40 and Iowa40 further drive the point that differences in the aggregation state alone of Aβ is not enough to dictate Fbg binding strength. Given that SPR response signal is known to be directly proportional to the change in bound analyte (Aβ) to the ligand (Fbg), the SPR response curves for Iowa40 were higher compared to Dutch40 (Figure 3.4E,F) at similar peptide concentrations most likely because Iowa40 aggregated into larger protofibrils compared to Dutch40 (Figure 3.4E,F). However, Dutch40 and Iowa40 had comparable binding affinities to Fbg, 12 ± 2.4nM and 6.8 ± 2.3nM, respectively, that are not statistically different. Taken together, our results indicate that while the aggregation state of the HCAA Aβ or WT Aβ may have an influence in its binding affinity to Fbg, it seems that is it not the sole factor in determining Fbg binding strength. It is possible that the amino acids substitutions in the Dutch-, Iowa-, Arctic-Aβ peptides may have a larger influence in their interaction with Fbg.

The possible mechanisms through which HCAA Aβs perturb clot structure and fibrinolysis are likely similar to as WT Aβ42's perturbation on clot structure and lysis (64). In non-HCAA AD patient cases, WT Aβ42 contributes to cerebrovascular pathology, CAA formation, and delays fibrinolysis by binding to two regions; the C-terminus of the β-chain of fibrinogen near the b-hole (63), and to a region of the αC-region of fibrinogen (Aα239-421)(67). This αC region of fibrinogen is known to bind plasminogen and includes Pn cleavage sites(68). The higher binding affinity of the mutant HCAA Aβs, specifically Dutch and Iowa Aβ peptides, to fibrin(ogen) may further impede plasmin(ogen) binding and access of tPA and plasmin(ogen) to fibrin clots, which can contribute to the increases in time to half-lysis times compared to WT Aβ (Figure 3.9C,D). Stronger binding to the region close to the b-hole of fibrinogen may further impair lateral aggregation of fibrin protofibrils(63) and can result in the observed Dutch- and Iowa-Aβ induced clot structures that are more irregular and have more gaps (Figure 3.7), thus also lowering the maximal OD as observed in the clot lysis kinetic curves (Figure 3.9A,B).

Although, Dutch and Iowa Aβ show similar interactions with fibrin(ogen), in terms of binding affinity, effects on fibrin clot structure, and effects on clot lysis, there are nuanced differences between the mutant Aβ peptides that should be noted. Differences in clot structure induced by Dutch40 (Figure 3.7E), compared to Iowa40's effect (Figure 3.7F), include qualitatively different fibrin clumps with a rosette-like appearance, more aggregates, and thinner fibers (Figure 3.7I,K). Possible reasons for these differences in fibrin clot perturbation includes differences in the Aβ aggregation profile and changes to the stoichiometry between WT and HCAA Aβ peptides for fibrin(ogen) (64, 67). Our TEM analysis of the structure of the oligomeric and proto-fibrillar forms of Aβ peptides (Figure 3.4) shows that while Iowa42 and Dutch42 peptides both have short proto-fibrillar forms, Dutch40 and Iowa40 peptides differ. Iowa40 peptide shows increased elongated proto-fibrils compared to Dutch40's aggregation pattern. Differences in aggregated peptide structures between Dutch40 and others Aβs could account for the differences in which they can affect fibrin clot structure. In addition, HCAA mutant Aβs may have additional binding regions within fibrin(ogen), which could lead to altered molar Aβ-Fbg stoichiometries, thus sleading to differential effects on clot structure.

Mutant Italian Aβ40 (E22K/E693K) found in HCAA-Italian disease (112), another autosomal dominant early-onset Aβ-type HCAA variant that clinically presents with severe CAA and ICH, was also investigated. There is no animal model for this HCAA variant. Its effect on clot lysis (Figure 3.18) was congruent with Dutch40 and Iowa40's effects. Dutch40, Iowa40, and Italian40 led to further prolongation of clot lysis relative to WT Aβ40. Although, we did not resolve Italian40's binding affinity for fibrin(ogen), its increased aggregation propensity (112, 114), its amino acid substitution at the same site as Arctic and Dutch Aβ (Figure 1.1) in a key Fbg-binding region (67), allows us to predict that it also binds strongly to Fbg.

5.3. The overlapping role of WT- and HCAA-linked Aβs and fibrino(gen) interaction in cerebral co-deposition AD and HCAA

My results in Chapter 3.7, show high levels of mutant Aβ-fibrin(ogen) co-deposition in HCAA-Dutch and -Iowa patient post-mortem occipital brain tissue, especially at cerebral blood vessel sites with a high burden of CAA pathology, which may be explained by the

stronger interaction between HCAA Aβ and fibrin(ogen) observed in binding, clot structure, and function. Our immunofluorescence (IF) analysis of HCAA patient brains (Figure 3.13 and Figure 3.14) helped corroborate the physiological relevance of our *in vitro* findings showing stronger interactions between mutant HCAA Aβ, specifically their oligomeric form, and fibrin(ogen). While, this strong interaction can occur throughout the brain, wherever there is CAA pathology, the brain area that we decided to compare among the three human groups (HCAA-Dutch, EOAD, and ND groups are described in Table 3.1) was the occipital cortex. Occipital brain tissue was selected based on the known predilection of CAA for posterior regions, including the occipital lobe (24, 25). This occipital localization is found in both sporadic CAA patients and in AD patients with concurrent CAA, with increasing occipital vascular involvement with increasing AD pathology (24). In the case of HCAA, vascular deposits also start in the occipital lobe, but in advanced cases all brain regions are involved (5, 11). It is important to note that although, in HCAA, similar to sporadic CAA, the Aβ40:Aβ42 ratio is elevated in vascular amyloid deposition (16, 21), Aβ42 is still a major component of CAA deposits(116, 117).

Our analysis of Aβ and fibrin(ogen) co-localization in human HCAA patient brains highlight the role the aggregated state of Aβ has in AD vascular pathology. In our analysis, the use of Congo Red detected highly aggregated and congophillic Aβ at Aβ parenchymal plaques and CAA sites in HCAA and EOAD patients, however, there was no distinction in Aβ deposit levels between the two groups (Figure 3.13C). In contrast, by using NAB61, we were able to reveal much higher levels of Aβ oligomers in HCAA-Dutch brains compared to EOAD brains, especially at sites of CAA (Figure 3.14B). Further stratification of our IF analyses based on vessel size indicated that there were different patterns of congophillic Aβ deposits in HCAA-Dutch and EOAD brains across larger (Figure 3.15A-E) and smaller (Figure 3.15F-J) vessels. In HCAA-Dutch brains, smaller vessels contained much lower congophillic Aβ deposits (Figure 3.15G) compared to EOAD brains, which is characteristic of HCAA-Dutch CAA pathology (39). EOAD brains also contained abundant CAA-laden large and small vessels with aggregated Aβ deposits (Figure 3.15B,G), which is in agreement with the high incidence of CAA pathology in AD patients (3). These differences in Aβ deposit patterns based on vessel size reflects the existence of substantial CAA pathology in both patient groups, with the added caveat that HCAA Dutch-type CAA is mostly restricted to the arterioles (39). Although, NAB61 was also able to detect parenchymal plaques in HCAA-Dutch and EOAD brains, its specificity in detecting vascular Aβ oligomers, including in larger (Figure 3.15C) and smaller (Figure 3.15H), highlighted the role cerebrovascular mutant Aβ oligomers have in their interaction and co-deposition with fibrin(ogen) along cerebral vessel of various sizes (Figure 3.15E,J). Furthermore, while smaller vessels in EOAD brains had noticeable levels of congophillic Aβ (Figure 3.15G) and Aβ oligomer (Figure 3.15H), fibrin(ogen) co-localization with Aβ oligomer (Figure 3.156J) was significantly lower compared to HCAA-Dutch brains. These results are in agreement with our previous *in vitro* binding experiments revealing that there is a strong binding affinity between oligomeric Aβ and fibrin(ogen), especially mutant oligomeric HCAA Aβs as observed in our SPR binding experiments (Figure 3.2), and fibrin(ogen), but weaker binding between fibrin(ogen) and Aβ aggregates and monomers (69).

Due to aging, genetic, and environmental influences, there are decreases in the clearance of Aβ, which leads to its accumulation at the cerebrovascular interface (31, 34). My results in Figure 3.11 indicate that even low nanomolar levels of HCAA Aβ can lead to alterations in fibrinolysis. Therefore, the BBB dysfunction typically seen in AD and HCAA patients (39, 79) may allow sufficient amounts, ranging from nanomolar to micromolar concentrations, of mutant HCAA-linked Aβ oligomers to transit through to the BBB, interact with circulating vascular fibrin(ogen), and then co-deposit with Fbg in HCAA patients' cerebrovasculature. This would lead to HCAA Aβ-induced clots that are severely structurally abnormal and resistant to fibrinolysis. Therefore, our findings would suggest there could be persistent HCAA Aβ-fibrin(ogen) along cerebral vessels, which can greatly contribute to the exacerbated CAA pathology observed in HCAA disease. The one caveat to this trend is Arctic Aβ that does not delay fibrinolysis relative to buffer (Figure 3.17). Although unclear, Arctic Aβ40's inability to delay clot lysis might be related to its lack of stimulation of *in vitro* tPA-mediated Plg activation, which is discussed in Chapter 5.5.

WT Aβ alone can cause endothelial and smooth muscle cell dysfunction, which can lead to BBB dysfunction (31, 34). In comparison, studies using Dutch42, Arctic42, Italian42, and Iowa42 have demonstrated they increase inhibition of neuronal viability and increase cell cytotoxicity in cell culture relative to WT Aβ42 (118, 119). Dutch40 and Iowa40 treatment of SMC explants from human cerebral microvessels has been shown to elevate proteolysis of SMC α-actin and decrease their viability compared to WT Aβ40 (120, 121). Dutch Aβ can lead to smooth muscle cell death via expression and activation of matrix metalloproteinase 2 (MMP-2) (109). Furthermore, *in vitro* studies have shown that soluble oligomeric HCAA Dutch Aβ is more neurotoxic compared to its more aggregated form (122), which complements our IF analysis in HCAA-Dutch brains (Figure 3.13). I showed there was abundant vascular Aβ oligomer (NAB61 signal)-Fbg co-localization at sites of CAA, which is likely composed of WT and mutant Dutch Aβ. As noted in AD mouse models, increased Aβ-fibrin(ogen) deposition at sites of CAA pathology can lead to detrimental effects in the microvasculature of AD mice, increased co-deposition, which can impair perfusion of the surrounding parenchyma (123), and lead to dystrophic neurites and neuronal death (59). The increased persistence of mutant HCAA Aβ-fibrin(ogen) co-aggregates may exacerbate the vast neuropathological changes typically observed in non-mutant AD CAA cases, which features cerebrovascular WT Aβ-Fbg co-deposition, and may lead to additional pathologies observed in HCAA brains, such as neuroinflammation, vascular wall remodeling, and Aβ clearance (38, 124). The possible ramification HCAA Aβ-fibrin(ogen) interaction in the brain has an added layer of complexity when considering the direct pathological effects of fibrin(ogen) in the brain. Although, the brain's innate immune system, including microglia and astrocytes, can be induced and activated by WT Aβ (125) and HCAA Dutch Aβ (79) alone, the persistence of fibrin(ogen) in CAA-laden vessels can also bring about severe local pro-inflammatory changes, which can contribute to vascular pathology in HCAA disease and AD (126, 127). Recent studies (128), have shown that fibrin can interact with receptors on innate immune cells in the brain and its deposition in the brain induces chronic inflammation in healthy mouse brains leading to synaptic dysfunction via loss of dendrites and spines.

Immunohistochemical studies of HCAA-Dutch patient brains have shown abundant activated microglial and reactive astrocytes surrounding vascular amyloid (i.e. CAA sites) and parenchymal plaques (21, 79), which have been implicated in having a detrimental role in AD pathology (73, 129) and most likely in HCAA. Ryu *et al.,* (73) showed that dense parenchymal and vascular plaques, indicative of fibrillar congophillic Aβ, were surrounded by activated glial cells devoid of cytoplasmic Aβ42+ granules, while non-reactive glial cells surrounding non-fibrillar plaques were Aβ42+ suggesting that mutant Dutch Aβ may have impaired clearance from the brain depending on its aggregated state. This highlights the importance of my results showing both congophillic and oligomeric Aβ's association with fibrin(ogen) in cerebral vessel walls in HCAA brain (Figure 3.13 and Figure 3.14). It is possible that the HCAA Aβ oligomer-fibrin(ogen) complex is harder to clear away due to defective fibrinolysis, as shown in this thesis, and by glial uptake. Additionally, HCAA Aβ may have impaired clearance from the brain because of their impaired degradation by proteolytic enzymes. While Pn's principal hemostatic role is to degrade clots to allow the continuous flow of blood in the circulation, it is known to cleave oligomeric and fibrillar WT Aβ (130, 131). However, closer examinations of mutant Aβ with increased aggregation propensities have showed that oligomeric HCAA Aβ40s, including Dutch40, Arctic40, and Italian40 are resistant to neprilysin-proteolysis (132) and to varying degrees, feature resistance to insulin degrading enzyme (IDE) and plasmin(Pn)-catalyzed (133) proteolysis.

While there is an extensive overlap in the clinical features and pathologies between HCAA- and Aβ-type CAA (Table 1.1), present in over 80% of AD patients, HCAA Dutch and Iowa-type patients present with a myriad of other neurovascular pathologies: they include additional ECM remodeling involving a deregulated TGF-β pathway (11), fibrosis/hyalinosis of the vessel wall, and loss of vessel wall integrity (6, 12-14). Another distinct pathology observed in HCAA are secondary CAA-associated vasculopathies, including "vessel-within-vessel" formation, perivascular astrogliosis, microgliosis, and neuritic degeneration. Neurofibrillary degeneration and presence of NFTs are absent or limited in HCAA disease (25). Mouse models that can recapitulate the pathophysiology specifically observed in HCAA and can distinguish it from pure forms of AD with CAA or sporadic CAA pathology is critical in understanding HCAA disease. A good HCAA model could lead to the development of treatments to a disease that is as of now still uncurable. While a few AD mouse models, like the 5XFAD mouse model, can exhibit CAA pathology (59), the TgSwDI mouse model, developed by the Van Nostrand group at Stony Brook, was one of the first animal models to dramatically develop large amounts of microvascular CAA relative to parenchymal Aβ plaques (134). The transgenic mouse model was made to express the human APP transgene containing 3 EOAD mutations, including the Swedish (K670M/N671L), Dutch (E693Q), and Iowa (D694N) mutations driven by the thymus cell antigen 1 (Thy1) promoter that leads to the predominant expression of transgenic APP in neurons and glia in the brain. The Swedish mutation results sits at the β-secretase cleavage site of APP, likely leading to increased cleavage of APP and increased Aβ production. This mouse line also develops neuroinflammation pathology and signs of cognitive impairments. Given that this mouse model develops extensive CAA and expresses mutant human Dutch and Iowa Aβ, it would be a great model to study in order to complement our HCAA-Aβ-Fbg binding results (Figure 3.2) and co-deposition analyses in HCAA-Dutch human brain (Chapter

3.7). The caveat is that the model does not precisely feature the severity of the cerebrovascular pathology in HCAA patients. TgSwDI mice do not feature abundant nor severe ischemic and hemorrhagic strokes and mostly develop capillary CAA, which largely contrasts with the large-to-medium sized vessel (arterial and arteriole) CAA observed in HCAA patients. Other useful and more recently developed transgenic mouse models of HCAA disease, include tg-APPDutch (16) and tg-ArcSwe (135, 136), which overexpress the HCAA Dutch and Arctic mutations, respectively. The ArcSwe model overexpresses human Arctic Aβ and models HCAA-Arctic disease given the development of CAA with lack of ICH, which also more closely resembles AD pathology (136). The APPDutch model overexpresses human Dutch Aβ and more closely resembles its human HCAA-Dutch analog since it presents with severe CAA, SMC degeneration, ICH, and neuroinflammation(16). It is likely that the HCAA-Aβ-Fbg interaction will have to be stratified by HCAA disease models.

5.4. HCAA-linked Aβ mutant variants greatly enhance tPA-Plg activation and components of the fibrinolytic system

Due to the potential crosstalk between coagulation and inflammation (137), it is difficult to discern what other pathways or mechanisms contribute to specific vascular pathologies in HCAA that include CAA and hemorrhagic strokes. Aβ's partner in CAA deposition, fibrin, the cleaved form of Fbg, plays a major role in Plg activation by stimulating the initial conversion of Plg into plasmin (Pn) via tPA binding/activation, and further enhancing the rate of tPA-Plg activation catalysis (68). However, fibrin is not the sole contributor to Plg activation. As mentioned in Chapter 1.5, small fragments of Aβ containing the Dutch mutation and other fibrillar Aβ peptides have been observed to enhance tPA-Plg activation *in vitro* (97, 138). Indeed in Chapter 4.1, I demonstrated that most of the full-length HCAA Aβs studied in this thesis increased the activities of tPA and Pn (Figure 4.2) and further stimulated tPA-Plg activation in chromogenic enzymatic assays (Figure 4.1) and in human plasma.

Merging results in Chapter 4 indicating that most HCAA Aβ increase fibrinolytic enzyme activity with results in Chapter 3 showing that there is increased HCAA Aβ-Fbg interactions, led to the formation of a hypothesis surrounding the role of the Aβ-Fbg-proteolytic/fibrinolytic system interaction in HCAA cerebrovascular pathology: a structurally altered clot with co-deposited HCAA Aβ-fibrin(ogen) that is resistant to Pn-mediated degradation, is not cleared effectively, and simultaneously dramatically enhancing the proteolytic activity of tPA and plasmin(ogen), both principal mediators of fibrinolysis. My Chapter 3 and 4 results for Dutch and Iowa Aβs were tabulated for easier comparison (Table 5.1). Effects that were quantitatively increased relative to WT Aβ were shaded in green. My data suggest that mutant oligomeric HCAA Aβ may be interacting and binding with vascular fibrin(ogen) with high affinity in and around cerebral blood vessels, which can lead to their co-deposition.

Table 5.1. Effect of HCAA Aβ-linked mutations on the Aβ-Fbg interaction and fibrinolytic enzymatic system compared to WT Aβ.

	Aβ42	Dutch42	Iowa42	Aβ40	Dutch40	Iowa40
Fibrinogen binding affinity (SPR)	14.0 ± 2.70nM	1.6 ± 0.5nM *	3.3 ± 2.3nM *	340 ± 87nM	12 ± 2.4nM ***	6.8 ± 2.3nM ***
% Increase in Clot time to half lysis time (normalized to Buffer)	27.5 ± 7.5%	40 ± 6.6%	72.5 ± 11.5% *	1.01 ± 3.75%	32.7 ± 6.25% **	25.9 ± 6.54% *
TEM morphology of Aβ peptides	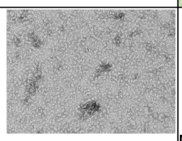 Oligomeric (dots)	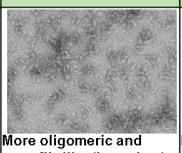 More oligomeric and protofibrillar (branches)	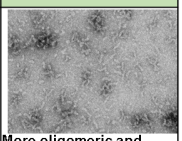 More oligomeric and protofibrillar (branches)	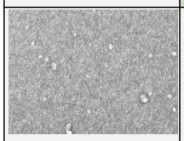 Very few oligomers (dots)	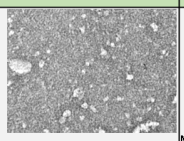 Slightly more oligomeric	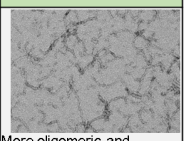 More oligomeric and protofibrillar
ScEM of fibrin clots incubated with Aβ	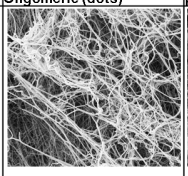 Thin and aggregated	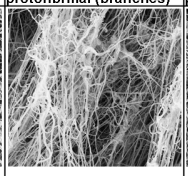 Thinner and more aggregated	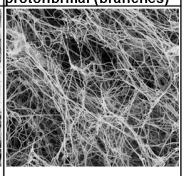 Thinner and slightly more aggregated	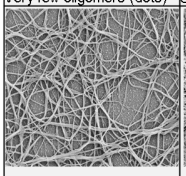 No change	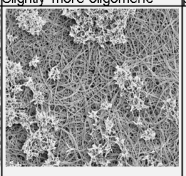 Thinner fibers and clusters of aggregates	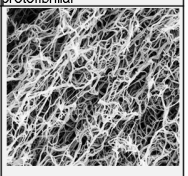 Slightly thinner fibers and very irregular structure
tPA-Plg activation (Vmax)	1.57 ± 0.09	1.76 ± 0.11	1.90 ± 0.05 *	1.27 ± 0.01	2.06 ± 0.07 ***	1.86 ± 0.15 **
tPA activity (Vmax)	1.89 ± 0.06	2.30 ± 0.03	2.26 ± 0.03	2.94 ± 0.11	4.06 ± 0.15 **	4.94 ± 0.21 *
Plasmin activity (Vmax)	1.36 ± 0.09	1.44 ± 0.02 ****	1.60 ± 0.004 ****	1.98 ± 0.17	2.97 ± 0.23 **	2.85 ± 0.19 ****

Statistical analysis: ****p<0.0001; ***p<0.001; **p<0.01; with statistical analyses using one-way ANOVA followed by Tukey's post-hoc test.

Overall, my results show that the most well studied HCAA disease variants, HCAA Dutch and Iowa Aβ, with special emphasis on their oligomeric forms, had increased Fbg binding and led to increase perturbation to fibrin clot structure and function. These mutant oligomeric Aβs also led to significant increases in *in vitro* tPA-Plg activation and in human plasma, which may create a local vascular hemorrhagic environment that is detrimental to the integrity of cerebral vessel walls. Taken together, these results would form the basis for our model (Figure 5.1) that presents the sequence of events that may interconnect these processes and highlights the new roles of mutant HCAA Aβ, fibrin(ogen), and proteolytic/fibrinolytic enzymes in HCAA vascular pathology. The sequence of events depicted in the model (Figure 5.1) are as follows: Akin to normal or WT Aβ-fibrin(ogen) co-deposition in AD patients and AD mouse models (59, 66), due to age-, environmental-, or genetic-related factors, [**Step 1**] there is increased transit across the BBB, with mutant HCAA Aβ oligomers efflux and Fbg influx (40, 62, 76, 77, 79). Mutant Aβ oligomers and congophillic aggregated Aβ can then start interacting within the various layers of the vessel wall. The stronger binding affinity of HCAA Aβ oligomer for Fbg leads to abundant mutant Aβ-Fbg co-deposition initially in and around cerebral blood vessel walls (mostly arteries and arterioles). Aβ can initiate coagulation and conversion of Fbg into fibrin via activation of the FXII-driven intrinsic coagulation and contact system leading to the generation of thrombin and bradykinin (65). Therefore, both Fbg and fibrin can interact with mutant Aβ, very often at sites of CAA, leading to the formation of persistent Aβ-fibrin(ogen) clot aggregates that are structurally abnormal. [**Step 2**] The fibrinolytic system, consisting of tPA and plasmin(ogen), are

activated by the presence of co-deposited/co-aggregated fibrin(ogen) and mutant Aβ, but cannot effectively degrade the structurally altered Pn-resistant clot (**not featured by Arctic-Aβ-induced clots**). In addition, the presence of vascular HCAA Aβ deposits may lead to the activation of the TGF-β pathway (11) and increased expression of MMP-2 from vascular smooth muscle cells (109), which can lead to extensive ECM remodeling, thus weakening the integrity of the vessel wall. [**Step 3**] Persistent vascular mutant Aβ-Fbg leads to further local enhancement and amplification of the fibrinolytic system, which include enhanced tPA-mediated Plg activation and increased tPA/Pn activity (**not featured by Arctic-Aβ-induced clots**). The excess proteolytic activity by the increased Pn generation and enhancements to Pn activity leads to abundant collateral and non-specific cleavage of the vessel wall ECM and tissue. [**Step 4**] Finally, due to a very compromised vessel wall, micro- and macro-intracerebral hemorrhages occur (i.e. lobar hemorrhages and microbleeds, respectively). Hemostasis can occur with circulating platelets and fibrin that can manage smaller cerebral bleeds (microbleeds) by forming clumps at sites of vessel injury. However, larger-caliber hemorrhages are largely lethal in HCAA patients. The first stroke in HCAA-Dutch patients is lethal in 1/3 of HCAA-Dutch patients (25).

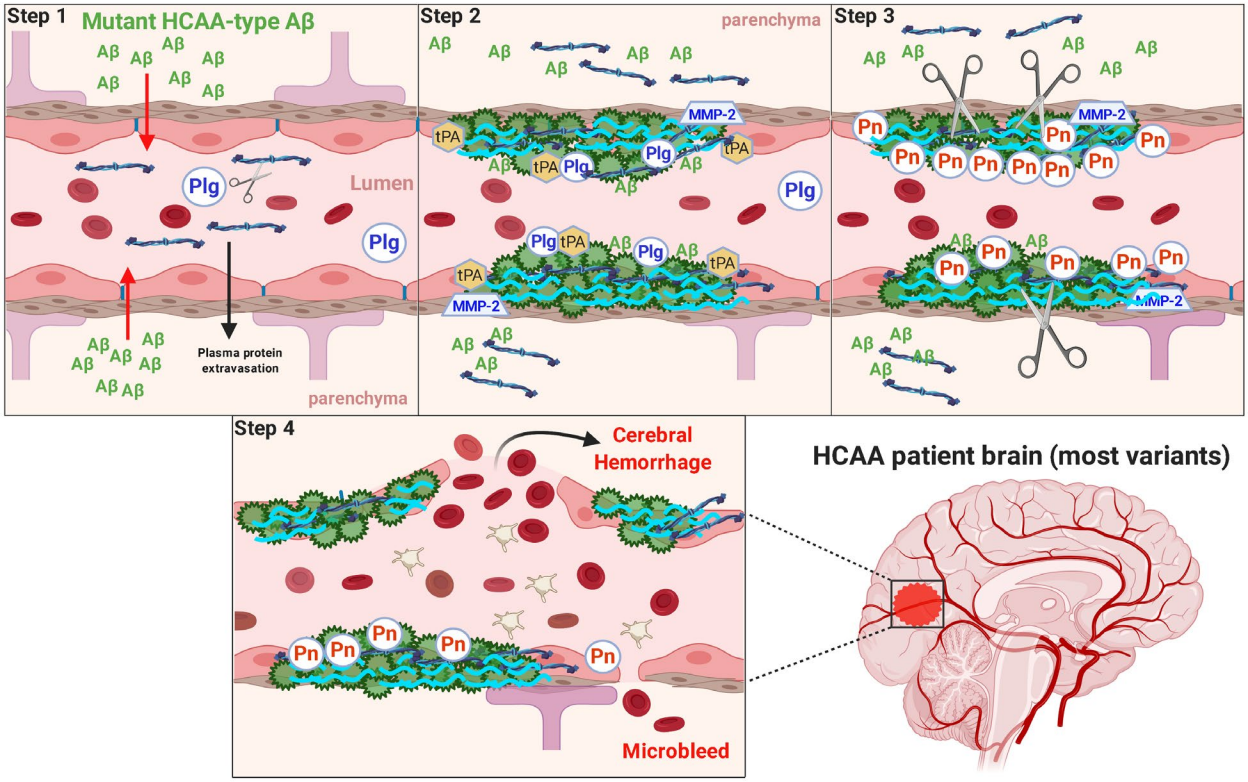

Figure 5.1. Model scheme: HCAA Aβ's effects on fibrin(ogen) structure/function and fibrinolytic enzyme activity are interconnected leading to HCAA pathology. **[Step 1]** Increased mutant **HCAA Aβ oligomers** efflux and Fbg (dark blue fibers) influx across the BBB, which leads to abundant vascular oligomeric and congophillic/aggregated (both are depicted as **green circles**) mutant Aβ deposition. Very often, vascular Aβ co-deposits/co-aggregates with Fbg in and around cerebral blood vessel walls. Aβ can initiate coagulation and conversion of Fbg into fibrin (light blue wavy fibers) via activation of the intrinsic coagulation system leading to the generation of thrombin, which cleaves Fbg into fibrin. Both Fbg/fibrin interact with mutant Aβ forming a persistent and stabilized Aβ-fibrin(ogen) aggregate at CAA sites. **[Step 2]** Structurally altered mutant Aβ-fibrin(ogen) clots exhibiting increased Pn-resistant proteolysis are not effectively degraded and are not cleared (**not featured by Arctic-Aβ-induced clots**). In addition, HCAA Aβ leads to extensive ECM remodeling (MMP-2 activation), weakening the integrity of the vessel wall. **[Step 3]** Persistent vascular mutant Aβ-Fbg leads to further local amplification of the fibrinolytic system: enhanced tPA-mediated Plg activation and increased tPA/Pn activity (**not featured by Arctic-Aβ-induced clots**). The excess proteolytic activity by the increased Pn generation and activity enhancements cleave the vessel wall. **[Step 4]** Finally, due to a very compromised vessel wall, micro- and macro-intracerebral hemorrhages occur (i.e. lobar hemorrhages and microbleeds, respectively). Hemostasis is started with circulating platelets and fibrin that can clump at sites of vessel injury.

Alterations, including enhancements to enzymatic activity, to the proteolytic system may be contributing to a local hemorrhagic environment in HCAA disease where proteolytic amplification could lead to focal degeneration of the vessel wall. Supporting this theory, previous analyses in AD mice show increased tPA and Plg protein

expression around cortical Aβ plaques (139), which suggests there could also be increases in these fibrinolytic proteins/enzymes around vascular amyloid deposits. Interestingly, recent RNA sequencing studies using postmortem HCAA-Dutch patient brain tissue has shown transcriptional up-regulation of *SERPINE1* (PAI-1) and *SERPING* (C1-inhibitor)(140), both of which play major roles in regulating aspects of hemostasis, including fibrinolysis, tPA activity, and Plg activation. Alterations to key regulators of fibrinolysis could be occurring in response to co-deposited fibrin(ogen)/HCAA Aβ in the vascular wall. Their results complement my findings in this thesis that show that HCAA Aβ may have critical roles in both impairing fibrinolysis and enhancing plasminogen activation, therefore altering the balance between thrombosis and fibrinolysis. These findings emphasize the more impactful pathophysiological role of mutant HCAA Aβs in CAA-associated vasculopathy in HCAA disease compared to WT Aβ in non-mutant CAA cases.

In a paradoxical manner, as mentioned in Chapter 5.3, proteolytic and fibrinolytic enzymes such as neprilysin, IDE, and Pn can degrade Aβ. Indeed, quasi-effective Pn-mediated degradation of vascular Aβ does occur in the context of AD disease. Induction of a focal cerebral vessel thrombosis (clot) in an AD model (TgCRND8) that exhibits abundant vascular Aβ-Fbg co-deposition showed delayed *in vivo* fibrinolysis relative to WT control-littermates (66). This phenomena may be occurring in HCAA brains, but to a much grander scale where there is much less efficient Aβ degradation and clot fibrinolysis due to the following: the ability of mutant HCAA Aβs alone to feature increased resistance to Pn-mediated proteolysis (133), delay Pn-mediated *in vitro* fibrinolysis in HCAA Aβ-induced clots (Figure 3.9), and have increased Fbg-co-deposition/co-localization in HCAA brains compared to EOAD brains (Figure 3.12).

There were a few nuanced differences between the effects the various HCAA Aβs had on fibrinolytic enzyme activity and tPA-Plg activation. The differences in tPA-Plg activation between WT Aβ40 and Dutch40 and Iowa40 were much more pronounced than the differences between the Aβ42 counterparts. Iowa42 led to increases in tPA-Plg activation relative to WT Aβ42, whereas Dutch42 showed an increased trend. Examination of the effect of HCAA Aβ40 variants in healthy control human plasma (Figure 4.4), showed that Iowa40 and the double-mutant Aβ peptide, Dutch-Iowa40, led to vast increases in tPA-Plg activation relative to WT Aβ. Interestingly, Italian40, expressed in hemorrhagic-type HCAA brains (HCAA-Italian), did show clear enhancements to enzyme activities of Pn (Figure 4.3B) and tPA (Figure 4.3C), but I did not observe a corresponding increase in tPA-Plg activation via chromogenic assays and in normal plasma (Figure 4.4). Italian Aβ40 only showed an increased trend in (not significant) tPA-Plg activation in plasma. Arctic40 clearly showed a lack of enhancements to tPA-Plg activation (and tPA/Pn activity) via chromogenic assay and in normal plasma, which very often resembled the effects of WT Aβ40. It was unclear why Dutch40 dramatically enhanced tPA-Plg activation (and tPA/Pn activity) in our chromogenic assays, but not in human plasma. The aggregated state of the Dutch40 peptide may have changed over the course of months at -80^{0}C between when the experiments were conducted, which may have had an impact on its ability to enhance tPA-Plg activation.

It is unclear why we observed these discrepancies in tPA-Plg activation. One possibility is that differences in the aggregation propensities of these HCAA Aβs, may differentially enhance the enzymatic approximation effect observed between Aβ-Plg-tPA as shown in Figure 4.7. Another possibility involves differences in binding affinity difference between these HCAA Aβ, Plg, and/or tPA, which merits future exploration to understand the exact structural and physicochemical mechanism behind mutant Aβ's ability to generally enhance fibrinolytic enzyme activity relative to WT Aβ.

5.5. The spectrum of effects of different HCAA Aβs on fibrinolysis and the fibrinolytic system

As mentioned before in Chapter 1.2, HCAA-Arctic disease pathology has many similarities to the other Aβ-type HCAA variants, however, the main difference is the more gradual onset of cognitive decline and lack of ICH and. My results regarding Arctic Aβ's interaction with fibrin(ogen) and the fibrinolytic system may partially explain the unique clinical features of this mutation, principally the lack of ICH in Arctic-carrier patients who are afflicted with abundant CAA. In Chapter 3.8.2, my results show that Arctic Aβ40 stands as an exception to the connection between stronger binding strength to fibrin(ogen) and delayed clot lysis as observed with the other HCAA Aβ40 variants tested (Dutch40, Iowa40, Italian40). Arctic Aβ's stronger binding to Fbg (Figure 3.17) may explain its effect in lowering the maximum clot turbidity (Figure 3.18), which could be indicative of its closer interaction with the b-hole of fibrin(ogen) thus altering its structure. However, unlike the other HCAA Aβs, it does not prolong clot lysis relative to WT Aβ40 (Figure 3.18). This would suggest that while Arctic40 could lead to alteration to clot structure it might be binding to fibrin(ogen) differently. The Aβ-Fbg molar stoichiometry and the Aβ binding sites on Fbg could be different for Arctic Aβ and in such a way that does not hinder plasminogen's access to fibrin.

My results in Chapter 4.1 indicated that while the most well studied HCAA Aβ variants, Dutch and Iowa Aβ, led to increased tPA-Plg activation *in vitro* (Figure 4.2) and in human plasma (Figure 4.4) relative to WT Aβ, Arctic40 did not. Arctic40 also exhibited other unusual characteristics. It enhanced Pn activity, but not tPA activity (Figure 4.2). Perhaps, in the realm of all configuration that could lead to more tPA-Plg activation, tPA activity is more important, which might be the reason why Arctic40 did not lead to more Plg generation. There is also the possibility that Arctic Aβ interacts with tPA and Plg differently based on its structure or binding affinity to tPA/Plg, which has not been yet explored. Overall, the nuanced differences observed between the various HCAA mutant Aβs in terms of degree of ability to delay fibrinolysis and stimulate tPA-Plg activation may be due to binding differences to these proteins and enzymes. HCAA Aβ may have additional binding regions within Fbg. The Strickland Laboratory has previously shown that there are two Aβ binding regions within fibrin(ogen); one is the C-terminus of the β-chain of fibrin(ogen) (b366-b414) near the b-hole (63) and the other is the αC-region of fibrin(ogen) (Aa239-421)(67). Since HCAA Aβs exist in several multimeric forms and Aβ-binding induces oligomerization of fibrin(ogen) (63), stoichiometric analysis of would be difficult. The interaction between HCAA Aβ and fibrin(ogen) may not only be stronger but may also be different among the various mutant Aβ, leading to different Aβ-Fbg molar stoichiometries.

Placed together, these findings suggest that while vascular Aβ in HCAA-Arctic brains may co-deposit with fibrin(ogen) extensively, due to their stronger binding affinity, there may be a lack of cerebral hemorrhage, due to Arctic40's inability to dramatically stimulate the fibrinolytic/proteolytic system, which is incongruent with other HCAA disease variants. Thus, the cerebrovasculature of HCAA-Arctic patients features sites of severe CAA with the incidence of ICH. Future experiments should be performed to probe how and where Arctic40 binds to fibrinolytic enzymes, Plg and tPA, and Fbg. This might help us further understand why HCAA-Arctic patients are afflicted with severe CAA, but not ICH. The model in Figure 5.1 illustrates how the interaction between HCAA Aβ variants, fibrin(ogen), and the fibrinolytic system could explain the development of CAA and the presence or absence of ICH in HCAA disease variants.

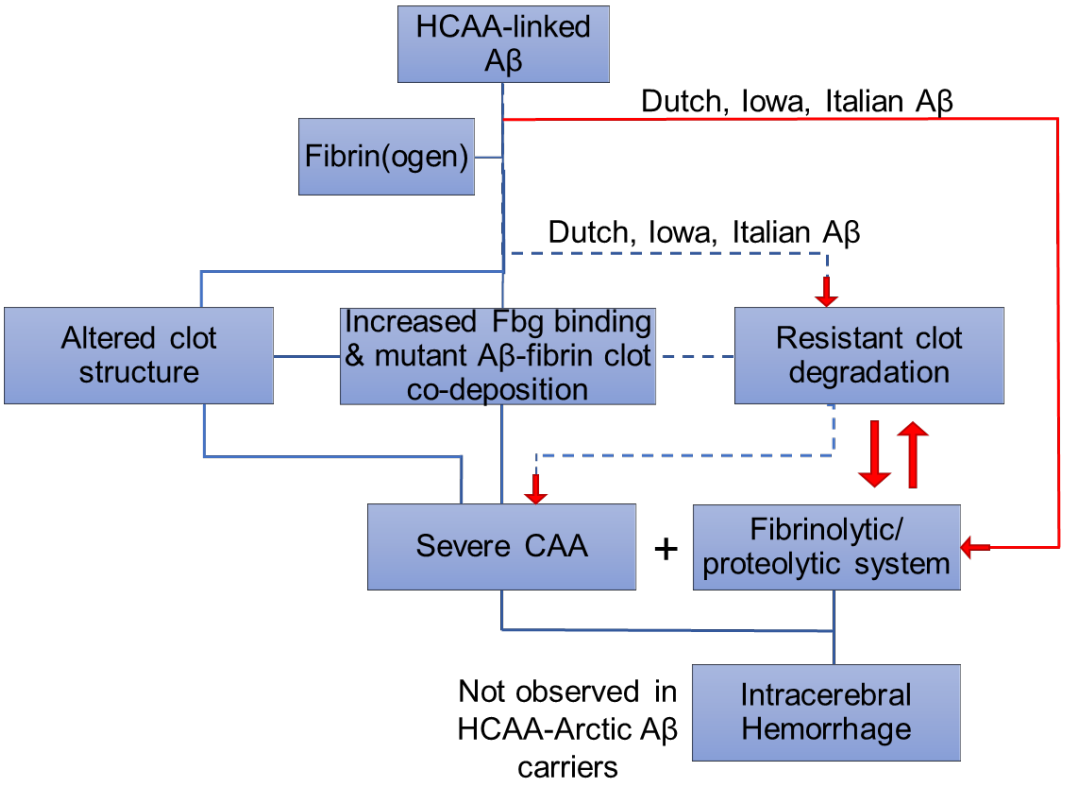

Figure 5.2. Model schematic of mechanisms of various HCAA-linked Aβ leading to HCAA pathology.
HCAA Aβ peptide variants bind strongly with Fbg (as shown in this thesis: Dutch, Iowa, Arctic Aβ) and lead to altered clot structures. However, not all mutant Aβs delay fibrinolysis. Atypically, Arctic Aβ variant does not delay fibrinolysis. It seems that these fibrin(ogen) effects are interconnected to an extent and can significantly contribute to the formation of severe CAA as seen in HCAA disease. Most Aβ variants can also further enhance tPA-Plg activation and tPA/plasmin activity relative to WT Aβ, but not Arctic Aβ. It is possible Arctic Aβ's minimal effect on a clot's resistance to plasmin-mediated degradation and minimal effect on plasmin generation creates a vascular environment where there is abundant Aβ-Fbg co-deposition (increased CAA) without an increase in proteolytic activity, which might be necessary to induce cerebral hemorrhage.

5.6. Longer length Aβs' interaction with fibrin(ogen) and the fibrinolytic system

I investigated the effects of longer length Aβs in Aβ-Fbg interaction and in fibrinolytic system activation as an extension of my thesis focused on probing the effect of various Aβs on elements of hemostasis, including clotting and fibrinolysis. My results in Chapters 3.9 and 4.3, show the differential effects of different length WT (non-mutant) Aβ (1-n), specifically Aβ38, Aβ43, Aβ46, in fibrin(ogen) interactions and with the fibrinolytic enzymatic system. The effects of these different length Aβs were also examined conjointly with Aβ42 and Aβ40 length peptides. The strong correlation observed between longer Aβs (≥ 42) and binding affinity strength for Fbg (Figure 3.20) suggests that Aβs of varying lengths interact with fibrin(ogen) in different ways, which can lead to different consequences for hemostasis. Although longer Aβs had weaker binding affinities for Fbg they did significantly prolong *in vitro* clot lysis (Figure 3.22). Particularly, Aβ46 drastically delayed clot lysis relative to shorter Aβ40 and Aβ42 peptides. As evidenced with my results in Chapter 3, the HCAA Aβ-fibrin(ogen) interaction is much stronger than WT Aβ and as previously discussed could lead to different Aβ-Fbg stoichiometries, which might be the case with these longer length Aβs. In addition, the majority of HCAA Aβ assumed a more aggregated state (Figure 3.4). While, I showed that inducing a more aggregated in Aβ did not directly increase Aβ's binding affinity for Fbg (Figure 3. 6), an increased aggregated state can still influence how it binds to fibrin(ogen). Indeed, TEM profiling of Aβ43 and Aβ46 peptides (Figure 3.19) showed that relative to Aβ40 and Aβ42, they exhibited increased formation of oligomeric and protofibrillar/fibrillar structures, respectively. These findings agrees with the literature indicating that Aβ43 features increased fibrillization capacity (106, 107) and the potential of longer length Aβs to be more amyloidogenic. Perhaps, the increased aggregated state of these longer length Aβs contributes to their ability to prolong clot lysis and alter clot structure (Figure 3.21), with special emphasis on Aβ46.

Interestingly, Aβ38 assumed a more aggregated state with rod-like protofibrillar structures (Figure 3.19) but did not prolong clot lysis. However, Aβ38's effect on clot lysis showed that it significantly lowered the maximum turbidity (Figure 3.22D), which is indicative of alterations to clot formation. Our scanning electron microscopy (ScEM) analysis of clot structures (Figure 3.21) incubated in Aβ (1-n), however showed that Aβ38 did not significantly alter the architecture of the fibrin network. A possible explanation for this Aβ38-associated discrepancy might involve Aβ38's selective ability to perturb clot formation in a dynamic reaction where thrombosis and fibrinolysis are occurring simultaneously in solution.

The increased aggregation state of Aβ38 and Aβ46 peptides might also explain why they both exhibited increased tPA-Plg activation in the chromogenic enzyme assay (Figure 4.5) and in human plasma (Figure 4.6). As explored in Chapter 4, I showed that Aβ46's increased ability to stimulate tPA-Plg activation is likely due to an enzymatic approximation effect (Figure 4.8). While all Aβs, except for WT Aβ40, usually led to increased tPA-Plg activation and enhancements to tPA and Pn activity, Aβ46's increased aggregated state relative to shorter length Aβs, might increase its ability to serve as binding template or scaffolding onto which tPA and Plg can be brought closer together enhancing the catalysis of Plg conversion into Pn. Aβ38's ability to increase

tPA-Plg activation might follow suit. My Chapter 3 and 4 results of Aβs (1-n) were tabulated for easier comparison (Table 5.2). Effects that were quantitatively increased relative to Aβ42 were shaded in green, effects that were decreased were shaded in light red.

Table 5.2. Effects of Aβ (1-n) on the Aβ-Fbg interaction and fibrinolytic enzymatic system relative to Aβ42

	Aβ38	Aβ40	Aβ42	Aβ43	Aβ46
Fibrinogen binding affinity (SPR)	46.3 ± 10.3nM	341 ± 86.8nM ***	17.7 ± 4.22nM	28.9 ± 7.70nM	63.7 ± 0.85nM **
% Increase in Clot time to half lysis time (normalized to Buffer)	24.2 ± 7.4%	4.6 ± 6.75% ** (t-test)	30.5 ± 6.08%	27.3 ± 8.05%	81.9 ± 19.4% *
Max Clot Turbidity (Turbidity Assay)	0.237 ± 0.020	0.301 ± 0.040 ** (t-test)	0.230 ± 0.015	0.305 ± 0.042	0.292 ± 0.021 ** (t-test)
TEM morphology of Aβ peptides	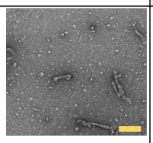 Rod-like protofibrils and Oligomers	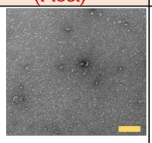 Very few oligomers (dots)	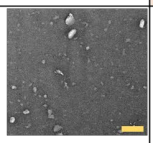 Some Oligomers (dots)	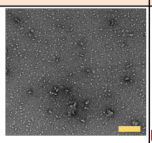 Highly Oligomeric (lots of dots)	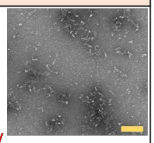 Heavily aggregated protofibrils
ScEM of fibrin clots incubated with Aβ	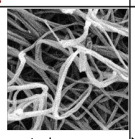 Not as thin, some aggregated	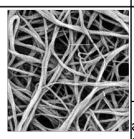 No change	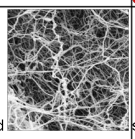 Thin, aggregated fibers	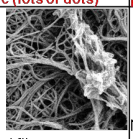 some aggregated fibers	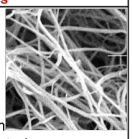 Not as thin or aggregated
tPA-Plg activation (Vmax)	5.0 ± 0.48 ****	0.63 ± 0.25	0.43 ± 0.01	0.51 ± 0.06	3.01 ± 0.73 *
tPA activity (Vmax)	1.52 ± 0.04 ****	2.062 ± 0.03 ****	2.76 ± 0.03	2.37 ± 0.05 ****	2.26 ± 0.04 ****
Plasmin activity (Vmax)	0.86 ± 0.01 ****	1.15 ± 0.01 *	1.55 ± 0.07	1.15 ± 0.01 *	0.95 ± 0.03 ***

Statistical analyses: ****p<0.0001; **p<0.01; with statistical analyses using one-way ANOVA followed by Tukey's post-hoc test. ****p<0.0001; ***p<0.01, *p<0.05; with unpaired two-tailed t-test

It is possible that there are longer length Aβs in parenchymal plaques and in CAA, in addition to the conventional Aβ42 and Aβ40 lengths typically studied (99-101). Sequential proteolytic activity of β-secretase and the γ-secretase/presenilin complex (11) of the amyloid precursor protein (APP) generates Aβ peptides of different lengths (108). The catalytic component of γ-secretase, presenilin (PSEN), further cleaves APP, which creates and releases 39-51 amino acid Aβ peptide fragments. A closer inspection of γ-secretase proteolytic activity reveals that an initial ε-endopeptidase cleavage of APP releases the soluble intracellular domain and long Aβs, including Aβ49 and Aβ48. Sequential carboxypeptidase-like γ-secretase cleavages can generate shorter Aβ peptides until it is released. It is not well known what drives the sequential processing of APP and how genetic (such as APP or PSEN mutations), environmental, and/or lifestyle risk (such as hypertension and diabetes) modifiers linked with AD leads to the production of amyloidogenic Aβ, including Aβ42. Recently, it's been shown that familial AD mutations in PSEN and APP destabilize *in vitro* the APP-γ-secretase/presenilin complex and processing of APP, therefore promoting the production of long amyloidogenic Aβ species (≥ Aβ43), including Aβ45 and Aβ46 (108). There is evidence

that longer length Aβs are deposited in the parenchyma and cerebrovasculature of AD individuals. Aβ43 levels have been found in diffuse parenchymal plaques in human AD brains (105, 141) and in vascular amyloid in human CAA deposits (106). Given my results in this thesis, longer Aβs, like Aβ46, may have a significant role in facets of AD-vascular pathology.

5.7. Future directions

While HCAA mouse models, including the TgSwDI, APPDutch, and TgArcSwe, as previously discussed, do not replicate human HCAA pathology perfectly, they could still help confirm the differences in cerebrovascular Aβ-Fbg deposition seen between mice expressing human WT and HCAA Aβ. We could compare a typically studied AD mouse model used in the Strickland Laboratory that develops abundant CAA (5XFAD or TgCRND8 models) to a HCAA mouse model(s) that forms more CAA. APPDutch mice (16) and tg-ArcSwe (135, 136) would be an ideal HCAA mouse model to investigate in comparison to WT Aβ-expressing mice. APPDutch and ArcSwe mice express human mutant Dutch and Arctic Aβ in the cerebrovasculature, respectively, and feature abundant CAA. Additionally, APPDutch mice feature large vessel CAA and hemorrhagic strokes. In this manner, we could recapitulate and expand on the human tissue analysis comparison between HCAA-Dutch and EOAD patient groups conducted in this thesis. We would quantify % fibrin(ogen) in CAA+ vessels and % Aβ-Fbg co-localization through the cortex across various HCAA variants disease models.

Since prior AD mouse studies have revealed that there is still quasi-effective Pn-mediated degradation when focal cerebral thrombosis were induced (66), it would be important to measure and compare *in vivo* fibrinolysis times between AD and HCAA mouse models. There might be further delays to fibrin degradation and clearance when two-photon induced *in vivo* cerebral clots are made in HCAA mouse models relative to AD mouse brains. Another approach to assess the importance of fibrin(ogen) in HCAA pathology in HCAA disease models involves using anti-sense oligonucleotide (ASO) technology that can target liver production of proteins such as Plg (129) and Fbg. ASO targeting of Fbg would knock down the levels of systemic circulating Fbg. As mentioned before, genetic and pharmacological depletion of Fbg in an AD mouse model reduced amyloid and vascular pathology, which lessened CAA burden (59, 62). ASO-mediated gene knockdown of Fbg (using a specific Fbg-targeted ASO) in an HCAA mouse model that features ICH, such as the APPDutch mouse model, would allow us to determine if early treatment lowering systemic Fbg could lessen mutant Aβ-associated CAA and its associated pathologies including vascular microgliosis and cerebral hemorrhage. Additionally, incorporating dual Fbg-specific and Plg-specific ASO treatments might help confirm the mechanism posited in this thesis. Manipulating Fbg and Plg levels could confirm the physiological mechanism behind how vascular mutant HCAA Aβ-Fbg co-deposition on vessel walls leads to an increased hemorrhagic environment as observed in HCAA patient brains.

In this thesis, I showed that mutant Aβs led to increased perturbation to clot structure and increased resistance to plasmin-degradation, thus likely to very persistent and abundant mutant Aβ-fibrin(ogen) clots co-deposited around sites of CAA in HCAA brains (Dutch and Iowa-brain). Most HCAA Aβ variants also led to increased *in vitro*

tPA-Plg activation in chromogenic assays and in human plasma relative to WT Aβ, which in part may explain the hemorrhagic phenotype observed in HCAA brains, specifically at sites of CAA. Taken together, these results would form the basis for our model (Figure 5.1). To test the validity of this model in human HCAA brain, we would have to inspect the enzyme activity and protein levels of tPA, Plg, and Pn in the cerebrovasculature across various human HCAA variants, including HCAA-Dutch, -Iowa, -Italian, and -Arctic carrier individuals. Excessive tPA and Pn proteolytic activity in HCAA may collaterally injure cerebral blood vessels in HCAA brains. It would be important to examine the protein abundance and enzyme activity of tPA/Plg/Pn in and around CAA sites in HCAA brains. As noted in my IF imaging results in Chapter 3.7, while the frequency and abundance of fibrin(ogen) co-depositing with Aβ around cerebral vessel walls was very high compared to EOAD brains, there were often CAA sites in HCAA brains that did not have Aβ-Fbg co-deposition. Therefore, it would be interesting to compare the amount of proteolytic enzyme levels and activity in CAA sites that are have abundant Fbg (Fbg+) and have less Fbg (Fbg-null). Immunohistological approaches using tPA/Plg-specific antibodies (129) and *in situ* tPA and Pn activity zymography (142) experiments would enable this assessment.

Since my HCAA brain tissue analysis consisted of only the Dutch patients due to limited availability of the tissue in brain banks around the world and used in research laboratories, it would be beneficial if we could procure more Dutch-, Iowa-, Italian-, and Arctic-brain samples if available. We can ask our collaborators at the Leiden University Medical Center, who provided the five HCAA-Dutch brain samples used in my IF analysis, for assistance. Increasing the number of samples and HCAA variants studied would help confirm the *in vitro* effects of HCAA Aβ on fibrinolysis and fibrinolytic enzyme activity that I observed in this thesis. In addition, more biochemical experiments are required to further elucidate the how and why different HCAA Aβ and different length Aβs differentially affect tPA-Plg activation and tPA/Pn activities. Binding experiments between the various Aβ and tPA/Plg/Pn via surface plasmon resonance and pull-downs might resolve their binding affinities and where they bind to each other, respectively. Pull-down experiments of Aβ-Fbg in HCAA brain tissue would also help corroborate the significance of the strong binding affinity for Fbg and high levels of mutant Dutch Aβ-Fbg co-deposition. Furthermore, isolation of microvessels in HCAA Dutch and Iowa brains would further elucidate the specific role of the mutant Aβ-Fbg binding in the cerebrovasculature compared to in parenchymal plaques. These experiments would also allow us to assess the aggregated state (oligomers, monomers, or higher order states) and role of Aβ at sites of CAA pathology.

Shorter length Aβ's may have a more important role in HCAA than in AD pathology. While, Aβ38 has been observed in human AD CSF, plasma, and brain extracts (143), immunohistological examinations of AD and HCAA brains show that there is not extensive Aβ38 deposition in cerebral vessels or in parenchyma plaques in AD brains (113). However, there was abundant cerebral cortical Aβ38 deposition in HCAA-Arctic and Italian-carrier patients' at sites of parenchymal plaques and capillaries/arterioles featuring CAA pathology (113). HCAA-Iowa patient brain analyses have also revealed the presence of Aβ38 in the parenchyma and vessels (144). Examination of the effect of

longer and shorter length Aβs harboring HCAA mutations in clot lysis and fibrinolytic enzyme activity would further elucidate their importance in CAA formation, CAA-associated vasculopathies, and the evolution of intracerebral hemorrhages.

5.8. Conclusion

This thesis provides evidence that mutant HCAA Aβ featured increased perturbation to *in vitro* fibrinolysis and fibrinolytic enzyme activity. These findings improve our understanding of the etiology and pathogenesis behind HCAA's main cerebrovascular pathologies and suggest a role for fibrin(ogen) and mutant HCAA Aβ oligomers in this disease. Amino acid mutations in the HCAA Aβ peptides increase the interaction between deposited Aβ and fibrin(ogen) along the cerebrovasculature in HCAA brains. While likely not the sole contributor, the stronger interaction could be a driver of the formation of the exacerbated CAA found in HCAA. Aβ-Fbg co-deposition might also simultaneously enhance local Pn activity and generation, which can contribute to ICH. If the mutant Aβ-Fbg interaction is a significant contributor to the deadly cerebral hemorrhages in HCAA disease, targeted inhibition of their interaction along the cerebrovasculature could provide a therapeutic opportunity for this uncurable disease and in AD patients afflicted by severe CAA pathology.

Furthermore, the findings in this thesis are not limited to our understanding of HCAA pathology. Since HCAA is an ideal disease to examine CAA pathology, these findings can help us further understand the molecular mechanisms underlying CAA formation, CAA-induced cerebrovascular pathology in AD, and cases of pure forms of sporadic CAA. The interaction between "normal" WT Aβ and fibrin(ogen) has a significant role in CAA formation (66, 69) though likely at a slower temporal scale compared to HCAA cases, due WT Aβ's weaker binding affinity for Fbg. While WT Aβ's featured lower enhancements to fibrinolytic/proteolytic enzyme activity compared to HCAA Aβs, their interaction may still have a significant in the formation of microbleeds in CAA cases. Although, not ubiquitous, microbleeds are found in 18-32% of AD patients (145) in cortical and subcortical regions observed via magnetic resonance imaging (MRI). While studies looking at the connection between vascular lesions and AD progression are limited, usually involve small sample groups, and show a loose correlation between severity of AD disease and large-scale ICH (macro-hemorrhages), there is precedent for a possible interaction between WT Aβ, fibrin(ogen), and the proteolytic/fibrinolytic system contributing to smaller cerebral bleeds. van Veluw *et al*. (78), has recently shown that there was frequent and abundant Aβ and fibrinogen deposition at sites of microbleeds and microinfarcts in CAA human cases. In addition, recent analyses conducted in the prospective population-based Rotterdam Study (146) have shown that there is an increased prevalence of cerebral microbleeds, especially around sites of CAA, in early-onset AD individuals (145), which was also associated with an increased risk for dementia, including AD dementia.

This research also provided evidence for a new potential role for longer length Aβ46. While its binding affinity for Fbg is not as strong as the Aβ42's, it interacts uniquely with fibrin(ogen) to drastically prolong clot lysis. It also features increased plasminogen activation. These findings highlight a possible role of long Aβs in facets of AD-related vascular pathology.

REFERENCES

1. Hebert LE, Weuve J, Scherr PA, & Evans DA (2013) Alzheimer disease in the United States (2010-2050) estimated using the 2010 census. *Neurology* 80(19):1778-1783.
2. Association As (2020) Alzheimer's and dementia.
3. Serrano-Pozo A*, et al.* (2013) Examination of the clinicopathologic continuum of Alzheimer disease in the autopsy cohort of the National Alzheimer Coordinating Center. *J Neuropathol Exp Neurol* 72(12):1182-1192.
4. Farkas E & Luiten PG (2001) Cerebral microvascular pathology in aging and Alzheimer's disease. *Prog Neurobiol* 64(6):575-611.
5. Humpel C (2011) Chronic mild cerebrovascular dysfunction as a cause for Alzheimer's disease? *Exp Gerontol* 46(4):225-232.
6. Kalaria RN (2002) Small vessel disease and Alzheimer's dementia: pathological considerations. *Cerebrovasc Dis* 13 Suppl 2:48-52.
7. Serrano-Pozo A, Frosch MP, Masliah E, & Hyman BT (2011) Neuropathological alterations in Alzheimer disease. *Cold Spring Harb Perspect Med* 1(1):a006189.
8. Jellinger KA & Attems J (2005) Prevalence and pathogenic role of cerebrovascular lesions in Alzheimer disease. *J Neurol Sci* 229-230:37-41.
9. Yamada M (2015) Cerebral amyloid angiopathy: emerging concepts. *J Stroke* 17(1):17-30.
10. Hardy JA & Higgins GA (1992) Alzheimer's disease: the amyloid cascade hypothesis. *Science* 256(5054):184-185.
11. De Strooper B (2003) Aph-1, Pen-2, and Nicastrin with Presenilin generate an active gamma-Secretase complex. *Neuron* 38(1):9-12.
12. Nunan J & Small DH (2000) Regulation of APP cleavage by alpha-, beta- and gamma-secretases. *FEBS Lett* 483(1):6-10.
13. Chen GF*, et al.* (2017) Amyloid beta: structure, biology and structure-based therapeutic development. *Acta Pharmacol Sin* 38(9):1205-1235.
14. Selkoe DJ (2000) The genetics and molecular pathology of Alzheimer's disease: roles of amyloid and the presenilins. *Neurol Clin* 18(4):903-922.
15. Qi XM & Ma JF (2017) The role of amyloid beta clearance in cerebral amyloid angiopathy: more potential therapeutic targets. *Transl Neurodegener* 6:22.
16. Herzig MC*, et al.* (2004) Abeta is targeted to the vasculature in a mouse model of hereditary cerebral hemorrhage with amyloidosis. *Nat Neurosci* 7(9):954-960.
17. Roher AE*, et al.* (1993) beta-Amyloid-(1-42) is a major component of cerebrovascular amyloid deposits: implications for the pathology of Alzheimer disease. *Proc Natl Acad Sci U S A* 90(22):10836-10840.

18. Shinkai Y*, et al.* (1995) Amyloid beta-proteins 1-40 and 1-42(43) in the soluble fraction of extra- and intracranial blood vessels. *Ann Neurol* 38(3):421-428.
19. McGowan E*, et al.* (2005) Abeta42 is essential for parenchymal and vascular amyloid deposition in mice. *Neuron* 47(2):191-199.
20. Verbeek MM, Otte-Holler I, Veerhuis R, Ruiter DJ, & De Waal RM (1998) Distribution of A beta-associated proteins in cerebrovascular amyloid of Alzheimer's disease. *Acta Neuropathol* 96(6):628-636.
21. Revesz T*, et al.* (2009) Genetics and molecular pathogenesis of sporadic and hereditary cerebral amyloid angiopathies. *Acta Neuropathol* 118(1):115-130.
22. Vinters HV (2015) Emerging concepts in Alzheimer's disease. *Annu Rev Pathol* 10:291-319.
23. Charidimou A*, et al.* (2017) Emerging concepts in sporadic cerebral amyloid angiopathy. *Brain* 140(7):1829-1850.
24. Viswanathan A & Greenberg SM (2011) Cerebral amyloid angiopathy in the elderly. *Ann Neurol* 70(6):871-880.
25. Zhang-Nunes SX*, et al.* (2006) The cerebral beta-amyloid angiopathies: hereditary and sporadic. *Brain Pathol* 16(1):30-39.
26. Neuropathology Group. Medical Research Council Cognitive F & Aging S (2001) Pathological correlates of late-onset dementia in a multicentre, community-based population in England and Wales. Neuropathology Group of the Medical Research Council Cognitive Function and Ageing Study (MRC CFAS). *Lancet* 357(9251):169-175.
27. Pfeifer LA, White LR, Ross GW, Petrovitch H, & Launer LJ (2002) Cerebral amyloid angiopathy and cognitive function: the HAAS autopsy study. *Neurology* 58(11):1629-1634.
28. Boyle PA*, et al.* (2015) Cerebral amyloid angiopathy and cognitive outcomes in community-based older persons. *Neurology* 85(22):1930-1936.
29. Yamada M (2002) Risk factors for cerebral amyloid angiopathy in the elderly. *Ann N Y Acad Sci* 977:37-44.
30. Moulin S*, et al.* (2016) Dementia risk after spontaneous intracerebral haemorrhage: a prospective cohort study. *Lancet Neurol* 15(8):820-829.
31. Hall CN*, et al.* (2014) Capillary pericytes regulate cerebral blood flow in health and disease. *Nature* 508(7494):55-60.
32. Zlokovic BV (2011) Neurovascular pathways to neurodegeneration in Alzheimer's disease and other disorders. *Nat Rev Neurosci* 12(12):723-738.
33. Attems J, Jellinger K, Thal DR, & Van Nostrand W (2011) Review: sporadic cerebral amyloid angiopathy. *Neuropathol Appl Neurobiol* 37(1):75-93.

34. Nelson AR, Sweeney MD, Sagare AP, & Zlokovic BV (2016) Neurovascular dysfunction and neurodegeneration in dementia and Alzheimer's disease. *Biochim Biophys Acta* 1862(5):887-900.
35. Dumas A*, et al.* (2012) Functional magnetic resonance imaging detection of vascular reactivity in cerebral amyloid angiopathy. *Ann Neurol* 72(1):76-81.
36. Reijmer YD, van Veluw SJ, & Greenberg SM (2016) Ischemic brain injury in cerebral amyloid angiopathy. *J Cereb Blood Flow Metab* 36(1):40-54.
37. Auriel E & Greenberg SM (2012) The pathophysiology and clinical presentation of cerebral amyloid angiopathy. *Curr Atheroscler Rep* 14(4):343-350.
38. Bornebroek M, Haan J, & Roos RA (1999) Hereditary cerebral hemorrhage with amyloidosis--Dutch type (HCHWA-D): a review of the variety in phenotypic expression. *Amyloid* 6(3):215-224.
39. Maat-Schieman M, Roos R, & van Duinen S (2005) Hereditary cerebral hemorrhage with amyloidosis-Dutch type. *Neuropathology* 25(4):288-297.
40. van Etten ES*, et al.* (2016) Recurrent hemorrhage risk and mortality in hereditary and sporadic cerebral amyloid angiopathy. *Neurology* 87(14):1482-1487.
41. Kamino K*, et al.* (1992) Linkage and mutational analysis of familial Alzheimer disease kindreds for the APP gene region. *Am J Hum Genet* 51(5):998-1014.
42. Basun H*, et al.* (2008) Clinical and neuropathological features of the arctic APP gene mutation causing early-onset Alzheimer disease. *Arch Neurol* 65(4):499-505.
43. Kalimo H*, et al.* (2013) The Arctic AbetaPP mutation leads to Alzheimer's disease pathology with highly variable topographic deposition of differentially truncated Abeta. *Acta Neuropathol Commun* 1:60.
44. Grand Moursel L*, et al.* (2018) TGFbeta pathway deregulation and abnormal phospho-SMAD2/3 staining in hereditary cerebral hemorrhage with amyloidosis-Dutch type. *Brain Pathol* 28(4):495-506.
45. Nishitsuji K*, et al.* (2007) Cerebral vascular accumulation of Dutch-type Abeta42, but not wild-type Abeta42, in hereditary cerebral hemorrhage with amyloidosis, Dutch type. *J Neurosci Res* 85(13):2917-2923.
46. Farrer LA*, et al.* (1997) Effects of age, sex, and ethnicity on the association between apolipoprotein E genotype and Alzheimer disease. A meta-analysis. APOE and Alzheimer Disease Meta Analysis Consortium. *JAMA* 278(16):1349-1356.
47. Tanzi RE (2012) The genetics of Alzheimer disease. *Cold Spring Harb Perspect Med* 2(10).
48. Fagan AM*, et al.* (2002) Human and murine ApoE markedly alters A beta metabolism before and after plaque formation in a mouse model of Alzheimer's disease. *Neurobiol Dis* 9(3):305-318.

49. Haan J*, et al.* (1994) The apolipoprotein E epsilon 4 allele does not influence the clinical expression of the amyloid precursor protein gene codon 693 or 692 mutations. *Ann Neurol* 36(3):434-437.
50. Bateman RJ*, et al.* (2006) Human amyloid-beta synthesis and clearance rates as measured in cerebrospinal fluid in vivo. *Nat Med* 12(7):856-861.
51. Jakel L, Biemans E, Klijn CJM, Kuiperij HB, & Verbeek MM (2020) Reduced Influence of apoE on Abeta43 Aggregation and Reduced Vascular Abeta43 Toxicity as Compared with Abeta40 and Abeta42. *Mol Neurobiol* 57(4):2131-2141.
52. Liu CC*, et al.* (2017) ApoE4 Accelerates Early Seeding of Amyloid Pathology. *Neuron* 96(5):1024-1032 e1023.
53. Shibata M*, et al.* (2000) Clearance of Alzheimer's amyloid-ss(1-40) peptide from brain by LDL receptor-related protein-1 at the blood-brain barrier. *J Clin Invest* 106(12):1489-1499.
54. Prelli F*, et al.* (1990) Expression of a normal and variant Alzheimer's beta-protein gene in amyloid of hereditary cerebral hemorrhage, Dutch type: DNA and protein diagnostic assays. *Biochem Biophys Res Commun* 170(1):301-307.
55. Thal DR*, et al.* (2002) Two types of sporadic cerebral amyloid angiopathy. *J Neuropathol Exp Neurol* 61(3):282-293.
56. Weber SA, Patel RK, & Lutsep HL (2018) Cerebral amyloid angiopathy: diagnosis and potential therapies. *Expert Rev Neurother* 18(6):503-513.
57. Iadecola C (2004) Neurovascular regulation in the normal brain and in Alzheimer's disease. *Nat Rev Neurosci* 5(5):347-360.
58. Niwa K*, et al.* (2002) Cerebrovascular autoregulation is profoundly impaired in mice overexpressing amyloid precursor protein. *Am J Physiol Heart Circ Physiol* 283(1):H315-323.
59. Cortes-Canteli M, Mattei L, Richards AT, Norris EH, & Strickland S (2015) Fibrin deposited in the Alzheimer's disease brain promotes neuronal degeneration. *Neurobiol Aging* 36(2):608-617.
60. Cortes-Canteli M, Zamolodchikov D, Ahn HJ, Strickland S, & Norris EH (2012) Fibrinogen and altered hemostasis in Alzheimer's disease. *J Alzheimers Dis* 32(3):599-608.
61. de la Torre JC (2004) Is Alzheimer's disease a neurodegenerative or a vascular disorder? Data, dogma, and dialectics. *Lancet Neurol* 3(3):184-190.
62. Paul J, Strickland S, & Melchor JP (2007) Fibrin deposition accelerates neurovascular damage and neuroinflammation in mouse models of Alzheimer's disease. *J Exp Med* 204(8):1999-2008.
63. Ahn HJ*, et al.* (2010) Alzheimer's disease peptide beta-amyloid interacts with fibrinogen and induces its oligomerization. *Proc Natl Acad Sci U S A* 107(50):21812-21817.

64. Zamolodchikov D & Strickland S (2012) Abeta delays fibrin clot lysis by altering fibrin structure and attenuating plasminogen binding to fibrin. *Blood* 119(14):3342-3351.
65. Zamolodchikov D & Strickland S (2016) The Alzheimer's disease peptide beta-amyloid promotes thrombin generation through activation of coagulation factor XII: reply. *J Thromb Haemost* 14(7):1489.
66. Cortes-Canteli M*, et al.* (2010) Fibrinogen and beta-amyloid association alters thrombosis and fibrinolysis: a possible contributing factor to Alzheimer's disease. *Neuron* 66(5):695-709.
67. Zamolodchikov D*, et al.* (2016) Biochemical and structural analysis of the interaction between beta-amyloid and fibrinogen. *Blood* 128(8):1144-1151.
68. Medved L & Nieuwenhuizen W (2003) Molecular mechanisms of initiation of fibrinolysis by fibrin. *Thromb Haemost* 89(3):409-419.
69. Ahn HJ*, et al.* (2014) A novel Abeta-fibrinogen interaction inhibitor rescues altered thrombosis and cognitive decline in Alzheimer's disease mice. *J Exp Med* 211(6):1049-1062.
70. Fiala M*, et al.* (2002) Cyclooxygenase-2-positive macrophages infiltrate the Alzheimer's disease brain and damage the blood-brain barrier. *Eur J Clin Invest* 32(5):360-371.
71. Lipinski B & Sajdel-Sulkowska EM (2006) New insight into Alzheimer disease: demonstration of fibrin(ogen)-serum albumin insoluble deposits in brain tissue. *Alzheimer Dis Assoc Disord* 20(4):323-326.
72. Noguchi M*, et al.* (2014) Roles of serum fibrinogen alpha chain-derived peptides in Alzheimer's disease. *Int J Geriatr Psychiatry* 29(8):808-818.
73. Ryu JK & McLarnon JG (2009) A leaky blood-brain barrier, fibrinogen infiltration and microglial reactivity in inflamed Alzheimer's disease brain. *J Cell Mol Med* 13(9A):2911-2925.
74. Craig-Schapiro R*, et al.* (2011) Multiplexed immunoassay panel identifies novel CSF biomarkers for Alzheimer's disease diagnosis and prognosis. *PLoS One* 6(4):e18850.
75. Vafadar-Isfahani B*, et al.* (2012) Identification of SPARC-like 1 protein as part of a biomarker panel for Alzheimer's disease in cerebrospinal fluid. *J Alzheimers Dis* 28(3):625-636.
76. Zipser BD*, et al.* (2007) Microvascular injury and blood-brain barrier leakage in Alzheimer's disease. *Neurobiol Aging* 28(7):977-986.
77. Freeze WM*, et al.* (2019) Blood-Brain Barrier Leakage and Microvascular Lesions in Cerebral Amyloid Angiopathy. *Stroke* 50(2):328-335.
78. van Veluw SJ*, et al.* (2019) Different microvascular alterations underlie microbleeds and microinfarcts. *Ann Neurol* 86(2):279-292.
79. Maat-Schieman ML*, et al.* (2004) Glial reactions and the clearance of amyloid beta protein in the brains of patients with hereditary cerebral hemorrhage with amyloidosis-Dutch type. *Acta Neuropathol* 107(5):389-398.

80. Song F*, et al.* (2011) Meta-analysis of plasma amyloid-beta levels in Alzheimer's disease. *J Alzheimers Dis* 26(2):365-375.
81. Andreasen N*, et al.* (1999) Cerebrospinal fluid beta-amyloid(1-42) in Alzheimer disease: differences between early- and late-onset Alzheimer disease and stability during the course of disease. *Arch Neurol* 56(6):673-680.
82. Murphy MP & LeVine H, 3rd (2010) Alzheimer's disease and the amyloid-beta peptide. *J Alzheimers Dis* 19(1):311-323.
83. Koffie RM*, et al.* (2009) Oligomeric amyloid beta associates with postsynaptic densities and correlates with excitatory synapse loss near senile plaques. *Proc Natl Acad Sci U S A* 106(10):4012-4017.
84. Suzuki N*, et al.* (1994) High tissue content of soluble beta 1-40 is linked to cerebral amyloid angiopathy. *Am J Pathol* 145(2):452-460.
85. Kumar-Singh S (2008) Cerebral amyloid angiopathy: pathogenetic mechanisms and link to dense amyloid plaques. *Genes Brain Behav* 7 Suppl 1:67-82.
86. Wisniewski T, Ghiso J, & Frangione B (1991) Peptides homologous to the amyloid protein of Alzheimer's disease containing a glutamine for glutamic acid substitution have accelerated amyloid fibril formation. *Biochem Biophys Res Commun* 180(3):1528.
87. Walsh DM, Lomakin A, Benedek GB, Condron MM, & Teplow DB (1997) Amyloid beta-protein fibrillogenesis. Detection of a protofibrillar intermediate. *J Biol Chem* 272(35):22364-22372.
88. Thal DR, Walter J, Saido TC, & Fandrich M (2015) Neuropathology and biochemistry of Abeta and its aggregates in Alzheimer's disease. *Acta Neuropathol* 129(2):167-182.
89. Nilsberth C*, et al.* (2001) The 'Arctic' APP mutation (E693G) causes Alzheimer's disease by enhanced Abeta protofibril formation. *Nat Neurosci* 4(9):887-893.
90. Norlin N*, et al.* (2012) Aggregation and fibril morphology of the Arctic mutation of Alzheimer's Abeta peptide by CD, TEM, STEM and in situ AFM. *J Struct Biol* 180(1):174-189.
91. Weisel JW & Litvinov RI (2017) Fibrin Formation, Structure and Properties. *Subcell Biochem* 82:405-456.
92. Weisel JW (2005) Fibrinogen and fibrin. *Adv Protein Chem* 70:247-299.
93. Tucker HM*, et al.* (2000) The plasmin system is induced by and degrades amyloid-beta aggregates. *J Neurosci* 20(11):3937-3946.
94. Van Nostrand WE & Porter M (1999) Plasmin cleavage of the amyloid beta-protein: alteration of secondary structure and stimulation of tissue plasminogen activator activity. *Biochemistry* 38(35):11570-11576.
95. Longstaff C*, et al.* (2011) The interplay between tissue plasminogen activator domains and fibrin structures in the regulation of fibrinolysis: kinetic and microscopic studies. *Blood* 117(2):661-668.

96. Kranenburg O*, et al.* (2002) Tissue-type plasminogen activator is a multiligand cross-beta structure receptor. *Curr Biol* 12(21):1833-1839.
97. Kingston IB, Castro MJ, & Anderson S (1995) In vitro stimulation of tissue-type plasminogen activator by Alzheimer amyloid beta-peptide analogues. *Nat Med* 1(2):138-142.
98. Kruithof EK & Schleuning WD (2004) A comparative study of amyloid-beta (1-42) as a cofactor for plasminogen activation by vampire bat plasminogen activator and recombinant human tissue-type plasminogen activator. *Thromb Haemost* 92(3):559-567.
99. Dulin F*, et al.* (2008) P3 peptide, a truncated form of A beta devoid of synaptotoxic effect, does not assemble into soluble oligomers. *FEBS Lett* 582(13):1865-1870.
100. DaRocha-Souto B*, et al.* (2011) Brain oligomeric beta-amyloid but not total amyloid plaque burden correlates with neuronal loss and astrocyte inflammatory response in amyloid precursor protein/tau transgenic mice. *J Neuropathol Exp Neurol* 70(5):360-376.
101. Benilova I, Karran E, & De Strooper B (2012) The toxic Abeta oligomer and Alzheimer's disease: an emperor in need of clothes. *Nat Neurosci* 15(3):349-357.
102. Selkoe DJ (1989) Molecular pathology of amyloidogenic proteins and the role of vascular amyloidosis in Alzheimer's disease. *Neurobiol Aging* 10(5):387-395.
103. Goust JM, Mangum M, & Powers JM (1984) An immunologic assessment of brain-associated IgG in senile cerebral amyloidosis. *J Neuropathol Exp Neurol* 43(5):481-488.
104. Powers JM, Schlaepfer WW, Willingham MC, & Hall BJ (1981) An immunoperoxidase study of senile cerebral amyloidosis with pathogenetic considerations. *J Neuropathol Exp Neurol* 40(6):592-612.
105. Welander H*, et al.* (2009) Abeta43 is more frequent than Abeta40 in amyloid plaque cores from Alzheimer disease brains. *J Neurochem* 110(2):697-706.
106. Jakel L, Boche D, Nicoll JAR, & Verbeek MM (2019) Abeta43 in human Alzheimer's disease: effects of active Abeta42 immunization. *Acta Neuropathol Commun* 7(1):141.
107. Burnouf S, Gorsky MK, Dols J, Gronke S, & Partridge L (2015) Abeta43 is neurotoxic and primes aggregation of Abeta40 in vivo. *Acta Neuropathol* 130(1):35-47.
108. Szaruga M*, et al.* (2017) Alzheimer's-Causing Mutations Shift Abeta Length by Destabilizing gamma-Secretase-Abetan Interactions. *Cell* 170(3):443-456 e414.
109. Stine WB, Jungbauer L, Yu C, & LaDu MJ (2011) Preparing synthetic Abeta in different aggregation states. *Methods Mol Biol* 670:13-32.

110. Lee EB*, et al.* (2006) Targeting amyloid-beta peptide (Abeta) oligomers by passive immunization with a conformation-selective monoclonal antibody improves learning and memory in Abeta precursor protein (APP) transgenic mice. *J Biol Chem* 281(7):4292-4299.
111. Singh PK*, et al.* (2018) Aminopyrimidine Class Aggregation Inhibitor Effectively Blocks Abeta-Fibrinogen Interaction and Abeta-Induced Contact System Activation. *Biochemistry* 57(8):1399-1409.
112. Bugiani O*, et al.* (2010) Hereditary cerebral hemorrhage with amyloidosis associated with the E693K mutation of APP. *Arch Neurol* 67(8):987-995.
113. Moro ML*, et al.* (2012) APP mutations in the Abeta coding region are associated with abundant cerebral deposition of Abeta38. *Acta Neuropathol* 124(6):809-821.
114. Miravalle L*, et al.* (2000) Substitutions at codon 22 of Alzheimer's abeta peptide induce diverse conformational changes and apoptotic effects in human cerebral endothelial cells. *J Biol Chem* 275(35):27110-27116.
115. Morimoto A*, et al.* (2002) Aggregation and neurotoxicity of mutant amyloid beta (A beta) peptides with proline replacement: importance of turn formation at positions 22 and 23. *Biochem Biophys Res Commun* 295(2):306-311.
116. Alonzo NC, Hyman BT, Rebeck GW, & Greenberg SM (1998) Progression of cerebral amyloid angiopathy: accumulation of amyloid-beta40 in affected vessels. *J Neuropathol Exp Neurol* 57(4):353-359.
117. Natte R*, et al.* (1999) Ultrastructural evidence of early non-fibrillar Abeta42 in the capillary basement membrane of patients with hereditary cerebral hemorrhage with amyloidosis, Dutch type. *Acta Neuropathol* 98(6):577-582.
118. Dahlgren KN*, et al.* (2002) Oligomeric and fibrillar species of amyloid-beta peptides differentially affect neuronal viability. *J Biol Chem* 277(35):32046-32053.
119. Murakami K*, et al.* (2002) Synthesis, aggregation, neurotoxicity, and secondary structure of various A beta 1-42 mutants of familial Alzheimer's disease at positions 21-23. *Biochem Biophys Res Commun* 294(1):5-10.
120. Wang Z, Natte R, Berliner JA, van Duinen SG, & Vinters HV (2000) Toxicity of Dutch (E22Q) and Flemish (A21G) mutant amyloid beta proteins to human cerebral microvessel and aortic smooth muscle cells. *Stroke* 31(2):534-538.
121. Van Nostrand WE, Melchor JP, Cho HS, Greenberg SM, & Rebeck GW (2001) Pathogenic effects of D23N Iowa mutant amyloid beta -protein. *J Biol Chem* 276(35):32860-32866.
122. Kumar-Singh S*, et al.* (2002) In vitro studies of Flemish, Dutch, and wild-type beta-amyloid provide evidence for two-staged neurotoxicity. *Neurobiol Dis* 11(2):330-340.

123. Klohs J*, et al.* (2012) Contrast-enhanced magnetic resonance microangiography reveals remodeling of the cerebral microvasculature in transgenic ArcAbeta mice. *J Neurosci* 32(5):1705-1713.
124. Greenberg SM*, et al.* (2003) Hemorrhagic stroke associated with the Iowa amyloid precursor protein mutation. *Neurology* 60(6):1020-1022.
125. Salminen A, Ojala J, Kauppinen A, Kaarniranta K, & Suuronen T (2009) Inflammation in Alzheimer's disease: amyloid-beta oligomers trigger innate immunity defence via pattern recognition receptors. *Prog Neurobiol* 87(3):181-194.
126. Adams RA*, et al.* (2007) The fibrin-derived gamma377-395 peptide inhibits microglia activation and suppresses relapsing paralysis in central nervous system autoimmune disease. *J Exp Med* 204(3):571-582.
127. Davalos D*, et al.* (2012) Fibrinogen-induced perivascular microglial clustering is required for the development of axonal damage in neuroinflammation. *Nat Commun* 3:1227.
128. Merlini M*, et al.* (2019) Fibrinogen Induces Microglia-Mediated Spine Elimination and Cognitive Impairment in an Alzheimer's Disease Model. *Neuron* 101(6):1099-1108 e1096.
129. Baker SK*, et al.* (2018) Blood-derived plasminogen drives brain inflammation and plaque deposition in a mouse model of Alzheimer's disease. *Proc Natl Acad Sci U S A* 115(41):E9687-E9696.
130. Exley C & Korchazhkina OV (2001) Plasmin cleaves Abeta42 in vitro and prevents its aggregation into beta-pleated sheet structures. *Neuroreport* 12(13):2967-2970.
131. Ledesma MD*, et al.* (2000) Brain plasmin enhances APP alpha-cleavage and Abeta degradation and is reduced in Alzheimer's disease brains. *EMBO Rep* 1(6):530-535.
132. Tsubuki S, Takaki Y, & Saido TC (2003) Dutch, Flemish, Italian, and Arctic mutations of APP and resistance of Abeta to physiologically relevant proteolytic degradation. *Lancet* 361(9373):1957-1958.
133. Betts V*, et al.* (2008) Aggregation and catabolism of disease-associated intra-Abeta mutations: reduced proteolysis of AbetaA21G by neprilysin. *Neurobiol Dis* 31(3):442-450.
134. Van Vickle GD*, et al.* (2008) Tg-SwDI transgenic mice exhibit novel alterations in AbetaPP processing, Abeta degradation, and resilient amyloid angiopathy. *Am J Pathol* 173(2):483-493.
135. Philipson O*, et al.* (2009) A highly insoluble state of Abeta similar to that of Alzheimer's disease brain is found in Arctic APP transgenic mice. *Neurobiol Aging* 30(9):1393-1405.
136. Cortese A, Delgado-Morales R, Almeida OFX, & Romberg C (2019) The Arctic/Swedish APP mutation alters the impact of chronic stress on cognition in mice. *Eur J Neurosci* 50(5):2773-2785.

137. Levi M, van der Poll T, & Buller HR (2004) Bidirectional relation between inflammation and coagulation. *Circulation* 109(22):2698-2704.
138. Davis J & Van Nostrand WE (1996) Enhanced pathologic properties of Dutch-type mutant amyloid beta-protein. *Proc Natl Acad Sci U S A* 93(7):2996-3000.
139. Bi Oh S, Suh N, Kim I, & Lee JY (2015) Impacts of aging and amyloid-beta deposition on plasminogen activators and plasminogen activator inhibitor-1 in the Tg2576 mouse model of Alzheimer's disease. *Brain Res* 1597:159-167.
140. Grand Moursel L*, et al.* (2018) Brain Transcriptomic Analysis of Hereditary Cerebral Hemorrhage With Amyloidosis-Dutch Type. *Front Aging Neurosci* 10:102.
141. Iizuka T*, et al.* (1995) Amyloid beta-protein ending at Thr43 is a minor component of some diffuse plaques in the Alzheimer's disease brain, but is not found in cerebrovascular amyloid. *Brain Res* 702(1-2):275-278.
142. Salles FJ & Strickland S (2002) Localization and regulation of the tissue plasminogen activator-plasmin system in the hippocampus. *J Neurosci* 22(6):2125-2134.
143. Maler JM*, et al.* (2007) Urea-based two-dimensional electrophoresis of beta-amyloid peptides in human plasma: evidence for novel Abeta species. *Proteomics* 7(20):3815-3820.
144. Tomidokoro Y*, et al.* (2010) Iowa variant of familial Alzheimer's disease: accumulation of posttranslationally modified AbetaD23N in parenchymal and cerebrovascular amyloid deposits. *Am J Pathol* 176(4):1841-1854.
145. Cordonnier C & van der Flier WM (2011) Brain microbleeds and Alzheimer's disease: innocent observation or key player? *Brain* 134(Pt 2):335-344.
146. Akoudad S*, et al.* (2016) Association of Cerebral Microbleeds With Cognitive Decline and Dementia. *JAMA Neurol* 73(8):934-943.